Tribological Studies of Modem orthopaedic biomaterial Combinations

Vassiliou, Katelia

Tribological Studies of Modern Orthopaedic Biomaterial Combinations

Katelia Vassiliou, BSc

A thesis submitted for the degree of Doctor of Philosophy at the University of Durham

Centre for Biomedical Engineering

University of Durham

South Road Science Labs

Durham

DH1 3LE

March 2005

"How high does the sycamore grow?
If you cut it down then you'll never know"

Colours of the Wind, Pocahontas
Lyrics by Stephen Schwartz

Abstract

Debris created during the wear of prosthetic joints is known to have an effect on the success of the implant. As such the factors affecting wear and lubrication need to be understood in order to reduce wear as much as possible *in vivo*. In this thesis a number of orthopaedic biomaterials were tested *in vitro*, and various factors affecting their tribology were investigated.

Load was found to affect wear for stainless steel on UHMWPE contacts, but not the wear factor which has a load term incorporated into it. Increasing nominal contact stress, however, was found to cause a decrease in wear factor particularly at low values of contact stress. The wear factor was less affected at higher values of contact stress.

Clearance and roughness were both seen to affect the lubrication mode under which ceramic-on-ceramic joints operated, as noted by extensive friction testing. Lower clearances and lower roughnesses respectively promoted fluid film lubrication. The wear remained very low in both cases and was undetectable gravimetrically. However, changes in the surface morphology throughout testing supported the fact that some wear did occur, but that this was so small as to be beyond the detection limits of the experiment. This is encouraging for the longevity of these joints *in vivo*.

The "running-in" phenomenon seen in metal-on-metal combinations was investigated using large diameter metal-on-metal resurfacing prostheses. During the course of wear testing the initially higher wear rate dropped to a much lower steady state wear. Friction testing indicated that the joints were operating closer to fluid film lubrication and the topography of the joint surfaces became more negatively skewed as the test progressed.

Acknowledgements

There are many people without whom this PhD would not have become a reality or taken its current form, and as such, I would like to use this space to offer my thanks to some of them:

Morgan Advanced Ceramics for the provision of test components and data for the ceramic clearance and roughness studies;
The EPSRC for funding part of the ceramic clearance project;
Arthur Newman, Kevan Longley, Colin Wintrip, and all the technicians in the mechanical and electrical workshops for their technical assistance and support;

Midland Medical Technologies, now Smith & Nephew (Bromsgrove) for funding the BHR study;
Dr Alistair Elfick with whom the author carried out this work jointly;

Christophoros, for taking some of my sketches and scanned images and turning them into readable and meaningful diagrams (All diagrams that have been re-worked from other sources are referenced to the original source);
Charalambos for his patience and assistance with printing and checking the thesis;
To all my family for their unending support;

My colleagues and officemates, and my co-supervisor for a portion of my studies, Dr Sarah Green;
My supervisor, Tony Unsworth for everything

Declarations

The work contained in this thesis has not been submitted elsewhere for any other degree or qualification and, unless otherwise referenced, is the work or the author.

Contents

List of Figures

List of Tables

Notation

Nomenclature

Symbol	Units	Explanation
a	m	Radius of contact in Hertzian contact theory
E	GPa	Modulus of elasticity in tension or compression
E′	GPa	Equivalent elastic modulus: $\frac{1}{E'}=\frac{1}{2}\left(\frac{1-\nu_1^2}{E_1}+\frac{1-\nu_2^2}{E_2}\right)$
f	-	Friction factor
F	N	Frictional Force
h_{min}	m	Minimum film thickness
k	-	Ellipticity parameter
k	-	Probability of inducing a wear particle (in Archard's equation)
K	mm^3/Nm	Wear Factor
L	N	Load
p		Hardness of the softer material (Archard's equation)
PV	μm or nm	Peak to valley height
R, r	m	Radius
R_a	μm or nm	Mean surface roughness value taken from a line scan across the surface
r_{max}, r_{min}	m	Maximum and minimum radius of the pin respectively
rms	-	Root mean squared value
R_{q1}, R_{q2}, R_{rms}	m	Rms value of surface roughness for surfaces 1 and 2 respectively
R_x	m	Equivalent radius of bodies in contact ($1/R_x= 1/r_1+1/r_2$)
S_{rms}, S_a	μm or nm	Roughness values obtained from Zygo based on area view not from a line scan
S_{sk}	-	Surface skewness parameter. Negative number indicates more valleys than peaks; positive number, more peaks than valleys. Taken from an area view not a line scan (see above).
T	N	Frictional Torque

Symbol	Units	Explanation
U		$u\eta/E'R_x$
u, v	m/s	Entraining velocity
V	mm^3	Wear Volume
W		$L/E'(R_x)^2$
W	N	Normal load
x	m	Sliding Distance
η	Pa s	Viscosity
θ	° (deg)	Maximum angle of incline for which no sliding occurs
λ	-	Parameter used to determine mode of lubrication
		$\lambda=h_{min}/(R_{q1}^2+R_{q2}^2)^{1/2}$
μ	-	Coefficient of Friction
ν	-	Poisson ratio
ψ		Plasticity index

Abbreviations

Abbreviation	In full
AFM	Atomic Force Microscopy
ASTM	American Society for Testing and Materials
CMC	Carboxymethyl Cellulose salt in solution
CMM	Coordinate measuring machine
EHL	Elastohydrodynamic Lubrication
HIP	Hot Isostatically Pressed
ISO	International Standard Organisation
NCOI	Non-contacting interference profilometer /profilometry
PMMA	Poly methyl methacrylate – Bone cement
PTFE	Polytetrafluoroethylene
rms	Root mean squared value
THR	Total Hip Replacement
TKR	Total Knee Replacement
UHMWPE	Ultra High Molecular Weight Polyethylene
XLPE	Cross linked poly ethylene

1 Introduction

The field of orthopaedic bioengineering is multi-disciplinary, with concepts such as friction, wear and lubrication, being considered alongside biocompatibility and application design. Materials chosen for use in orthopaedic applications within the body should obviously not cause a foreign body response, but in addition they must be sterilisible, have a relatively long shelf life, and be easily stored in hospital conditions. In joints, where two surfaces articulate against one another by their very nature, it is important that wear be minimised, both to avoid foreign body response to the wear debris and also to maintain the design of the prosthesis. Materials and designs of prostheses should be adequately tested before implantation, necessitating the development of adequate testing procedures *in vitro*.

Joint designs are tested in simulators, where the motion and loading in a normal walking cycle are mimicked. Often the joints are tested in the presence of protein-containing lubricants, and the wear is assessed either gravimetrically or dimensionally. Simulator testing is useful not just for testing new designs but also for assessing the factors which affect joint performance. For example, the motion could be altered to simulate faster walking or running, or loading could be altered to assess the differences caused by patient weight. In addition, various differences within the samples can be investigated, such as clearance or roughness.

Supplementing this, the friction within a joint can be tested, which can give insight into the lubrication mechanism under which the joint is operating. The effect of design and test parameters on the lubrication mechanism can be investigated.

The changes in the surface condition throughout testing can also give some insight into what may be occurring in the joints. In ceramic joints this can be one of the few indicators that wear is in fact occurring since the wear is often so small as to be immeasurable.

All these *in vitro* tests can help to assess the suitability of a joint for implantation, whether a new design or a modification to an existing one, and can also help shed light on the mechanisms under which joints may fail *in vivo*.

In this thesis simulator testing of both materials and manufactured components is used to investigate the effect of various factors on tribology. The effects of load, stress and area of contact on wear are investigated for metal-on-polymer contacts in a pin on plate machine. Ceramic hip components are tested in both friction and wear simulators to discern the effect of surface roughness and radial clearance on lubrication and wear. Then the change in the tribology over the course of a wear test was investigated using metal-on-metal resurfacing prostheses.

2 Literature Review

2.1 Joint anatomy

A joint in the body is where two or more bones are connected to one another with the ability to give tangential motion. Joints are the bearings of the human "machine", allowing motion often while transmitting a load. There are many types of joint in the human skeleton, each allowing varying levels of motion. In the skull for example there is virtually no movement in the joints, a type of joint known as a synarthrosis. Joints such as those on the vertebral column are known as amphiarthroses, and allow restricted motion. Diarthroses are the most common joints and allow considerable movement. These are joints such as the wrist, ankle, shoulder, knee and hip.

A diarthrodial or synovial joint, such as the knee or hip, generally involves two or more bones whose ends are covered with articular cartilage, surrounded by the synovial membrane. Since articular cartilage does not have its own blood supply[1], it is nourished through synovial fluid, the lubricant encapsulated in the joint cavity. In the normal walking cycle the maximum load can be up to 4 times the person's weight[2].

Joints are among nature's miracles: bearings with low friction and wear, capable of supporting high loads while, often simultaneously, allowing large ranges of motion, and which can work successfully for a lifetime. However, circumstances can undermine their purpose: wear, disease or trauma can reduce a joint from a useful and necessary means of mobility to a debilitating and disfiguring mass of pain and stiffness.

It is for this reason that prostheses have been developed and utilised over the years, although in general arthroplasty is only employed as a last resort: once all other options have been exhausted. Their main purpose: to replace the damaged or diseased joint, allowing the patient to enjoy freedom from pain, inflammation, stiffness and any other symptoms caused by the breakdown of their natural bearings.

Prostheses should simulate natural movement as closely as possible. The hip is a typical ball and socket joint, and perhaps its seemingly simple design is the reason hip

prostheses have enjoyed such success even in their earlier designs. The head is located at the top of the femur and articulates against the cup located in the acetabulum. The head of the femur is covered with articular cartilage, which is thicker in the centre than on the edge, except for a small pit near the centre of the head which is called the fovea capitis. The entire acetabulum is lined with articular cartilage although this is thicker on the top surface than the bottom[3,4].

2.2 Forces on joints

Stresses in the hip joint rarely exceed 6.9MPa[5], but in the knee they can be significantly higher. The load across the hip can be up to 4 times the body mass during normal activities, while it can be many more times this during sports activities and during falling or stumbling.

During the walking cycle, the forces transmitted across a joint vary. The force in the hip joint was found[2] to be high at the points during the walking cycle where the body mass is transferred from one foot to the other (around 4 times the person's body weight). During the stance phase the loads reduce to as low as 1-1.5 times the person's weight. During the swing phase, the loads are again much lower than during heel strike. The 'Paul' cycle is shown in Figure 1:

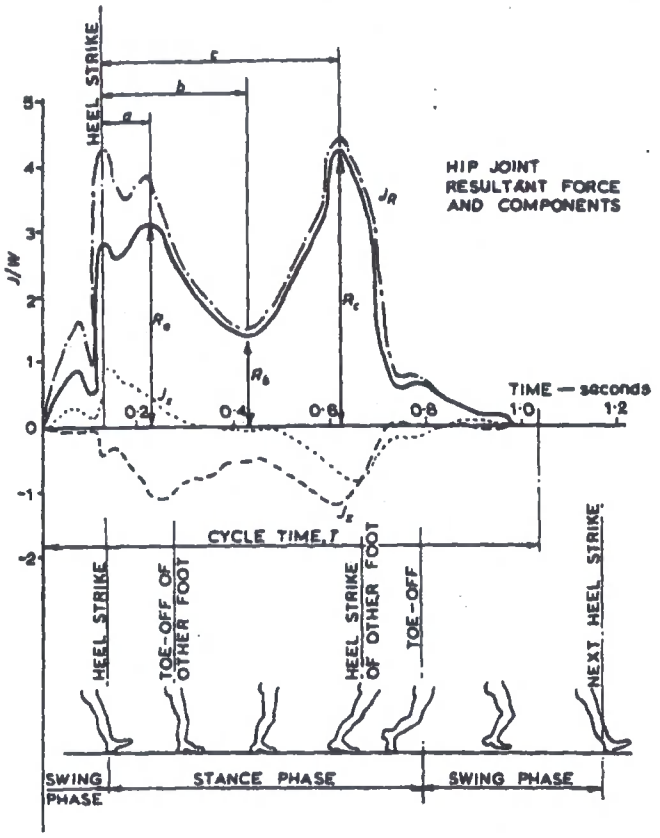

Figure 1. The Paul cycle for hip joints during the gait cycle[2]

Other work on the loading seen within a hip joint has highlighted the differences between individuals, but the work is not significantly different to the Paul cycle[6,7]. The Paul cycle remains the most widely adopted profile for hip loading.

In addition, the loading profile for running has been investigated and reported[7], and has been adopted by Bowsher *et al*[8] in simulator studies.

2.3 Arthritic and rheumatic diseases

Arthritis is a general term encompassing all inflammations of joints. Various types of arthritis include rheumatoid arthritis and osteoarthritis.

Rheumatoid arthritis initially affects the small joints usually of the hand or foot, often in a bilaterally symmetrical manner (e.g. both hands or both feet). In severe cases the disease may begin to affect larger joints like the knee, hip, elbow or shoulder. The

joints are often swollen and disfigured, a feature caused by inflammation to the synovium[9].

While rheumatoid arthritis primarily affects the synovial membranes, osteoarthritis affects the articular cartilage. It is a non-inflammatory, degenerative joint disease, involving deterioration and erosion of the articular cartilage. Osteoarthritis affects weight bearing joints such as the hip, knee and spine, and joints that are in constant use such as the fingers. It is a disease associated with aging, and traces of osteoarthritis can be found in most adults over the age of 50, although younger people can be affected. By the age of 70 around 90% of the population will have some osteoarthritis.

In cases of severe arthritis the last remaining option is often to replace the joint with an artificial one. Mobility can often be restored and pain and swelling can be reduced significantly. A successful prosthesis will enable the patient to return to a higher level of activity than before the operation, and can continue to do so for many years. The Charnley joint, for example, has been shown to have a survivorship rate of 77% at 25 years[10]

2.4 Wear debris

Just like the natural joint, however, replacement joints can eventually fail. Unlike the healthy natural joint, a prosthesis is seen not to operate under such favourable lubrication conditions, and the surfaces of the replacement joints wear.

In the case of total joint replacement surgery, the wear debris, regardless of the mechanism of its production, can be extremely significant. Wear debris from a replacement joint is thought to induce osteolysis, and late aseptic loosening, causing pain and instability, necessitating revision surgery[11,12].

The normal response of the body to a foreign particle, including micro-organisms, is for a macrophage to engulf and digest it, as part of the immune response. Following this, cytokines are released encouraging inflammation and repair at the site. Foreign particles may be introduced to the body in a number of ways, including trauma,

infection or surgery, or in the case of an implant, due to the wear of the articulating surfaces.

However, wear debris from joint prostheses is generally indigestible to macrophages. UHMWPE is a bio-inert material, making phagocytosis attempts unsuccessful. This results in large numbers of cytokines being released, and more cells migrating to the site to assist in the attack on the particles. Multi-nucleated giant cells are formed by the fusion of the macrophages in an attempt to shield the particles from the body[13]. During revision surgery large numbers of macrophages and multi-nucleated giant cells are present in the joint area, as seen in retrieved joint studies both from revision surgery and post-mortem retrieval[14]. The particle size may also play a role in determining the body's exact response[11].

It is unclear whether the macrophages affect bone remodelling directly, or whether it is the cytokines released during the above process which affect it. The presence of high concentrations of macrophages is seen in areas where bone resorption is readily visible from radiographs[14]. However, normal bone remodelling is negatively affected. This results in osteolysis, weakening of the bone in the area, which in turn can cause loosening of the prosthesis, necessitating revision surgery.

Wear debris from simulator tests under different conditions was found to be similar to the debris harvested from peri-prosthetic tissue during revision[15]. In the search for total joint replacements that will produce less wear (and hence fewer particles), analysis of simulator debris may provide an indication of the 'loosening hazard' *in vivo*.

2.5 Reasons for failure of total hip replacements

The Swedish hip arthroplasty registry (2003 report[16]) reports that in Sweden, aseptic loosening is by far the most common reason for revision surgery, this being the reason behind 73.9% of all hip arthroplasty revision operations. Primary deep infection is the next largest reason for revision operations, and constitutes only 7.9% of revisions. This has not changed dramatically in the last few years (2000 report[17]). Other reasons for

revision include dislocation, technical error, implant fracture and secondary infection. Since aseptic loosening is by far the most common reason for revision of hip arthroplasties, minimising this as much as possible would be of immense benefit to the patients.

As discussed above, it is thought that a reaction to wear debris is one of the major causes of aseptic loosening. Thus, minimising the amount of wear debris would be beneficial to the long term success of total hip replacements. Equally, the body's reaction to wear debris depends on the material[18], so alternative materials, which provoke a smaller response, may also be of benefit.

2.6 Tribology

2.6.1 Wear

Wear may be defined as the removal of material from solid surfaces as a result of mechanical action[19]. It can be useful in some applications such as surface production (by abrasive means), writing, sharpening of blades or teeth in the case of animals. Wear and transfer of material may occur on such a small scale that sensitive detection techniques must be used to discern it. In other cases wear may be so great as to compromise the structure of the materials due to the removal of the bulk of the material. As discussed below, it is favourable to reduce wear in joint applications, both to retain the structural integrity of the joint, and to minimise the production of wear debris, which can cause adverse biological effects.

The simple model of wear, according to the Lancaster equation[20] states that $V = KLx$, where V = wear volume (mm^3), L = load (N), x = sliding distance (m) and K is the wear factor, and is expressed in mm^3/Nm. This indicates that the wear volume is dependent on the load and the sliding distance for any given configuration. The nominal contact stress across the interface does not appear. This is because the real contact area increases with load, while the apparent contact area remains constant[21]. Therefore since the load and the actual contact area are related, the load itself is responsible for the actual contact stress seen at the contact points and the apparent contact area should not

affect the wear volume. There is some experimental evidence to the contrary, and this is discussed further in Section 2.8.1.

The Lancaster equation is a simplified form of the Archard wear equation[22], which included a term for the hardness. In this case, the hardness term has been incorporated into the wear factor, although this is discussed further in Section 2.7.6.

Some of the main wear mechanisms are discussed below. In any particular application in which wear occurs, it is not always possible to determine a single wear mechanism by which all wear is induced. Often one wear mechanism will dominate in a certain application, but in many applications wear is caused by a combination of wear mechanisms.

2.6.1.1 Adhesive wear[19,23]

In the case of contact between two solids, interfacial bonding occurs between the surfaces. In the case of lubricated contact there may be little or no bonding of the two surfaces at low loads. At higher loads, as the surfaces are forced closer together contact and bonding will almost certainly occur. Interfacial layers (such as a boundary lubricant or an inert oxide layer) may prevent strong bonding between molecules and atoms of the two materials. However, for the majority of solid contacts, there will be at least some weak bonds between the two surfaces due to the physical attraction of one body for another (van der Waal's forces) which are easily ruptured. In many contacts the surfaces will come into close enough contact for stronger interfacial bonding to occur. In the case of chemical bonding for example, the attractive forces between the surfaces will be very strong.

If a tangential motion is applied to the two surfaces, these forces may be ruptured by shearing. In the case of strong bonding between the two surfaces, this rupture is likely to be inside the weaker of the two materials, rather than at the original site of contact. This causes a transfer of material from one surface to the other, due to adhesion between the surfaces. Tangential motion is not necessary for adhesive wear to occur. The

surfaces may be separated in a normal direction, still causing the rupture of intermolecular forces at a weak contact point.

Adhesive wear is the most difficult to eliminate but also the most common form of wear. 'As far as is known, this form of wear is universal in all mechanical systems in which two solids slide in contact with each other. It cannot be eliminated, only reduced.' [19]

2.6.1.2 Abrasive wear

Abrasive wear occurs when a rough hard surface (or soft surface embedded with hard particles) slides over a softer surface. Hard particles plough a series of grooves into the softer material. Material removed from the grooves is released from the surface as wear debris. If the hard surface is very smooth, and care is taken to avoid hard third body inclusions in the soft material, then wear due to this mechanism can be reduced, although it should be noted that the wear rate is dependent upon the roughness of the hard bearing material, as will be discussed in Section 2.8.3.

2.6.1.3 Fatigue wear

Fatigue wear occurs during repeated sliding or rolling over a track. Repeated loading cycles on the surface induce surface or subsurface cracks, resulting in the break-up of the material surface. Large fragments are formed resulting in large pits on the surface. The effects of surface fatigue can be reduced in cases where other mechanisms operate since all others remove material from the surface, preventing it from becoming fatigued. However, in cases where there is a high stress concentration below the surface, the subsurface fatigue can take place, regardless of the presence of other wear mechanisms. In joint replacements, fatigue wear has been seen particularly in total knee arthroplasties. The polyethylene tibial tray was seen to wear profusely and destructively, due to cracks induced below the articulating surfaces[24]. Polyethylene components fitted to a metal backing plate, and where the polyethylene layer was thin, were seen to wear through to the metal backing, exposing the femoral condyles to the backing surface. The surfaces were manufactured with hot pressing techniques, which

altered the crystallinity of the polyethylene and created a layer near the surface which was markedly different from the bulk material. This interface happened to be remarkably close to the zone of maximum shear stress and cracks appeared at the interface between these two 'layers' of the material, which propagated due to the large repetitive stresses, resulting in catastrophic failure of the implants.

2.6.1.4 Corrosive wear

When sliding occurs in a corrosive atmosphere, corrosive wear can occur. Without sliding, a corrosion layer is formed on the surface, but sliding action wears the layer away and corrosive attack continues. Corrosive wear can be eliminated by ensuring that the surfaces are unreactive with the lubricant and atmosphere. In bioengineering, this wear mechanism is one which is not generally seen, since the materials implanted into the body are corrosion resistant, and thus should not be compromised by the environment in which they are implanted.

2.6.2 Friction[19,25]

In an artificial joint the friction between the articulating surfaces should be low in order to minimise the frictional torque. The frictional force occurs due to the shear stresses developed by the motion of the two surfaces under a normal load. When these surfaces are moved tangentially to one another, a force is required to initiate the motion, and another, lower, force is required to maintain it. This force, F, is related to the normal load, L, in the form $F = \mu L$, where μ is the coefficient of friction. Therefore, there are two such coefficients, the static and the dynamic. In general the dynamic coefficient of friction is lower than the static, hence the larger force required to initiate motion (static) than to sustain it (dynamic). The frictional force acts to oppose motion, or impede the initiation of motion.

Frictional forces originate from the nature of the surfaces, both mechanically and chemically. Since real surfaces are rough, only the asperities come into contact. This reduces the area of contact, and yields extremely high stresses at these points. These high stresses can induce adhesion at the asperities of the two surfaces which, when

moved over one another, can require a large force to separate them. The nature of the contact stress is such that the point of maximum shear stress is below the contacting surface (Hertzian contact theory). Hence failure often initiates below the free surface of the weaker material. Tangential motion will create additional stress, which will add to the subsurface stress generated by Hertzian contact pressure.

For flat surfaces, the coefficient of friction can also be determined by $\mu = \tan\theta$, where θ is the maximum angle of incline for which no motion occurs. The frictional force is independent of both the apparent contact area and the sliding velocity, with the notable exception of initiating motion.

The friction factor is subtly different from the coefficient of friction[26]. In many systems the surfaces articulating are not flat. For example a sphere may oscillate in a hemispherical cavity, as in a hip joint.

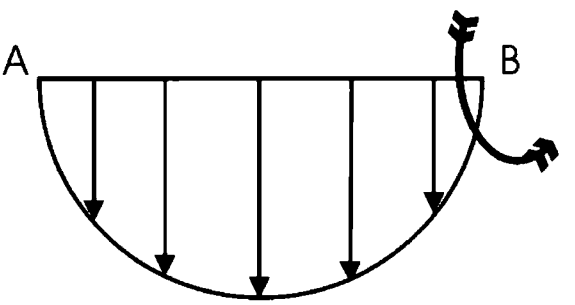

Figure 2. When a sphere oscillates in a hemispherical cavity, the moment arm at which the frictional force acts is not the same for all contact points.

In this case the frictional forces do not all act at the same distance from the axis of motion (AB) as seen in Figure 2. If the frictional torque is measured, this is related to the friction factor by the relation f=T/LR, where f= friction factor, T= frictional torque, L= normal force and R=radius of the sphere. The friction factor allows for the surface geometry, although it will be of the same order of magnitude as the coefficient of friction. For a point contact configuration, where the entire load acts at the same radius, the friction factor and the coefficient of friction are the same[26,27].

2.6.3 Lubrication[28]

A lubricant keeps two surfaces apart, reducing asperity contact between them. This will obviously have an effect on the level of friction seen, and the amount of wear which occurs, although these two are not directly related. Many factors affect the mode of lubrication for a particular application. These include the viscosity of the lubricant, the shear rate, the load and the surface roughnesses of the two surfaces.

2.6.3.1 Fluid film lubrication

When the surfaces are completely separated by the lubricant, fluid film lubrication occurs. In the case of full fluid film, there is no contact between the asperities of the two surfaces, as seen in Figure 3, and all of the load is transmitted through the lubricant layer.

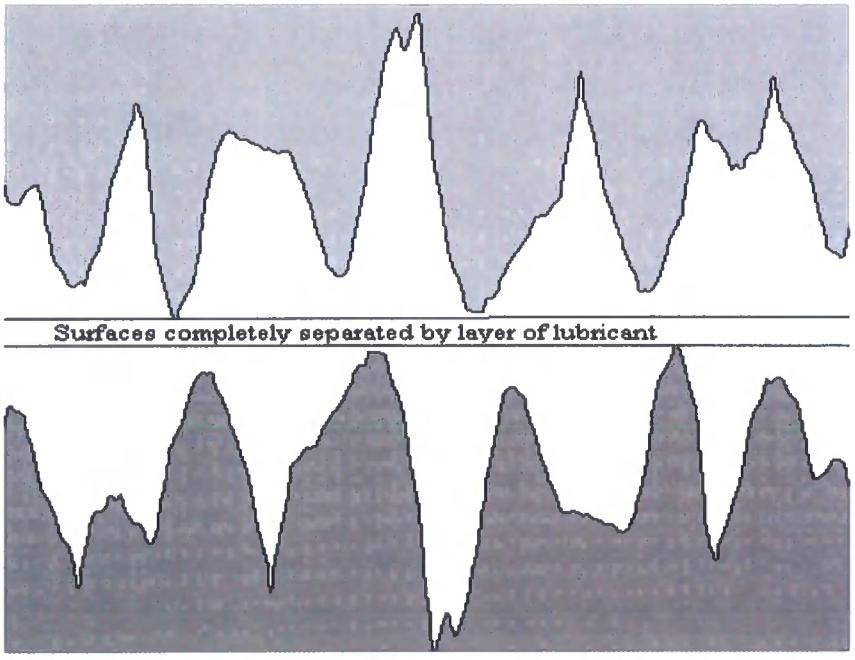

Figure 3. Surfaces completely separated by a layer of lubricant are in full fluid film lubrication.

The frictional behaviour of the joint is thus determined mainly by the shearing of the lubricant. Wear should not occur, except at start up, since there is no asperity contact. Fluid film lubrication can be hydrodynamic, elastohydrodynamic (EHL), squeeze film or externally pressurised, although the latter mechanism is not seen in the case of human joint lubrication. Squeeze film occurs when two surfaces are pushed together or pulled

apart either with or without shearing motion, such as occurs during the loading/unloading of a joint during the gait cycle.

Under hydrodynamic lubrication, two rigid surfaces move tangentially across one another. When there is a converging wedge configuration, a positive pressure is generated between the two surfaces, and load can be supported across the interface.

Under EHL at least one surface is elastic. Due to the pressure generated between the surfaces, the surface of the elastic material deforms. For a given load this increases the film thickness across the interface as compared with a similar configuration under hydrodynamic lubrication. In the body, cartilage acts as a layer of elastic material attached to the more rigid substrate of bone and it is the two cartilage surfaces which form the bearing.

The lubrication within natural healthy joints is a combination of these lubrication mechanisms[29,30]. For example during the swing phase of the normal walking cycle, a low load across the joint during the motion allows a full fluid film to develop. During the heel strike and toe off, however, the velocity will reduce to zero while the load increases rapidly. For these portions of the gait cycle, squeeze film lubrication maintains the separation of the joint surfaces over this short time. During the stance phase of the gait cycle, the loads are lower than those of heel strike, but the entraining velocity is high. Theory and experiment suggest elastohydrodynamic lubrication during this portion of the gait cycle[29-31] Thus during walking, in a normal, healthy joint, the articular surfaces are kept separated by the lubricating synovial fluid. Trauma and disease can cause this ideal lubrication situation to break down, bringing the articular surfaces together, and making the joint more susceptible to wear.

2.6.3.2 Boundary Lubrication

When two surfaces are in contact while sliding and not completely separated by a lubricant, wear will occur and the frictional behaviour will be affected. A polar active molecule in the lubricant would adsorb onto the surfaces providing a low shear strength material layer. This layer may be sheared off during the sliding but nevertheless this

protects the surfaces, leaving the material relatively undamaged. Those molecules removed are then replaced by more from within the lubricant. This protects the material itself, effectively reducing wear. The friction in this case would remain constant since it would be dominated by either shearing of the polar active molecule or dry contact of the surface asperities. It is thought that surface-active phospholipids perform this function in the human body[32].

2.6.3.3 Mixed Lubrication

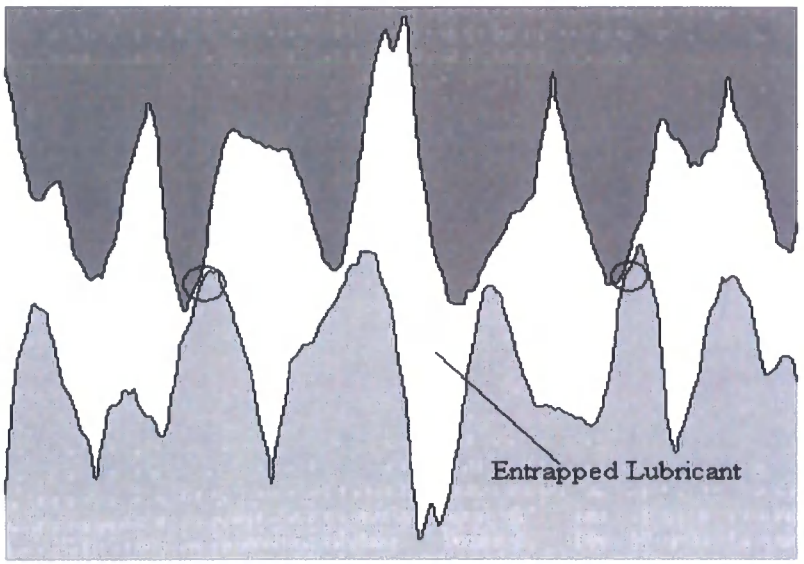

Figure 4. Surfaces in mixed lubrication condition; some of the load is carried by the entrapped lubricant while some is carried by the asperity contact of the surfaces.

In many cases a mixture of boundary and fluid film lubrication takes place in different places along the surface. This regime is called mixed lubrication. Some of the load across the bearing is carried by the lubricant, as in the case of fluid film lubrication, but also some of the load is carried by the asperity contact between the surfaces as seen in Figure 4.

The surface roughness of the two materials produces a height variation of the surfaces which is similar to the thickness of the lubricant film[33]. The minimum film thickness between two surfaces depends on their equivalent radius, the combination of materials

and the conditions under which they are configured. Hamrock and Dowson[34] predict the minimum film thickness for materials of low elastic modulus. This is given by the following relation:

$$h_{min} = R_x 7.43(1-0.85e^{-0.31k})U^{0.65}W^{-0.21}$$

Where, R_x=equivalent radius, defined by: $\frac{1}{R_x} = \frac{1}{R_1} + \frac{1}{R_2}$, k=ellipticity parameter and U, W are the dimensionless speed and load parameters respectively, defined by:

$$U = \frac{u\eta}{E'R_x} \text{ and } W = \frac{L}{E'R_x^2}$$

Where, u=entraining velocity, η=viscosity, E'=equivalent modulus of elasticity, L=normal applied load.

The ellipticity parameter, k, is equal to 1 for circular or point contact, as in the case of a spherical femoral head in a hemispherical acetabular cup. Thus for the special case of a replacement hip joint, the equation reduces to:

$$h_{min} = 2.798R_x\left(\frac{u\eta}{E'R_x}\right)^{0.65}\left(\frac{L}{E'R_x^2}\right)^{-0.21}$$

This relation has been shown to apply to hard bearing combinations provided hydrodynamic pressure is not so high as to cause increase in the lubricant viscosity[35]. For this to hold, the radius of contact should be large compared with the film thickness. It should be noted here that the minimum film thickness is the distance between the average heights of the two surfaces and not the distance between the highest asperities on each surface.

2.6.4 Synovial Fluid

Synovial fluid is basically blood plasma and hyaluronic acid (a long chain polymer). Without the polymer, the viscosity of the plasma reduces to that of water. The pH, temperature and concentration of salts in solution are also factors which affect the viscosity. It is a highly non-Newtonian liquid when healthy, its viscosity decreases with increased shear rate (shear-thinning). A Newtonian fluid is one for which the viscosity remains constant regardless of the shear rate. Similar to water and unlike mineral oils and silicone fluids, the viscosity of synovial fluid is not very sensitive to pressure changes[36].

The shear thinning nature of synovial fluid means that the viscosity will be higher when the entraining velocity is low. Synovial fluid from diseased joints is less viscous, and shows more Newtonian behaviour than synovial fluid obtained from healthy joints. A test on fluid obtained from a joint fitted with a metal on polyethylene joint replacement, showed that it had similar rheological properties to synovial fluid from rheumatoid arthritic joints[36]. Carboxymethyl cellulose (CMC) salts show non Newtonian behaviour, and the viscosity can be controlled by the concentration of the salt dissolved in water[36]. This makes CMC fluids a suitable choice of lubricant for in vitro testing of artificial joints, particularly if only physical aspects of lubrication modes are to be investigated.

However, if the physio-chemical nature of lubrication is to be examined, a lubricant containing proteins is needed. During wear testing in a simulator, most often a solution of bovine serum is used as a lubricant. This product contains high levels of proteins and has been adopted as the lubricant of choice amongst researchers. However, the concentration of the serum in the lubricant, and of the chemicals added to resist bacterial degradation are many and varied[37-43].

In some of the studies herein, friction testing has been carried out using both bovine serum and CMC separately (Chapters 5 and 6) and combined (Chapter 7). This was done in order to combine the high viscosity available from high concentrations of CMC, while also determining the effect of a lubricant containing proteins.

2.6.5 Stribeck curve [44]

A dimensionless Sommerfeld-type number, $\frac{\eta v r}{L}$, [45] (where η=viscosity of lubricant, v= entraining velocity of the two surfaces, L=radial load and r=radius of the joint) is often plotted against the friction factor[26] defined as $\frac{T}{Lr}$ (where T is the frictional torque). The resulting diagram is a type of Stribeck plot[44] (Figure 5) and is generated experimentally.

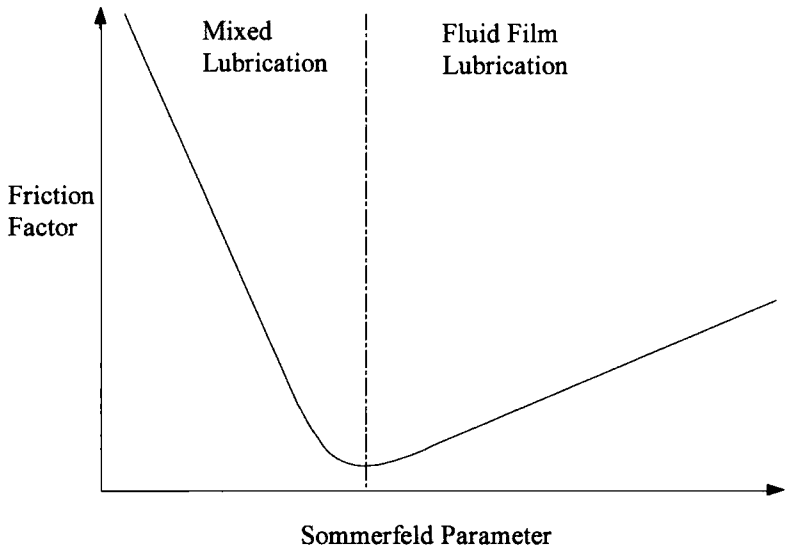

Figure 5. Ideal Stribeck plot

When the gradient of the Stribeck curve is negative, then the mixed lubrication regime is predicted. A positive gradient combined with a low coefficient of friction (below around 0.01) suggests fluid film lubrication. An indication as to which mode of lubrication occurs in any situation is the λ ratio: $\lambda = \frac{h_{min}}{(R_{q1}^2 + R_{q2}^2)^{1/2}}$ [46].

When: $\lambda > 3$ fluid film lubrication

$1 < \lambda < 3$ mixed lubrication

$\lambda < 1$ boundary lubrication

This holds true for most materials and where h_{min} is the minimum film thickness and R_{q1}, R_{q2} are the root-mean-square values of the surface roughnesses of the two

materials. Therefore the condition for fluid film lubrication is that the minimum film thickness is approximately 3 times the combined roughness of the surfaces. The dotted line in Figure 5 corresponds to λ=3.

2.6.6 Predictions of joint performance

Using these ideas, it is possible to perform theoretical calculations in an attempt to predict the performance of a particular joint. From the λ condition above, we see that the lubrication mode is affected by the minimum film thickness and the roughness of the surfaces. For a given surface roughness a thicker film would result in a more favourable lubrication regime. Equally for a given film thickness, a smoother pair of surfaces should result in more favourable lubrication. The film thickness depends on both test parameters, such as load, lubricant viscosity and entraining velocity, and also on the materials and joint design. The equivalent elastic modulus, E', depends upon the materials from which the joint components are manufactured. R_x depends on both the actual radius of each bearing surface but also on the radial clearance: the difference in the two articulating radii. Some of these ideas are discussed in more depth in later sections of this chapter.

2.6.7 Contact mechanics

Considering the simplest case of Hertzian contact theory for continuous and non conforming bodies, we have solids of revolution under an axisymmetric normal load. The initial contact will be circular, and will increase in size with an increase in the normal load. The theory assumes that the area of contact is small with respect to the relative radius of curvature, and to the macroscopic dimensions of the bodies in contact. This allows each body to be considered as an elastic half space loaded over a small area of its surface, the area of contact, when considering the stress induced in the contact region. The stress over this area is high, and the assumption that the area of contact is small ensures that these high stresses are not affected by and do not affect, the boundaries or edges of the body itself. The contact is also assumed to be frictionless allowing only a normal pressure to be transmitted over the region. In addition the

deformation of the bodies must be elastic, indicating that the strains induced should be small[47].

Hertzian contact theory approximates the contact mechanics of spherical elastic contacts. A case of bodies in contact can be reduced to a sphere on a plane. Assuming an axisymmetric load, the contact area between the two surfaces will be circular and dependent upon the load and the radius of the sphere, as well as the elastic moduli of the materials. A slightly simplified version of Timoshenko and Goodier's[48] equation for the radius of the area of circular contact is given by:

$$a = \left(\frac{3}{2} \frac{WR_x}{E'} \right)^{\frac{1}{3}}$$

Where a= the radius of contact, W = Normal Load, R_x = equivalent radius of contact, E = equivalent modulus of elasticity defined by $\frac{1}{E'} = \frac{1}{2}\left(\frac{1-\nu_1^2}{E_1} + \frac{1-\nu_2^2}{E_2} \right)$. (In some texts [47] this is given as, $E'^{-1} = (1-\nu_1^2)/E_1 + (1-\nu_2^2)/E_2$ resulting in the radius of contact having a 3/4 coefficient instead of 3/2.) Thus the area of contact is:

$$\text{area} = \pi a^2 = 1.31\pi \left(\frac{WR_x}{E'} \right)^{\frac{2}{3}}$$

The contact pressure is not uniform throughout the area of contact. There is a maximum pressure at the origin of the circular contact, which is 3/2 times the average pressure (Load divided by area of contact). Some deformation of either or both of the surfaces may occur with a very large normal load.

Greenwood and Williamson developed a theory of surface contact for nominally flat surfaces relating the real contact area and load to the separation of the surfaces. The separation of the two surfaces is dependent on the nominal (apparent) contact pressure, while the real area of contact is only determined by the load[21]. The area of contact and

the load depend on the separation in a similar way, giving an almost linear relation between the two, allowing prediction of one from the other.

The contact between solid surfaces is determined by the elastic modulus and the hardness of the materials, as well as by their surface topography: the density, the height distribution and the mean radius of the asperities. These quantities define the contact mechanics of nominally flat solid contacts for the Greenwood-Williamson theory of elastic contact. The plasticity index suggested in the theory provides an indication of the type of contact: elastic if the plasticity index is low (<0.6), plastic if it is high (>1.0). The plasticity index combines both material and topographic properties and as such the type of contact. The plasticity index, ψ, is defined as follows:

$$\psi = \left(\frac{E'}{H}\right)\sqrt{\frac{\sigma}{\beta}}$$

Where E' is the equivalent elastic modulus, H is the hardness, σ is the standard deviation of the height distribution of the asperities, and β is the radius of the asperity summits (assumed to be the same for all asperities). While this can in theory have any value from 0 to ∞ in practice it was found to that most surfaces have a value of 0.1 to over 100. Further to this, the range of plasticity index for which the plastic or elastic contact is uncertain is 0.6-1.0.

2.7 Biomaterials

2.7.1 UHMWPE

Polyethylene is a polymer of ethylene molecules (CH2=CH2). In the case where the units join up in a line, high-density polyethylene is formed. Alternatively if a branched polymer chain is formed then low-density polyethylene is formed, due to packing of the molecules. In UHMWPE, the molecular chains are linear, but extremely long. This causes the polymer chains to get tangled up and thus not be as tightly packed. In the molten state it has very high viscosity and thus cannot be moulded. It is pressed into bars, rods or sheets and machined into the necessary shapes. For use as a prosthetic

material its tensile strength should be no less than 21 N/mm^2 and its ultimate tensile strength should be no less than 34 N/mm^2. [49,50]

A study by Barbour *et al*[51] compared a standard compression moulded UHMWPE (GUR1120) and a standard ram extruded UHMWPE (GUR4150HP) using uniaxial reciprocation pin on plate tests. The ram-extruded sample gave lower average wear rates in each test performed. However, due to the small number of data points, this was not found to be a statistically significant difference. It does, however, underline the importance of using a single batch of material in comparative tests.

2.7.2 Stainless steel

The stainless steel used in bioengineering should, like all biomaterials, conform to international standards such as the ASTM or the ISO. General specifications for stainless steel include that there should be no inclusions such as sulphide stringers, which can arise from unclean steel making practices. It should be single-phase austenite (face centred cubic) with no free body centred cubic phases. The grain size should be fine, around 100 μm or less, and fairly uniformly distributed. Approximately 0.03% or less carbon should be present to reduce the possibility of *in vivo* corrosion. There should be 60-65% Iron, 17-19% Chromium, 12-14% Nickel and minor amounts of nitrogen, manganese, molybdenum, phosphorous, silicon and sulphur. The presence of the chromium promotes the production of a corrosion resistant and adherent Cr_2O_3 oxide layer[52].

2.7.3 Ceramics

The two main ceramics used in joint replacements are alumina and zirconia. They have been used both articulating against themselves and articulating against other materials such as UHMWPE. Alumina-on-alumina articulations have the advantage of producing significantly smaller volumes of wear debris than polyethylene[53]. This is the driving factor in the development of ceramic bearing couples since, it is thought that wear debris could be a contributing factor to osteolysis and prosthesis loosening[11,12,14].

Alumina often contains small quantities of CaO or MgO to prevent grain growth, resulting in higher material strength and in a fully dense material. Zirconia has a higher strength and as such has become desirable as an alternative. An all-ceramic bearing couple, however, is usually alumina, due to the higher wear of zirconia against itself[53,54].

It is possible to produce a ceramic with a higher fracture toughness, by combining zirconia and alumina in varying ratios[55,56]. In addition, the wear resistance of this type of material is optimum at a particular proportion of ZrO_2, the exact level of which depends on the load[56].

Ceramics are ionic or covalent in structure, often leading to a hydrophilic surface, due to interaction with the polar nature of water based fluids. This wettability is thought to aid lubrication of the articulation by assisting the entrainment of lubricant into the joint.

2.7.4 CoCrMo Alloy

Cobalt-Chromium-Molybdenum alloys are often used as bearing surfaces in orthopaedic applications. The exact material composition can vary, as can the manufacturing procedure, both of which affect the final properties of the material. Typically the alloy will also contain smaller quantities of other materials; the percentage of carbon in particular can affect the hardness and wear properties greatly. High carbon materials typically contain 0.2% carbon or more, while low carbon materials contain below 0.07% carbon[57]. High and low carbon CoCrMo alloys can be paired in various configurations (high-high, low-low, high-low) and different wear rates are seen in each case. High carbon combinations have been shown to produce lower wear than low carbon combinations[58] and mixed carbon content combinations[59] in pin on plate testing, both for uni-and multi-directional motion. Other constituents of the alloy can be Fe, Mn, Ni, Ti and Si.

In addition to this, the material properties differ according to the manufacturing procedure. Typically hot-isostatically pressed (HIP) material has a higher Young's modulus and tensile strength than the as cast material[52]. HIPed then heat treated large

diameter metal-on-metal bearings showed no significant difference in wear characteristics compared with as cast material in simulator tests[60]. Other tests have shown better wear resistance from the as cast material, although in this case the carbon fraction was found to be highest in the as cast over all other heat treated materials, whose carbon contents and wear rates were statistically indistinguishable[61].

2.7.5 Other materials

2.7.5.1 XLPE

There is a trend towards cross linking polyethylene in order to produce a lower wearing material for joint prostheses. Some cross linking often exists in polyethylene especially when the sample has been sterilised by irradiation (20-30 kGy). In order to induce higher degrees of cross linking, much higher doses of radiation (up to 1000 kGy[62]) are used. This induces bonds between the molecules which makes the removal of the molecules by wear less likely. Cross linking can also be achieved chemically, such as by mixing UHMWPE powder with peroxide and then compression moulding directly into the required shape[62].

Cross linking is the induction of intermolecular carbon – carbon covalent bonds. This reduces the amount of chain slippage that can occur during sliding, and prevents the reorientation of the chains into the direction of sliding. This significantly reduces the wear rate of the material, for both methods of cross linking, when worn against CoCr alloy heads in a hip simulator[62]. Similarly, the Durham metacarpo-phalangeal prosthesis (silane cross linked polyethylene for both components) shows low wear rates in simulator tests[63].

XLPE was seen to perform better than conventional polyethylene under normal conditions in knee simulator tests. However, when both materials were then worn against a rough counterface the wear was seen to greatly exceed the wear of conventional polyethylene[64]. The roughness is seen to have a greater effect on the wear of XLPE under simulated conditions of increased patient activity in a hip simulator test[8]. The greater hardness of XLPE is thought to lower its abrasion resistance as compared with conventional polyethylene.

2.7.5.2 PTFE

Polytetrafluroethyne was one of the first plastic materials to be used in a replacement joint. Acetabular cups were made from this material articulating against metal. It was chosen initially for its low frictional properties[65]. However, PTFE was soon found unsuitable due to its incredibly high wear rates. It was subsequently abandoned for this application.

2.7.5.3 Bioactive materials

Hydroxyapatite is a material which promotes bone growth, and is thus classed as a bioactive material. The stems of some prostheses are coated with a layer of such materials in order to promote bone growth into or onto the prosthesis and hence provide better fixation[66].

Another method of promoting bone growth into the prosthesis is to texture its outer surface. Tiny beads of metal are often sintered or moulded onto the stem. This promotes the growth of bone into the beads providing a mechanical bond between the bone and the prosthesis. Bone growth has even been seen to occur into porous alumina ceramic[67]. In modern devices a combination of beads and hydroxyapatite is often used, and while not a bioactive material, bone cement is also still widely used for fixation of the prosthesis.

2.7.6 Hard bearing combinations

Concerns over the effects of polyethylene wear debris, have promoted research into hard bearing couples such as ceramic-on-ceramic or metal-on-metal. In general these combinations give lower wear rates, hence a smaller volume of wear particles. This is in accordance with the wear equation. The full version of the wear equation[22] includes a term for the hardness as follows:

$$V = \frac{kLx}{3p},$$

where V = wear volume, L = load, x = sliding distance, as before; k is the probability of inducing a wear particle, and p is the hardness of the softer material. Therefore it is expected that increasing the hardness of the softer material should decrease the wear volume.

As such there is hope that hard bearing combinations will be particularly favourable for younger patients who may be more active, but for whom longevity of the prosthesis is particularly important, especially considering that subsequent revision procedures are associated with a progressively higher failure risk[68]. Currently, the 12-year survivorship for patients younger than 50 is only 73.9% while in the over 75's this is much higher at 95.5%[16] despite the higher number of implants in older patients. This includes all types of joints both hard-bearing and the conventional metal-on-polymer, but nonetheless underlines the need for more options for younger patients, both in terms of joint longevity but also bone stock preservation.

Tests have been carried out both in the laboratory and on retrieved components[69], and the results for hard bearing combinations are encouraging. It can be difficult, however, to assess the wear accurately on explanted joints as often information on the surface condition and geometry before implantation is not available.

Hard bearing joints are well known to show a wearing in period during simulator wear tests[70-72], although the final steady-state wear can be more difficult to discern in ceramic-on-ceramic joints even over 14 million cycles[71]. Friction tests have revealed lower friction factors post wear than initially in metal-on-metal joints[70] pointing towards more favourable lubrication after testing. All of this suggests that the articulating surfaces run-in during early stages of the wear test, moving towards a condition of better lubrication and hence lower wear as the tests progress.

2.7.6.1 Ceramic-on-ceramic

Alumina-on-alumina joints were first used in the early 1970's by Boutin[73-75] due to the favourable wear and friction characteristics combined with good biocompatibility. Alumina manufacture has improved over the years, notably since the late seventies when standards for production were introduced. It has been noted that older generation alumina was seen to wear more than more recently produced specimens[76].

It is mostly agreed that the results for ceramic-on-ceramic joints show encouragingly low wear rates, both in simulator work and by follow up analysis, where survivorships such as 86.2% at 11 years[74], 93.7% after 9 years[77] are quoted in various studies (Table 1). While these results are not completely consistent, this is to be expected from different populations, sample sizes and surgeons. Hamadouche *et al*[78] report immeasurable wear and limited osteolysis at a minimum of 18.5 years postoperatively.

Type of joint	Time *in vivo*	Survivorship	Period of implantation	Study
Alumina-on-alumina joints: Total joint Cemented cups Uncemented cups	 9 years 20 years 20 years	 93% 61.2% 85.6%	Various: 1977-2002	[76]
Alumina-on-alumina joints	5 years 10 years 11 years	97.5% 89.4% 86.2%	Various: 1977-1990	[74]
Alumina-on-alumina joints	9 years	93.7%	1991-1992	[77]
Alumina-on-alumina joints	11.3 years	88.6%	1976-1979	[73]
Alumina-on-alumina joints (autophor) heads and cups	4 years	65%	1982-1985	[79]
Alumina-on-alumina joints Ceraver - Osteal	10 years	98%	1977-1986	[80]
Charnley metal-on-polymer	25 years	77.5%	1969-1971	[10]
All joint types implanted in patients under 50 years	12 year	73.9%	1992-2003	[16]
All joint types implanted in patients over 75 years	12 years	95.5%	1992-2003	[16]
Wagner resurfacing hip arthroplasty (CoCrMo-on-polyethylene)	1 year 5 years 8 years	98% 70% 40%	1978-1980	[81]
Birmingham Hip (metal-on-metal) resurfacing arthroplasty	5 years	98%	1997-1998	[82]
Conserve plus (metal-on-metal) surface arthroplasty	4 years	94.4%	1996-2000	[83]

Table 1. Survivorship rates of various hip replacements from the literature.

Sedel *et al*[76] report that a study of a well fixed device after the natural death of a patient (12 years implantation) showed that while there was no direct bone-alumina contact, fibrous tissue and bone did enter into the grooves on the alumina surface, resulting in good fixation.

However, some negative reviews of all-ceramic prostheses are noted: Mahoney and Dimon[79] show a 35% failure rate (combined femoral and acetabular) over 4 years using the autophor (uncemented) prosthesis. This high rate of failure is attributed to osteolysis and loosening thought to be caused by trauma at the bone-prosthesis interface. They do note however, that the wear of these components was fairly low, as seen by other workers, and that the wear characteristics of the joint did not contribute to the unsatisfactory results they observed.

However, in the case of cemented all-alumina prostheses, it has been found that most of the debris is generated by mechanical factors that cause cement fragmentation[84]. Uncemented cups have shown better survivorship than cemented at 20 years[76]. Also damage to the joint during the implantation procedure (at the time of reduction) has been seen, and this was immediately revised[85].

Simulator tests have echoed the low wear rates seen in retrieved joints. Scholes *et al*[86] have reported wear of less than 0.1mg over 5 million cycles, equivalent to approximately 5 years in vivo. Saikko and Pfaff[87] have also seen low wear rates in simulator tests of various lengths up to 5 million cycles, and using a variety of nominal diameter joints.

Factors such as metal transfer to the components are thought to confound these very low gravimetric wear results partially. To investigate this, Brown *et al*[88] loaded various joints on their trunnions without any articulating motion and followed a standard cleaning protocol, also using a control head. They found large losses on some of the trunnions, which were not mirrored by any measurable transfer on the ceramic heads. They suggest that there is no need to correct for metal transfer or that long-term conditioning and harsh cleaning methods are not necessary. The conditioning events

were however, rather short, a maximum of 13,800 cycles, with cleaning taking place after between 300-600 cycles.

2.7.6.1.1 Microseparation

Researchers at the University of Leeds in particular have been investigating ceramic-on-ceramic wear under a condition they have named microseparation[89,90]. This involves allowing the joint to separate completely during the gait cycle, causing rim contact when the joint is loaded again. This has been in an attempt to simulate the "stripe wear" which has been seen on some explanted ceramic components[91-93] and to induce a larger amount of wear in the ceramic components.

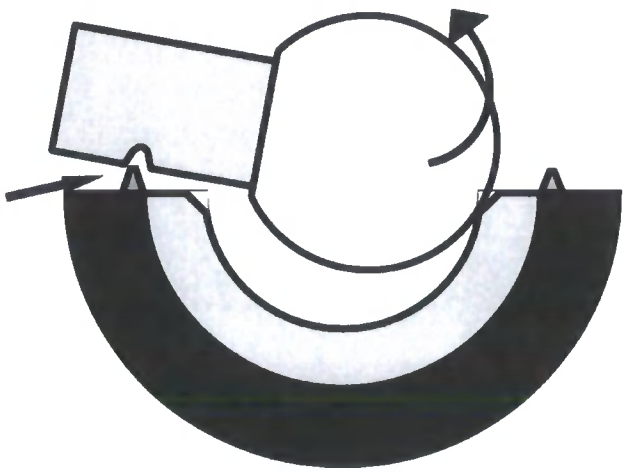

Figure 6. Eickmann *et al*'s explanation for the appearance of stripe wear on retrieved ceramic-on-ceramic hip joints[94]

Dorlot *et al*[91,95] have noted gross wear of the ceramic cup in explanted alumina joints, which they found to be caused by rim contact of the ceramic cup onto the stem, indicated by a corresponding worn area on the stem and also by metal transfer onto the cup rim. Impingement of the cup rim on the stem was seen in other case studies[94,96]. In each case sub optimal alignment of the components is suggested as a reason, in some cases due to migration of the component. Eickmann *et al* further state that the impingement of the outer metal lining of the cup on the stem created a fulcrum for

subluxation and dislocation, which was the cause of stripe wear seen over the wear area on the head[94].

Additionally a long, thin peripheral wear zone is seen which showed high wear[94,96]. This wear zone followed the outside edge of the main wear area on one side of the head. The stripe of wear seen by Dorlot *et al*[91] however, was not along the periphery of the main wear area, but across the centre of the main wear area. Neither study suggests a reason for the elliptical wear shape seen.

Dennis *et al* observed separation of the femoral head from the acetabulum in unconstrained metal-on-polymer THA[97]. During hip abduction all unconstrained THA patients in the study presented separation of the femoral head from the acetabulum of at least 1mm and up to 5.2mm (average 3.3mm). In the same study, patients with a natural hip showed no separation, and those with a constrained THA showed a much smaller separation (average 0.4mm) which was smaller than the detection error in the experiment (0.75mm). In some cases during this separation, the head was observed to pivot on the lip of the acetabular liner.

2.7.6.2 Metal-on-metal prostheses – conventional and resurfacing

Early, small diameter, metal-on-metal hip joints were prone to premature failure[98], although some specimens are known to have been in place successfully for up to 20 years or more[99-101]. This suggests there being a favourable tribological condition in some cases, although not in the majority of cases.

Although early metal-on-polymer resurfacing procedures showed encouraging results in the medium term, the longer term results were poor[81]. New generation, larger diameter metal-on-metal hip joints have been more successful in the mid term[83,102], although long term results are not as yet available, since the joints have only been in use for around 10 years.

Theory points to the diameter being a large contributing factor to this, as discussed in Section 2.8.2 and these joints have shown fluid film lubrication in laboratory tests[103]

(See Chapter 7). However, van Kampen *et al*'s work[104] showed that the joints were not initially fluid film lubricated.

Wimmer *et al*[105] have noted a deposit on McKee-Farrar explanted joints which is organic in nature, and hence most likely a layer of adhered denatured proteins. However, McKellop *et al* report a tenacious deposit on explanted joints which is shown to contain calcium phosphate[106].

Aseptic loosening is seen to be a lower risk in metal-on-metal implants than metal-on-polymer, although not significantly so[107].

2.7.6.3 Comparison of all-metal and all-ceramic

Ceramic-on-ceramic joints show lower wear rates than metal-on-metal articulations[71]. Skin patch tests for alumina and nickel sulphate in human subjects also showed a smaller immuno-allergic reaction to alumina[108]. Furthermore it has been found that in mice there is a smaller biological reaction to ceramic particles than to polyethylene or titanium alloy particles and fewer osteolytic lesions are noted[18]. Similar results have been seen in other studies[84,109]

Hard bearing combinations all show a wearing-in phase of higher wear in simulator studies, which is easily discernible[70,71,110-112]. It has also been noted that the average linear wear rate (μm/year) for retrieved metal-on-metal joints is lower for joints with a longer survivorship, indicating that this wearing-in phase may also occur *in vivo*[110]. Steady state wear in ceramic-on-ceramic joints can be confounded by large fluctuations in mass of the components around very low wear rates[71,113,114]. Rieker *et al* found that although all-ceramic joints show a lower wear rate than all-metal, the difference was not statistically significant, owing to the fluctuations shown by both these types of joints[112]. However, changes in the surface conditions are much easier to determine and indicate that, although sometimes undetectable gravimetrically, wear does occur on all-ceramic joints[86,113,115].

Scholes *et al*[39] have shown that all-alumina pairs produce lower friction factors than all-metal (CoCrMo) or metal-on-UHMWPE joints of the same diameter (28mm), for CMC fluids. In addition, fluid film lubrication was achieved with the all-alumina joints, while the other two combinations operated in a mixed lubrication regime. When tested with bovine serum lubricant, Scholes *et al*[116] found that the friction factor increased significantly for the all-ceramic joints, but decreased significantly for metallic ones. This was attributed to adsorption of proteins from the bovine serum onto the articulating surfaces in both cases. In the all-ceramic joints this adsorbed layer may have penetrated the fluid film; in the all-metal joints the protein shearing protects the surface from metal to metal contact, reducing the friction. The friction factor of all-metal total hip replacements was found to be significantly lower after wear testing, which is also the case for metal on UHMWPE.

2.8 Factors affecting the tribology of artificial hip prostheses

2.8.1 Effect of stress and load on wear rate of UHMWPE on Stainless Steel

Although the Lancaster equation suggests that the wear volume is dependent only on the particular configuration of materials, the load and the distance slid, the situation may not be quite so simple. The literature is divided as to the exact effect of load and stress on the wear of UHMWPE. This is made more difficult by the different operating conditions in each study, including differences in apparatus and lubricants.

Barbour *et al*[117] indicated that the wear factor decreases with increasing nominal contact stress. In the study, two pin diameters were used (3.4mm and 5.3mm) with various loads (80 – 240N) in order to vary the contact stress in the range of 3.4 to 28.3MPa. The data from the two pins overlapped and as such were treated as one data set. The authors suggested that this indicates an increase in wear rate with decreasing load, which initially appears to contradict previous work[5,118]. However, these studies presented the wear factors as mass loss per unit sliding distance and penetration depth per unit sliding distance respectively, neither taking into account the load under which

the surfaces articulated. Both studies showed an exponential increase in wear with increasing stress.

Sathasivam *et al*[119,120] used five different diameters of pin (8, 10, 12, 17 and 23 mm), giving stresses in the range of 3-20MPa. The study found that the average mass loss on the pins at first increased, then decreased with increasing diameter (all pins were under the same load thus increasing diameter corresponds with decreasing nominal stress). The load was 1200N, which is significantly higher than the loads involved in Barbour *et al*'s study, but more appropriate to the knee applications. Since in the two studies the contact stress range overlaps greatly, this indicates that other factors may determine the behaviour of wear rate.

In Sathasivam *et al*'s study, the tibial tray (counterface) was reciprocated in ± 5mm wear track and the pins were rotated by ± 5° about their own axis. In Barbour *et al*'s study the pins were reciprocated only, and the pin – plate pairings were changed each time the apparatus was dismantled for measurement. Sathasivam used 30% bovine serum while Barbour used 89% bovine serum (3ml of 1% sodium azide solution to each 25ml of serum). Barbour's pins were microtomed to remove the machining marks.

In an earlier study Rostoker and Galante[5], suggested that the amount of wear shows a small contact stress dependence below 6.9MPa, but an increased dependence at higher stresses. Fisher and Dowson[49] suggest that the higher wear rates in Rostoker and Galante's study occur when close to the limiting compressive stress of the UHMWPE. Regression analysis had suggested an exponential relation between wear rate and contact pressure, where wear rate was found in terms of the depth of wear per unit sliding distance. The test was carried out at 37° lubricated with water. Rose *et al*[118] find an exponential increase of mass loss per unit sliding distance with increasing contact stress.

A recent study by Wang *et al*[121] showed the effect of maximum contact stress on the wear of UHMWPE using artificial hips, by altering the radial clearance. The study indicates that over a maximum stress range of 5 - 25MPa the wear factor decreases with

increasing maximum stress. The study also indicated that the coefficient of friction similarly decreases with increasing maximum stress. These findings agree with the Barbour *et al* study

Landry *et al* studied the effect of contact conditions on wear debris[122]. This indicated that at a low stress (6.9MPa), the mean particle size was smaller than for a higher stress (13.8MPa). The average particle sizes were given as 0.48 ±0.1 μm and 0.91 ± 0.3μm respectively. The authors suggest that this indicates a higher wear factor for higher stresses, although no measurements of wear rate were made in this study.

Mazzucco and Spector[123] found that the wear factor for UHMWPE against CoCrMo alloy pin on flat tests was neither dependent upon the load nor upon the contact stress, but rather it was dependent on the apparent contact area. They tested 2 different designs of pin at 2 loads resulting in contact stresses of 3.1, 3.5 and 7.0MPa.

In an attempt to solve this contradiction, Vassiliou and Unsworth carried out a similar study and showed that neither the contact area, nor the load affected the wear factor. The nominal contract stress however, caused an exponential decrease in the wear factor, indicating a large dependence at low stresses, and much lower dependence at higher stresses[43] (See Chapter 4).

2.8.2 The effect of radial clearance on tribology

Returning to the equation of film thickness, h_{min}, we can see that the overall dependence of h_{min} on R_x is 0.76. Since this is a positive exponent h_{min} will increase as R_x increases, if all other testing and material conditions remain constant. Looking again at the equation for R_x: $R_x=R_1R_2/(R_2-R_1)$ reveals that R_x is the product of the radii divided by the radial clearance. Hence larger radii and smaller radial clearances should induce a thicker film, while a combination of small radii and a larger clearance should induce a thinner film, assuming all other parameters affecting the film thickness remain the same. There is of course a practical limit to the radial clearance, since if this is too small then the joint will not function. This is partly due to manufacturing tolerances, but also due

to deformation of the cup during loading, which can cause a decrease in the radial clearance.

Schmidt and Farrar[124] found that the diameter had no significant effect on wear for 3 sizes of metal-on-metal joints (22, 28, 35mm), but the effect of large variations in the radial clearance (0.030-0.139mm) was not taken into account. Medley *et al*[125] also indicated no effect of diameter on the wear of metal-on-metal hip joints, but they do note that the lowest wear was seen on the joint with the combination of the largest diameter and smallest clearance.

There have been some investigations into this experimentally, for various material combinations. Schott and Schroeder[126] showed higher wear for larger radial clearances in 28mm metal-on-metal wear tests. Scholes *et al*[70] also showed higher wear on 40 micron radial clearance than on 22 micron in a metal-on-metal wear test. They found similar initial friction factors for the two clearances but post wear the 40 micron joints showed slightly lower friction than the 22 micron. Direct measurements of surface separation in 36mm diameter metal-on-metal joints in a simulator have shown a larger degree of separation for smaller clearances[127].

In ceramic-on-ceramic joints the steady state wear rates are often more difficult to discern due to large fluctuations in the mass of the components, as discussed earlier in Section 2.7.6.3. Clarke *et al*[71] tested 3 radial clearances (5, 25 and 80 microns) for 14.4 million cycles and the wear trends for all three clearances were indistinguishable.

In addition, for 28mm joints there is no discernible effect of radial clearance on friction factor, and the friction factors and lubrication regimes remained mostly unchanged throughout wear testing[128,129].

2.8.3 The effect of roughness on tribology

The roughness of the components in a wear couple will have an effect on its tribological performance. This is evident from the earlier discussions regarding film thickness and fluid film lubrication (Section 2.6.5). If the roughness is higher, then the asperities of the material are more likely to be able to break through the lubricant film and come into

contact with the asperities of the counterface. As a rule of thumb, the quantity λ, the ratio of film thickness to combined roughness, should be greater than 3 for fluid film lubrication. Hence, the combined roughness of the two articulating materials should be 3 times smaller than the calculated film thickness; remembering that the film thickness is not the minimum separation of the surface asperities, but the separation of the average surface heights.

This is well investigated experimentally for metal-on-polymer combinations. An increase in wear factor with counterface roughness has been seen in pin-on-disk results both with conventional and cross-linked UHMWPE[130]. Explanted CoCrMo heads with a much higher roughness than new heads (although still within the British standard) showed much higher wear rates when worn against UHMWPE cups in a hip simulator than their new counterparts[131]. Bowsher and Shelton have shown that increased roughness on the metallic component increased the wear of cross linked polyethylene significantly under simulated walking and even more so under simulated jogging indicating that increased patient activity could seriously compromise the longevity of a metal-on-polymer joint[8].

An increased roughness of the metallic component is known to cause an increase in the minimum polyethylene particle size produced from a hip joint in simulator studies[15]. In the same study it is noted that the morphology of the debris is somewhat different for rougher heads which showed more "shred-like" particles, perhaps indicating an increase in abrasive wear.

It is generally seen that the wear rate of UHMWPE is smaller for ceramic counterfaces than metallic ones, a fact often attributed to their superior surface finish and hardness[131]. The effect for ceramic-on-ceramic combinations is less well investigated.

Aims and Objectives

Aims

The literature review shows that friction lubrication and wear of artificial joints depends on the contact stress, the joint clearances the surface topography and the length of time in the joint has been in service. The aims of this thesis therefore are to investigate these in a consistent and coherent range of experiments.

- To resolve the contradictions regarding the effect of contact stress on wear factor, the first aim is to investigate this in the context of UHMWPE on stainless steel.
- While clearance is known to affect lubrication in a well defined way, there is little published evidence of this for ceramic-on-ceramic total hip replacements.
- Increased surface roughness is detrimental to the production of fluid film. Ceramic components are generally polished to a very low roughness, with only very small variations. There are no studies investigating the effects of large variations in ceramic surface roughness.
- A higher wear rate during the early stages of the life of a hard-on-hard material combination is well documented, particularly for hip joints. Thus the relationship between running-in and changes in lubrication during the lifetime of the joint would help elucidate the mechanisms which are called into play.

The aim of this thesis is to investigate a number of factors known to affect tribology in an attempt to solve some of the contradictions in the literature or to more fully investigate aspects which have hitherto not been published.

Objectives

- A pin on plate test has been used to determine the effects of load, contact stress and contact area on the wear factor, using UHMWPE pins against stainless steel plates.
- Then the effects of clearance and roughness have been separately investigated using ceramic-on-ceramic hip joints. Friction testing has been used to investigate the lubrication on a large number of samples and a wear test has been carried out on a smaller number.
- Then the effect of running in on tribology has been examined using a metal-on-metal resurfacing device. Friction testing has been monitored on one joint throughout a wear test in order to asses the changes in lubrication induced by the running in.

3 Apparatus

3.1 Pin on plate machines

The pin on plate machine was manufactured in house, designed by A. Unsworth and described in detail in [37]. It was a four-station machine, allowing four pins to be tested against four plates with independently generated reciprocating and rotational motion. Figure 7 shows the set up of the rig.

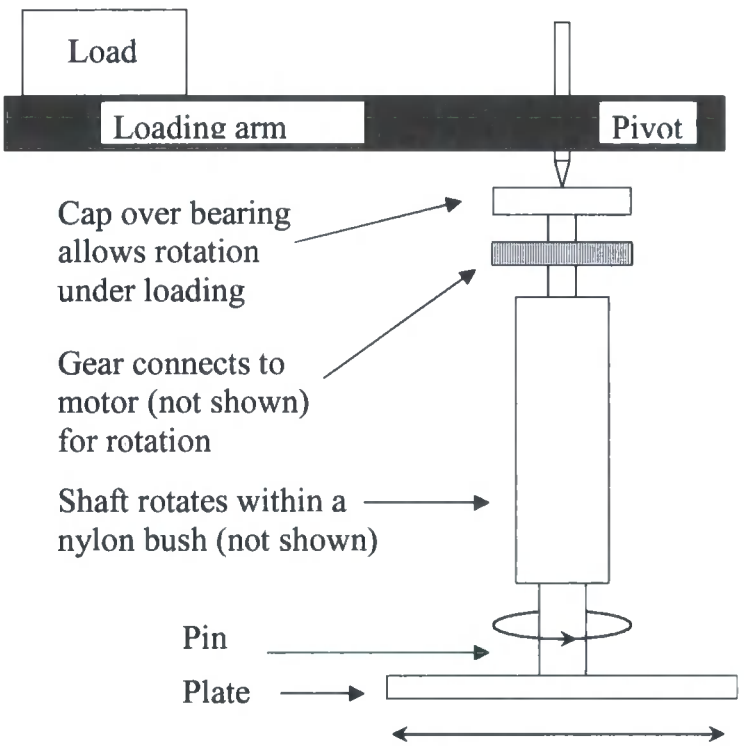

Figure 7. Schematic diagram of pin-on-plate set-up.

The plates were positioned in a stainless steel bath with a plastic plate holder to hold them in position. The entire bath with the plates was reciprocated by an external motor/crank arrangement. The pins were held in pin holders, each of which was attached to a motor, rotating the pins around their central vertical axis. In this manner reciprocation and rotation of the pins was achieved. The pins were each independently statically loaded by placing masses at various moment arms along four loading arms. Bovine serum diluted to 30% was placed in the stainless steel bath to lubricate the pin–

plate interface. The rig was covered by a Perspex box to avoid contamination of the specimens by external debris, and for safety from the moving parts.
The stroke length was set to 25mm, producing a sliding distance of 50mm per cycle. This was achieved by adjusting the throw of the crank which was attached to the motor. By attaching a pen to the pin holder arm, a trace of the reciprocation length was drawn and measured. This defined the reciprocation length. The bath was reciprocated along linear rails. The reciprocation frequency was set at 1Hz by timing the number of reciprocations over a period of time. The number of cycles was continuously measured by a non-contacting Hall-effect probe.

The rotational motion of the pins was achieved by using a small motor attached to the drive shaft using gears. The drive shaft had a blind hole in which the pin was held in position by a grub screw. Each of the four stations had a separate motor. The shaft was lubricated using olive oil, since mineral oils absorbed by the UHMWPE test pins would cause a significant mass gain distorting the wear results. The shaft of each motor was cleaned and oil reapplied every 0.5 million cycles. There was an oil catcher attached to the bottom of the shaft, held in place by an O-ring. This prevented the oil from the shaft dripping into the lubricant bath and contaminating the lubricant.

The temperature was measured by a K-type thermocouple, which enabled the control of the heating element beneath the lubricant bath, via a feedback circuit. The temperature was kept at a constant 37°C. A level sensor was attached to one side of the bath to control the amount of lubricant in the bath. The sensor was made of three platinum pins, one shorter than the other two. By monitoring the current between the pins, the level of the lubricant in the bath could be kept constant. When only the two longer pins were in the circuit (ie immersed) the lubricant level was satisfactory. When the level fell to below these two pins, distilled water was added to the bath, from a reservoir, until the third, shorter, pin was immersed. Thus the minimum and maximum lubricant levels were controlled.

3.2 Friction Simulators I & II

Frictional studies were performed on the Durham Hip Function Friction Simulator I (Figure 8). This comprised a low friction carriage into which the acetabular cup was placed, and a moving frame into which the femoral head was placed. The joint was inverted with respect to its position in vivo. The head was lowered into the cup, applying the load to the joint hydraulically. Approximately 5ml lubricant was placed in the cavity of the cup. The simulator was controlled by a microprocessor, through a standard PC interface. Data collected by the microprocessor was analysed by the PC and a text file output of friction factors and Sommerfeld numbers was obtained.

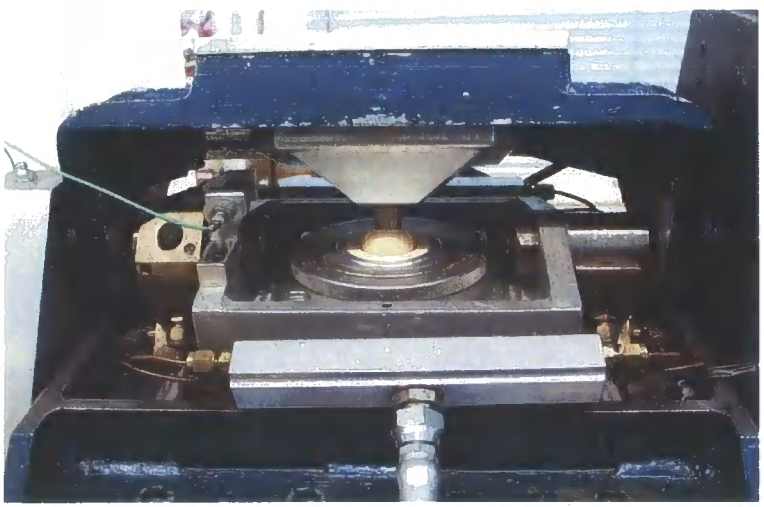

Figure 8. Durham Hip Function Friction Simulator I

The head was oscillated in the flexion extension plane, in simple harmonic motion with amplitude +/-24° and period 1.2 seconds. A square wave loading profile (Figure 9) was applied to the head during this motion, similar to that measured by English and Kilvington[6] or a smoothed version of that found by Paul[2]. The maximum load applied was 2000N and the minimum 100N.

The carriage into which the cup was placed, was mounted on two sets of externally pressurised bearings. The first set allowed the cup to centre itself around the head in the anterior-posterior plane, while the second set provided medio-lateral alignment. This prevented any misalignments between the centres of rotation of the head and cup. Since the cup was allowed to find its own centre around the head, and was fixed in the

extremely low-friction carriage, motion of the carriage would be caused by a frictional torque from within the prosthesis, and this was measured by a piezoelectric transducer (Kistler 9203).

Each complete run comprised a normal and inverse run, which were then combined by the software to eliminate any misalignment errors that remained. Data were recorded digitally for the 1st, 21st and 41st of the 41 cycles in each normal and inverse run, and stored in a file with a unique name and extension. The normal and inverse files for each run were then merged. The friction factors quoted were taken from the high load and high velocity phase of motion, equivalent to the stance phase of walking from the 41st run and are an average of 3 independent runs at the viscosity quoted.

The merging of the normal and inverse loading cycle was done by phase shifting the inverse file so that the encoder positions for each portion of the cycle coincided. Since the loading cycles for the two runs were 180° out of phase this corresponded to a shifting of the inverse cycle by half a cycle. Thus encoder position i on the normal run, corresponded to encoder position $i+64$ on the inverse run (total of 128 positions). Then, an average was taken of the values recorded for each encoder position. The absolute values were used since the frictional torque recorded in the reverse cycle will be in the opposite direction to that recorded in the normal cycle.

The frictional torque, T, was converted to a friction factor using the relation:

$$f = \frac{T}{rL}$$

where f=friction factor, L=load and r=radius of the joint (see Section 2.6.1 in Chapter 2). The friction factor and Sommerfeld numbers were computed within the simulator software and some of the Sommerfeld numbers checked manually for accuracy.

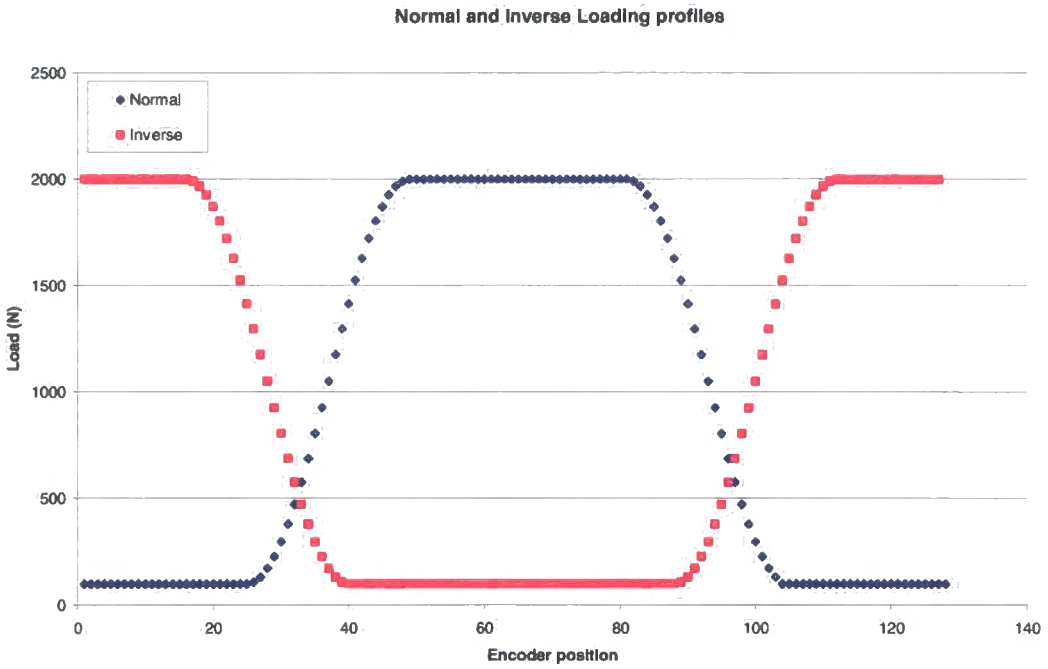

Figure 9. Applied loading profiles for the friction simulator

The metal-on-metal hip resurfacing study was done using Friction simulator II. The conditions of testing are the same for both rigs, as are the methods of measuring and analysing the results.

3.3 Hip Wear Simulator II

The ceramic hip wear studies were performed on the Durham Hip function Wear Simulator Number 2[132]. The joints were anatomically positioned. The head oscillated in the flexion extension plane, while the cup was rotated around its polar axis to simulate internal/external rotation. Motion in both planes was near simple harmonic. The head was loaded into the cup pneumatically, with a square wave profile (Figure 10), similar to that measured by English and Kilvington[6] or a simplified version of that found by Paul[2]. This configuration has been found to give comparable wear results to a simulator applying a Paul cycle dynamic loading profile[133].

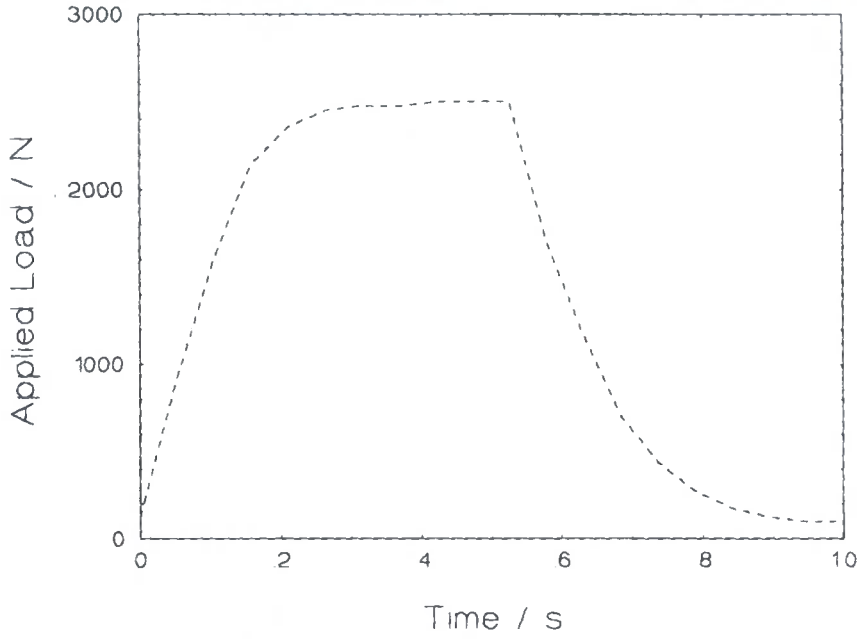

Figure 10. Loading profile for Hip Wear Simulator II[132]

The simulator comprised 5 active wear stations plus a creep control station. Each of the 6 stations had an independent closed lubricant bath of 500ml. The ceramic head was mounted onto a PMMA coated taper (Figure 12), while the cup was clamped into an UHMWPE holder. The taper was machined from bone cement cast onto a metal core. This minimised metal transfer to the head and made removal of the head easier. The metal core of the taper was machined from the top part of a 16mm diameter threaded bar, which was used to attach the head to the stainless steel plate, which formed the bottom of the test cell. The top of the test cell was formed by the UHMWPE cup holder. A rubber gaiter completed the cell into which the lubricant was enclosed.

The motion was controlled by a single motor rotating at 1Hz, from which two connecting rods provided the swinging motion on the heads (flexion extension) and the internal-external rotation on the cups. While both motions were near simple harmonic they were 90° out of phase with one another.

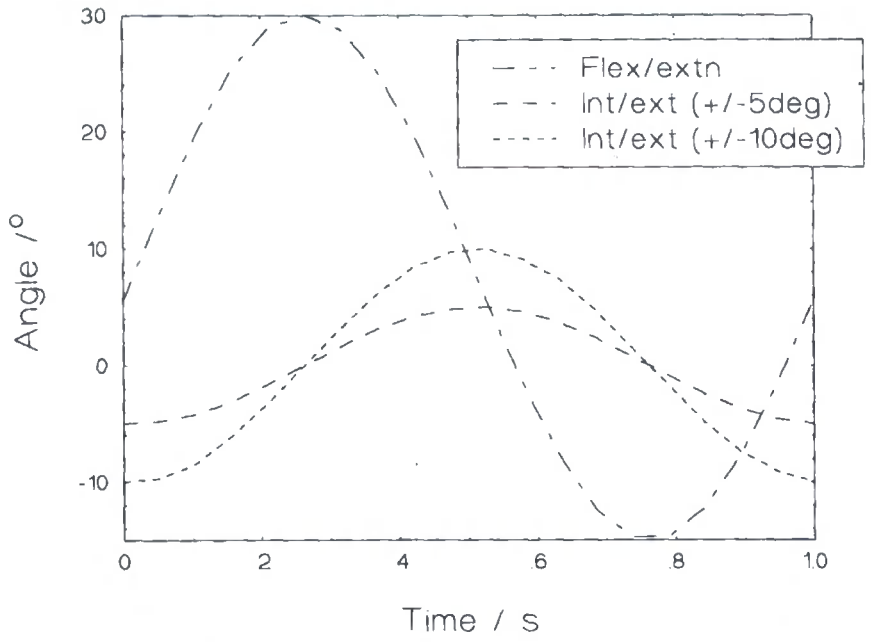

Figure 11. Motion applied to Hip Wear Simulator II[132].

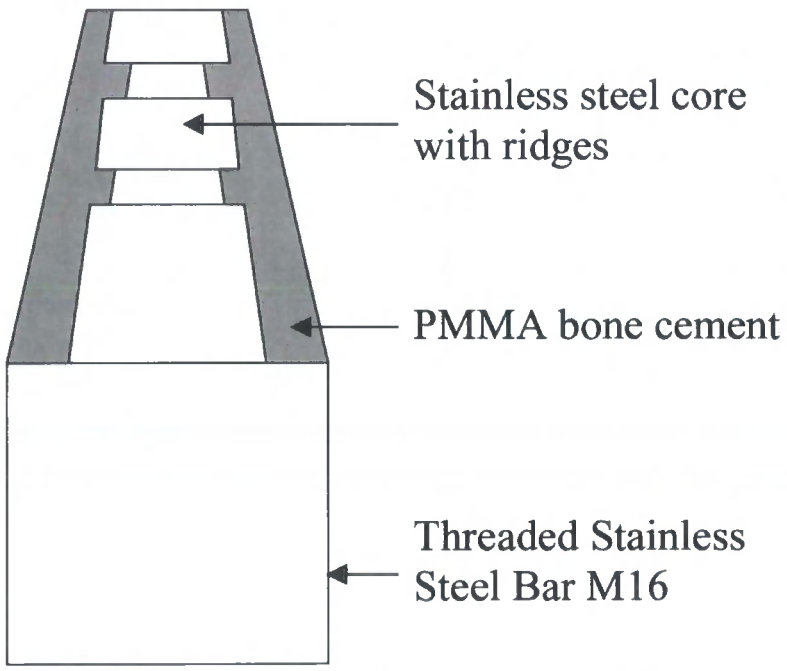

Figure 12. Schematic diagram of the taper used for the ceramic femoral head in the wear simulator

Two non-contacting Hall-effect counters were attached to the rig to count the number of cycles undergone. One was attached to the flexion extension arm, and the other to the rotating shaft which controlled the internal external rotation. Each cycle was thus

counted once by each counter, providing a check on the number of cycles completed during the test

3.4 Hip wear simulator I

The Birmingham hip resurfacing device study was conducted on the Durham Mark I hip wear simulator. This consists of 5 active stations and one control station. The 5 active stations were controlled by two servo-motors: one for each of the flexion-extension and internal-external rotation motions. The forces were applied pneumatically with a manifold serving each individual station including the control. As such each active joint underwent the same motion and loading, while the control joint underwent the same loading profile as the active joints without any tangential motion.

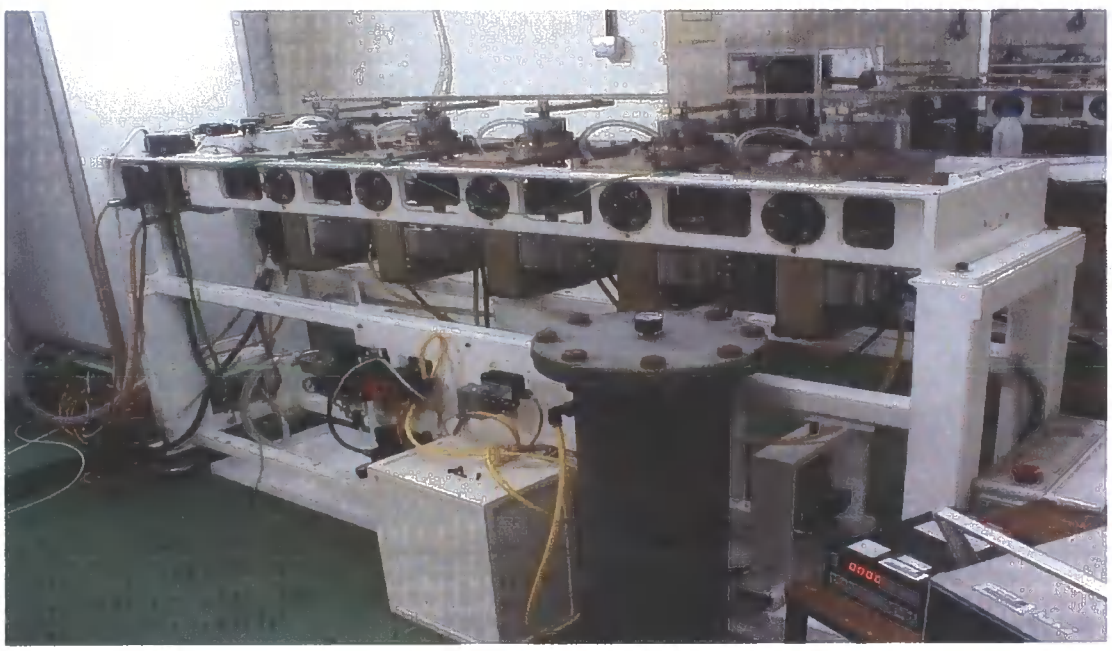

Figure 13. Mark I Durham hip wear simulator.

The heads were mounted in a similar way to that described above, although with metallic holders appropriate to the head configuration. The cup holder was oriented at 33° to the horizontal to achieve the same contact regions on the components as in vivo. As in the case of the Mark II simulator described above, each joint was mounted in an

individual sealed cell with 500ml of lubricant, thus avoiding cross contamination of the lubricant.

The force applied is shown in Figure 14, and is based on the Paul cycle[2]. The minimum load applied was 100N and the maximum was 2975N.

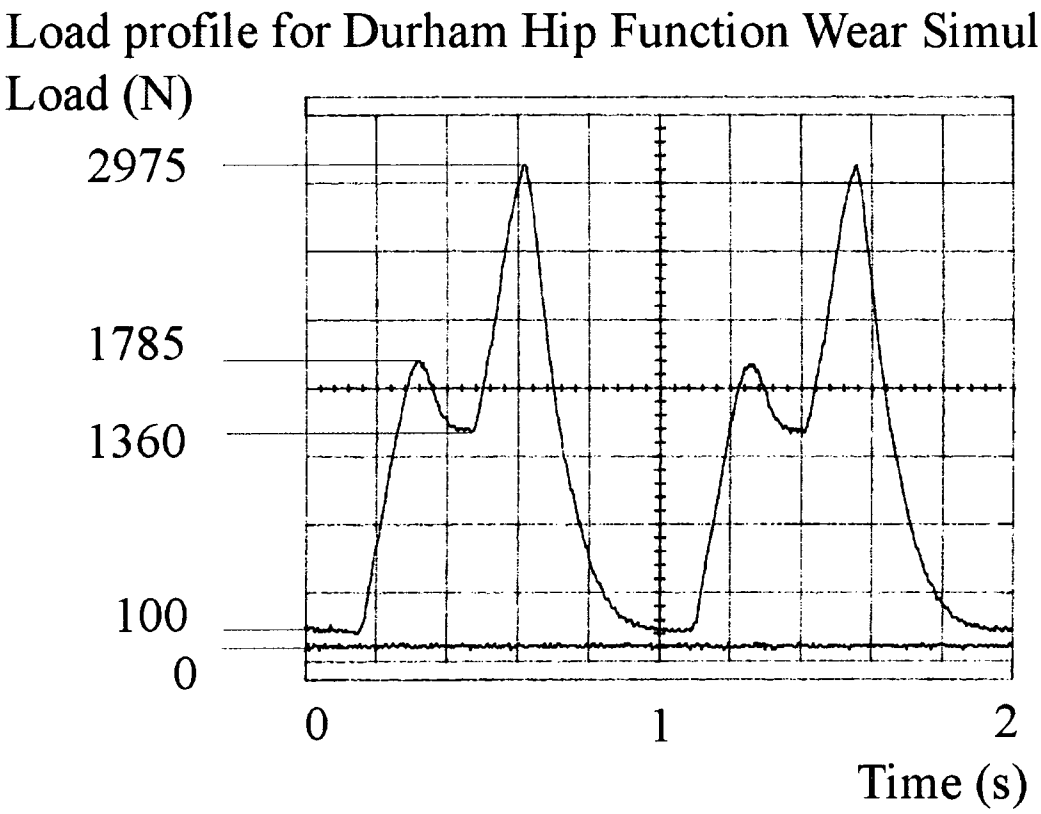

Figure 14. Load profile for Mark I Durham hip simulator

The results given by the Mark I and Mark II Simulators have been found to be comparable to one another and to other simulators [134,135]

3.5 Non-contact surface profilometer

The Zygo (NewView 100) non-contacting interference profilometer was used to measure the surface roughness of each plate surface, before, during and after testing. The device works by splitting a light beam into a reference beam and an incident beam. The incident beam is reflected from the surface, and the difference in path length

between the reference and reflected beams causes an interference pattern. Since the reflected light has only interacted with the surface, the interference pattern produced is dependent only on the surface. As such the interference pattern is analysed by the software to give surface profile information. The maximum z-height variation that can be measured is 100μm, and the vertical resolution is less than one nanometre. The horizontal area of view depends on the magnification, but the number of pixels always remains the same at 320x240. This means that the horizontal resolution is different for different magnifications (Table 2). The on-screen magnification is 10 times the lens magnification.

Lens/Zoom	Area of view (μm)	Area depicted by one pixel (μm^2)
x10/x1	720 x 540	5.06
x10 /x2	363 x 272	1.28
x40/x1	181 x 136	0.32
x40/x2	91 x 68	0.08

Table 2. Resolution of the Zygo interference profilometer at different magnifications.

3.6 Atomic Force Microscope [136]

The TopoMetrix Explorer atomic force microscope (AFM) was used for surface analysis of the ceramic heads in the ceramic clearance study. This was not used for cup surface analysis since the scanning tip could not be lowered into the cup cavity. The AFM used a piezoelectrically driven scanning probe mounted on a cantilever. A laser focussed on the cantilever reflected onto a photoelectric detector, allowing deflections of the cantilever to be monitored by a feedback system (see Figure 15). These data were then used by the software to determine topographic and other information. A 100μm X, Y scanner was used, which had an X and Y range of 100μm and a Z range of 10μm. The maximum scan speed was 5 lines/sec and its non-linearity and non-orthogonality were both less than 1%.

The contact-mode tip on the underside of the cantilever (V-shaped) was a silicon nitride pyramidal tip of 4μm base and height (aspect ratio ~1:1) with a tip radius of less than 50 nm.

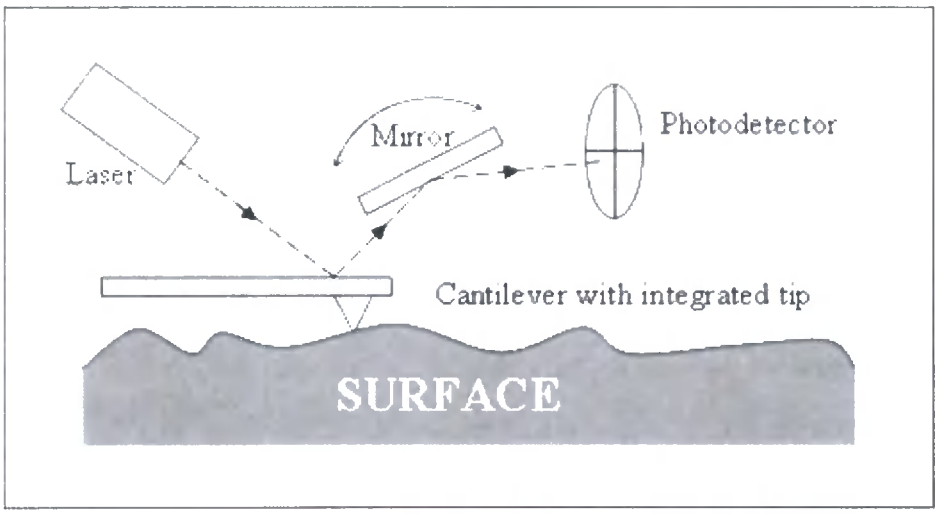

Figure 15. Schematic diagram of AFM set up

3.7 Balances

Three different balances were used. The balance used to find the mass of the pins was the Mettler Toledo AT20 with a maximum mass of 22g and a sensitivity of 2μg. The balance used for the plates was the Mettler AE200 which had a sensitivity of 0.1mg. This was used since the mass of the plates was outside of the range of the other balance. For the later tests the Mettler Toledo AX205 was used for the plates, with a sensitivity of 0.01mg. This balance was also used for the ceramic-on-ceramic and metal-on-metal tests. The mass of a small metallic object was measured using both of the AE200 and the AT20 and the temperature and humidity of the laboratory was also monitored. Due to the results of this test, as detailed in Appendix A, a mass control was included in later pin on plate tests to correct for the differences in mass recorded. The AX205 was internally calibrated prior to each use and was also checked with an external calibration mass borrowed for the purpose from Mettler. This was found to read correctly and no further external checks were deemed necessary.

4 Is wear factor dependent on stress in UHMWPE contacts?

4.1 Introduction

Both the Archard equation[22] and the Lancaster equation[20] suggest that the only factors affecting the wear factor are the materials themselves, the load under which they articulate and the distance of articulation. However, experimentally there is evidence that some other factors may come into play, although no consensus of agreement has been reached regarding exactly what these are and how they affect the wear factor. One factor that has been investigated somewhat is the nominal contact stress.

Barbour *et al*[117] found a decreasing trend of wear factor with respect to nominal contact stress over a range of 3.4-28.3 MPa, while Sathasivam *et al*[119] found that the wear factor first increased and then decreased over the similar range of 3-20MPa.

Mazzucco and Spector[40] found, however, that the wear factor was not dependent on nominal contact stress, but on the apparent contact area. This was a small study but the range of stresses investigated were within those tested in the two studies mentioned above.

Earlier studies found that there was an exponentially increasing trend of linear wear rates with increasing contact stress[5,118].

In the present study[43] a number of pin designs are used in an attempt to shed some light on some of these points. A set of pins of different diameters were tested under the same load, giving a range of contact stresses. Then a set of pins with the same contact area but different outside radii (annular cross section) were used to test the material under the same load and the same stress. Finally a number of tests were carried out with different loads providing further variation in the nominal contact stress.

4.2 Materials and Methods

4.2.1 Materials

4.2.1.1 Stainless Steel

Stainless steel plates of length 48mm were machined from 25.4mm x 3.175mm bar stock supplied by RS components, resulting in a plate of dimensions 48 x 24 x 3mm. The stainless steel was 316 high corrosion resistant material, due to the inclusion of molybdenum. The plates were ground using Bueler Metaserv Rotary Grinder and subsequently polished using Bueler Metaserv Universal Polisher using firstly 6μm diamond paste, then 1μm diamond paste. The surface roughness of each plate was measured using the Zygo non-contacting interference profilometer. While the British standard recommends an Ra < 50μm, the initial Sa values of the plates used were between 5.25 and 13.30 nm, which is more consistent with the manufactured products.

4.2.1.2 Ultra High Molecular Weight Polyethylene

The pins were machined from a rod of UHMWPE supplied by DePuy. It was irradiated with gamma radiation with a minimum dose of 25.4kGy and a maximum dose of 29.7kGy on 26/9/1996. All pins were machined with the same orientation within the bar to prevent any possible directional effects.

For Test A four different pin designs were used, to achieve four different pin face areas, and hence four different nominal contact stresses for the same load. The four designs chosen were used to reflect various designs used in the literature, and were named appropriately. Two Leeds University designs were used. The Leeds flat is a cylinder of diameter 9.5mm. The Leeds tapered is identical to the flat design but has a tapered end, so that the initial face diameter is 3mm. The Durham University pin is a cylinder of 5mm diameter, while the ASTM pin is a 9mm diameter cylinder. The details were summarised in Table 4. All pins had a 5mm diameter connector to fit into the pin holder.

Test Number	Test Pair	Load (N)	Contact Stress (MPa)	Pin type
Test A	1	40	5.66	Leeds Tapered
	2	40	2.04	Durham
	3	40	0.63	ASTM
	4	40	0.56	Leeds Flat
Test B	5	40	1.46	5.9mm solid face (Table 5)
	6	40	1.47	Annular face (Table 5)
	7	40	1.47	Annular face (Table 5)
	8	40	1.50	Annular face (Table 5)
Test C	1	70	2.56	5.9mm solid face (Table 5)
	2	70	2.58	Annular face (Table 5)
	3	70	2.58	Annular face (Table 5)
	4	70	2.62	Annular face (Table 5)
Test D	5	33	1.68	Durham
	6	61	3.11	Durham
	7	79	4.02	Durham
	8	49	2.50	Durham
Test E	1	33	1.68	Durham
	2	61	3.11	Durham
	3	79	4.02	Durham
	4	49	2.50	Durham
Test F	1	180	9.17	Durham with larger midsection
	2	250	12.73	Durham with larger midsection
	3	90	4.58	Durham with larger midsection
	4	120	6.11	Durham with larger midsection

Table 3. Conditions and pin design for each test

Pin	Face diameter (mm)	Face area (mm^2)	Nominal contact stress under 40N (MPa)
Leeds Tapered	3.0	7.07	5.66
Durham	5.0	19.63	2.04
ASTM	9.0	63.62	0.63
Leeds Flat	9.5	70.88	0.56

Table 4. Details of the pin designs for Test A.

For Tests B and C, the pins were required to have similar face areas, while differing in radius. As such the centre of pins 2-4 was machined out, resulting in the pin's face being an annulus for three of the pins, and only one pin having a circular face area. The inner and outer diameters of the pins are given below. The depth of the hole was 2mm, while the pins were 20mm long. All pins were placed under a 40 and 70N load respectively, and therefore, were under similar contact stresses. These details are summarised in Table 5.

Pin	Inner diameter (mm)	Outer diameter (mm)	Face area (mm^2)	Contact Stress (MPa)	
				40N	70N
1	0.00	5.9	27.34	1.46	2.56
2	3.00	6.6	27.14	1.47	2.58
3	6.00	8.4	27.14	1.47	2.58
4	8.00	9.9	26.71	1.50	2.62

Table 5. The dimensions of pins manufactured to have similar face areas, for the two tests at constant load and constant nominal contact stress.

For Test F, a pin of face diameter 5 mm was used. However, due to the large loads applied during this test, a pin with a larger midsection was manufactured to decrease

any buckling or bending of the pin under load. For Tests D and E a Durham pin, as described for Test A was used.

4.2.1.3 Bovine Serum Lubricant

The lubricant used was newborn calf serum supplied by Harlan Sera-Lab; batch number 8030901. Chemical analysis of the serum by the supplier showed that the total protein concentration in undiluted serum was 5.2g/dL. The serum was diluted to 30% concentration by volume with distilled water. 0.2% sodium azide was added to reduce bacterial degradation. This resulted in a protein concentration of 15.6g/L in the lubricant. Both diluted and undiluted serum was kept frozen until needed.

4.2.2 Methods

4.2.2.1 Cleaning Weighing Protocols

4.2.2.1.1 Plates

The plates were cleaned according to the protocols in Appendix C, Section C.1.

Each plate was weighed 4 times and the mean and standard deviation of the readings was found.

4.2.2.1.2 Pins

The pins were cleaned according to the protocol as detailed in Appendix C, Section C.2, closely following the ASTM recommendation (ASTM F732-00, part A6)[137].

The mass of each active pin and control pin was found and recorded 4 times. The mean and standard deviation of these readings was used to calculate the relevant mass losses or gains and subsequently determine the wear rate of each pin. A control pin was used to correct for absorption of lubricant by the UHMWPE. The mass of the pins was corrected for fluid uptake as detailed below

M_0, M_i = initial mass reading and *ith* mass reading respectively for a test pin

C_0, C_i = initial mass reading and *ith* mass reading respectively for control pin
Wi = wear on plate between intial and *ith* reading.

M_i-M_0 =mass change of test pin
C_i-C_0 = mass change of control pin
$(M_i-M_0)-(C_i-C_0) = W_i$

In the case where C_i is smaller than C_0 then the mass loss on the control pin is added to the change in mass of the test pins. In the case where C_0 is smaller than C_i then the mass gain on the control pin is subtracted from the test pin mass change.

4.2.2.2 Experimental Procedure

4.2.2.2.1 Pin on Plate study

For each individual test the experimental procedure was the same. After approximately 250,000 cycles the experiment was stopped and the pins and plates removed, cleaned and weighed according to the protocols described in section 4.2.2.1. The mass loss measured was converted to a volume loss using the density of UHMWPE (953μg/mm^3), and stainless steel (7.85mg/mm^3) for the pins and plates respectively. This was plotted on a graph against the product of the sliding distance and load. The wear factor is the gradient of this line, and was found using linear regression analysis in Microsoft Excel. All wearing-in data were disregarded and each test was terminated after a minimum of 1.5 million cycles of steady state wear.

The lubricant was discarded and replaced with fresh serum each time the machine was stopped for weighing. In addition, the plates were imaged on the Zygo profilometer approximately each 0.5 million cycles, to monitor the surface roughness of the wear track throughout the wear test.

4.2.2.3 Effect of the rotational element of motion on the sliding distance

Due to the rotational motion, paths taken by different points on the pin surface differed according to position[37]. Since the rotation and reciprocation frequencies were both 1Hz, the path lengths of different points on the perimeter also differed. Figure 16[37] shows the paths taken by points which began at different positions on the circumference of the pin. Clearly not all points traversed the same path or have the same path length.

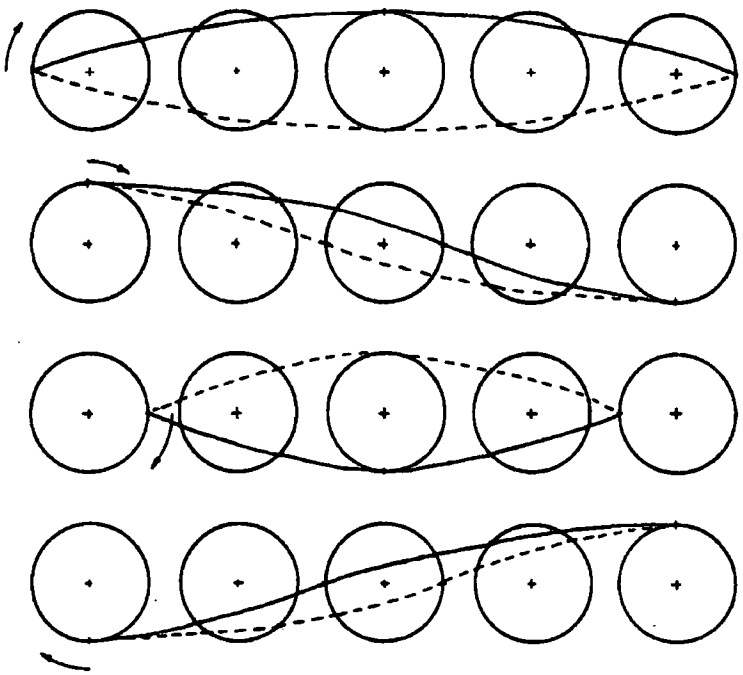

Figure 16. The paths taken by various points along the circumference of the pin during one cycle[37].

Scholes (1999)[138] developed a computer program to find the actual sliding distance of pins undergoing the particular motion used in the Durham machines. The sliding distance was different for each point on the surface of the pin and was dependent on the full set of starting conditions, r, the distance from the centre of the pin face and θ_0, the initial angle from the direction of reciprocation. For any given r, points along the direction of reciprocation, $\theta_0 = 0°$ and 180°, the sliding distance was a minimum and a maximum respectively. Scholes took these two values at various radii across the pin and found their numerical mean, to give the average overall sliding distance. The

sliding distance was higher than the reciprocation distance for each pin, when the rotational motion was taken into account. The rotational motion on the Durham pin (5mm diameter) gives an average increase in path length of 2.1% over the entire surface of the pin[138].

In a similar study, Lloyd[139] constructed a spreadsheet in Microsoft Excel to work out the additional sliding distance due to the rotation. The result obtained was remarkably similar to that found by Scholes. In this case the absolute velocity of various points on the pin face was found and then multiplied by a small time increment to find the distance moved by that point. Summing over the time taken for a whole cycle, gave the overall distance.

In the present study, the extra sliding distance of each pin, due to its rotation was calculated by modifying the computer program (written in C) used by Scholes. The program was altered slightly to calculate the overall sliding distance for more than just these two initial angles over the pin face, and to consider smaller radial intervals. These sliding distances were then averaged to find the average sliding distance of the pin face. For small increments in angle and radius, this is a numerical integration over the surface of the pin, and gives a more reliable value of the additional sliding distance than the method used by Scholes. For the annular pin faces, the integration parameters were altered to take this into account, and only values between the internal and external radii were considered. The modified code is included in Appendix B.

When the modified program was set to the same number of points and precision as in Lloyd's case, a lower percentage increase was found. This could be due to the fact that at each stage of the calculation, rounding errors were introduced to excel which could compromise the value of the average, although this does not explain the agreement between the Scholes and Lloyd calculations for the Durham pin.

As the number of points taken into account was increased, the output values settled to the values given in Appendix B. The percentage increase found for each pin was used

to adjust the values of the sliding distance, and it was always these adjusted values that were used for the sliding distance rather than the reciprocation distance.

4.3 Results

The test conditions and wear rates found for all tests are summarised in Table 6, below. Analysis and graphical representation of these data follow. In all cases the wear factor has been adjusted to take into account the true average sliding distance resulting from the rotational element of the pin motion, as described in Section 4.2.2.3. The percentage increase in the sliding distance for each pin radius is given in Appendix B for reference. Each test was stopped after a minimum of 1.5 million cycles of steady state wear, and all wearing-in data were disregarded.

Test	Load (N)	Stress (MPa)	External pin radius (mm)	Internal pin radius (mm)	Steady-state wear factor (mm^3/Nm)	Standard Error in wear factor (mm^3/Nm)	N, No. of Samples
A	40	2.04	2.5	0	5.47E-07	2.09E-08	12
	40	5.66	1.5	0	6.96E-07	2.72E-08	12
	40	0.63	4.5	0	1.41E-06	5.41E-08	12
	40	0.56	4.75	0	1.85E-06	4.91E-08	12
B	40	1.46	2.95	0	1.38E-06	6.88E-08	8
	40	1.47	3.3	1.5	1.44E-06	6.84E-08	8
	40	1.47	4.2	3	1.42E-06	8.08E-08	7
	40	1.50	4.95	4	1.25E-06	2.96E-08	7
C	70	2.56	2.95	0	6.77E-07	2.62E-08	8
	70	2.58	3.3	1.5	5.95E-07	3.10E-08	8
	70	2.58	4.2	3	6.05E-07	2.77E-08	8
	70	2.62	4.95	4	3.27E-07	1.90E-08	8
D	33	1.68	2.5	0	1.06E-06	3.97E-08	11
	61	3.11	2.5	0	8.35E-07	4.24E-08	10
	79	4.02	2.5	0	4.41E-07	2.20E-08	11
	49	2.50	2.5	0	9.25E-07	4.10E-08	11
E	33	1.68	2.5	0	1.58E-06	3.14E-08	8
	61	3.11	2.5	0	8.61E-07	3.31E-08	8
	79	4.02	2.5	0	5.62E-07	1.64E-08	8
	49	2.50	2.5	0	8.50E-07	2.62E-08	7
F	180	9.17	2.5	0	3.31E-07	9.55E-09	18
	250	12.73	2.5	0	1.21E-07	8.16E-09	12
	90	4.58	2.5	0	2.48E-07	8.80E-09	13
	120	6.11	2.5	0	1.54E-07	1.34E-08	12

Table 6. Test Conditions and wear factors found for all pins.

4.3.1 The effect of pin radius on wear factor

Figure 17 shows the wear factors for the two tests carried out with pins of equal contact area. The wear for the 40N test was not affected by the outer radius of the pin (R^2 = 0.353). However, the 70N test does show some variation over the range of radii (R^2 = 0.719). Statistical analysis of the raw data for the 70N test showed that the wear factors on pins 1, 2 and 3 were not significantly different from one another, but all were significantly different from the wear factor on pin 4 (all $p<1x10^{-6}$). There is a slight drop in wear factor for the highest radius pin in the 40N test also, although this is not statistically significantly different from any of the wear factors on pins 1, 2 and 3.

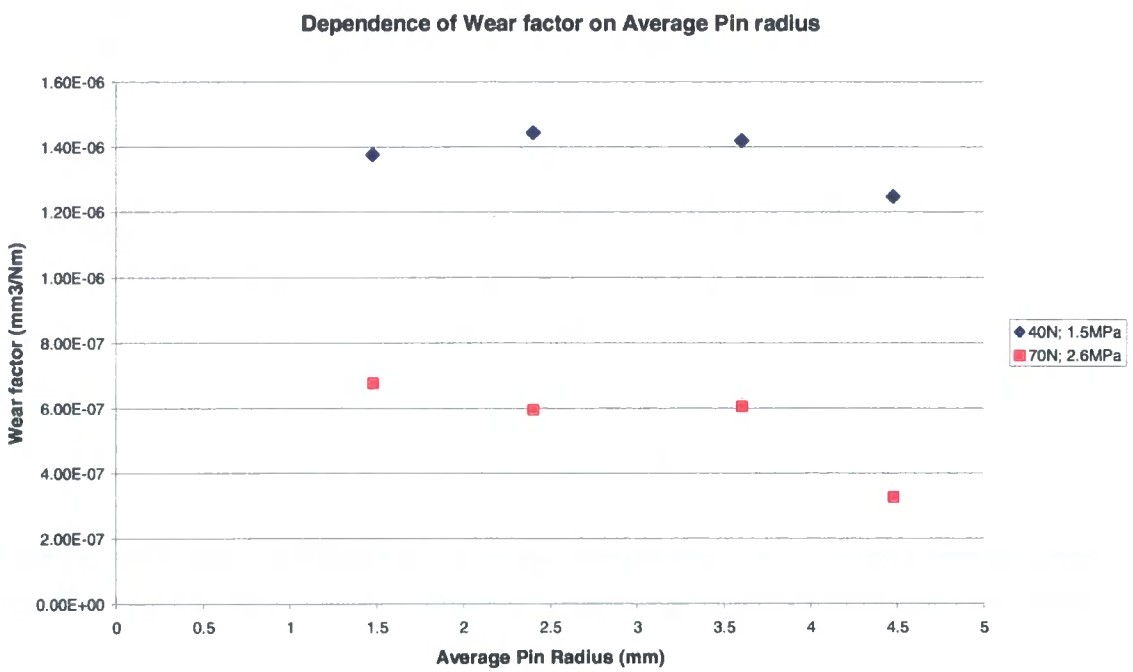

Figure 17. Dependence of wear factor on average pin radius for two conditions of constant stress: 1.5MPa and 2.6MPa.

Taking into account all the other tests, regardless of experimental conditions, Figure 18, shows that there was no clear correlation between the external pin radius and the wear on the pin. The results for the 2.5mm radius were particularly indicative since they span almost the entire range of the wear factors seen. Regression analysis of all the data

gives R^2=0.162, indicating the lack of correlation between the pin radius and the wear factor.

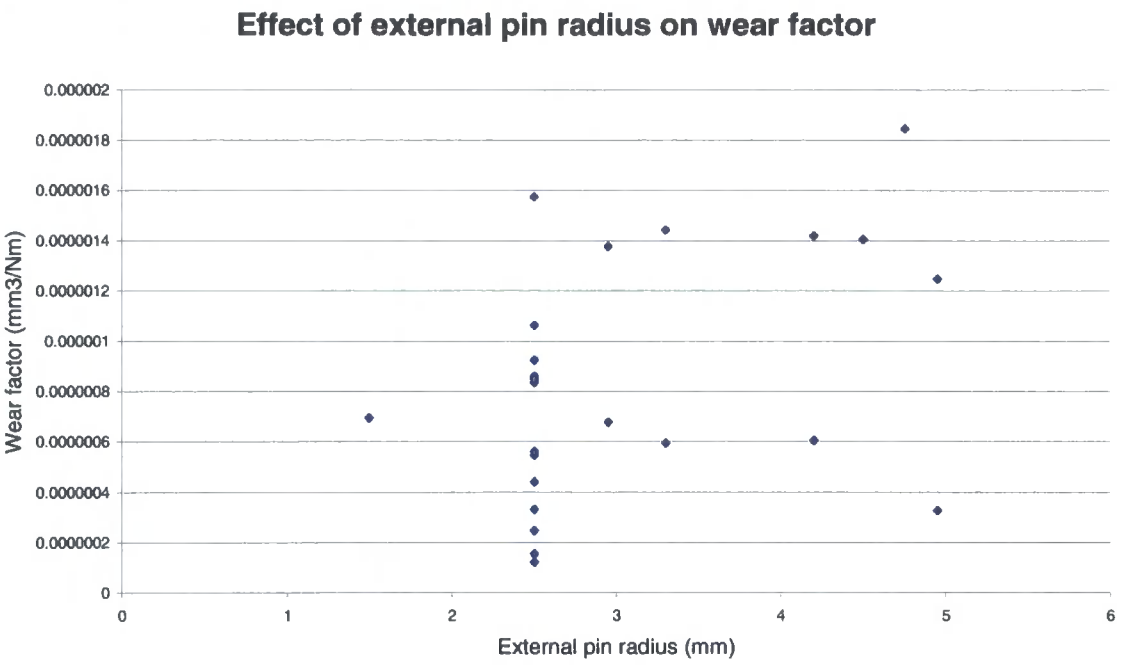

Figure 18. The effect of external pin radius on wear factor for all test conditions.

4.3.2 The effect of Load on wear factor

As can be seen from Figure 19, the dependence of the wear factor on the applied normal load showed a different trend for two different contact stress values. Moreover, the R^2 values are very low (0.0231 and 0.1954 for the 1.5MPa and 2.5MPa cases respectively) indicating a very low correlation between wear factor and normal load. This implies that some other factor affects the wear rate more significantly than just the load applied.

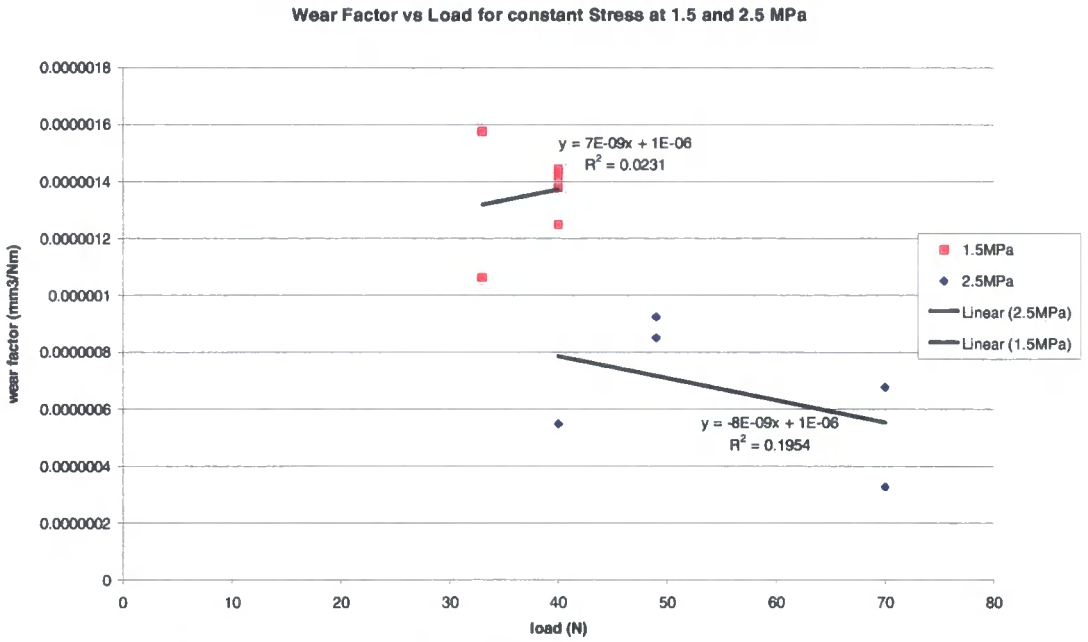

Figure 19. The effect of normal load on wear factor for two nominal contact stress values: 1.5MPa and 2.5MPa.

4.3.3 The effect of nominal contact stress on wear factor

From the results in Figure 17, we can see that at higher load/stress, lower wear factors are achieved. While this difference is not found to be statistically significant ($p=0.15$), a closer analysis including results from all test conditions follows.

Including only all data at 40N the effect of the stress on the pin wear can be seen, and this is shown in Figure 20. A decrease in wear factor is noted with increasing stress, although this is clearly not a linear dependence.

Figure 21, shows all data regardless of the experimental conditions. The remaining data were found largely to overlap the 40N data, and are thus considered as one data set. A power-law fit to these data gives the relation $K=2x10^{-6} \times \sigma^{-0.84}$ with $R^2=0.71$. This means that at low stresses the wear factor is highly dependent upon the stress, whereas for higher stresses the wear factor is less dependent on the stress.

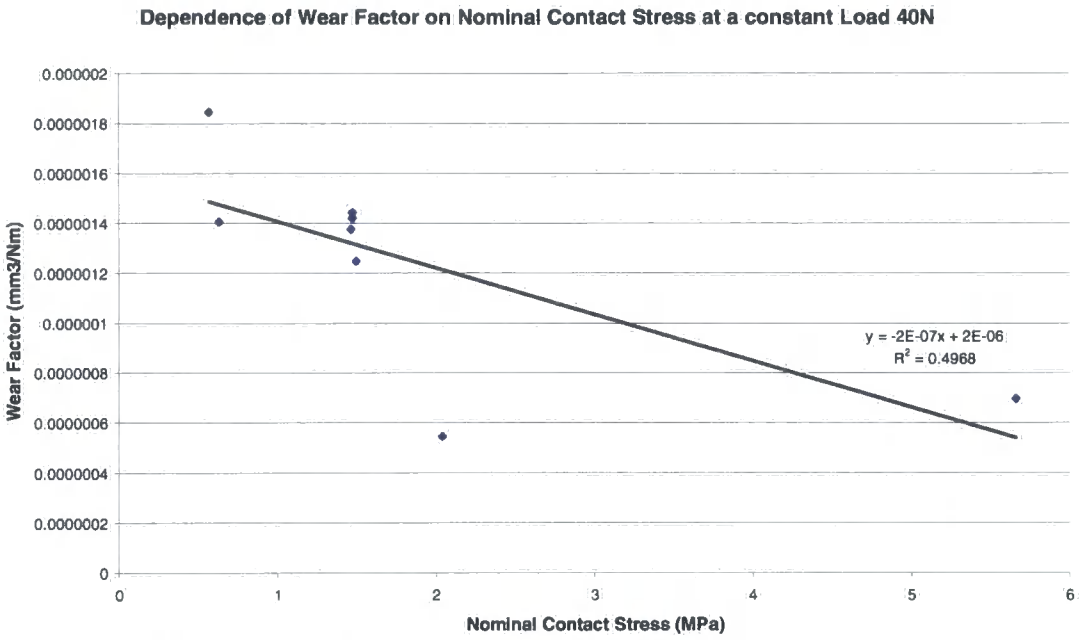

Figure 20. The dependence of Wear Factor on Nominal contact stress at a constant load of 40N.

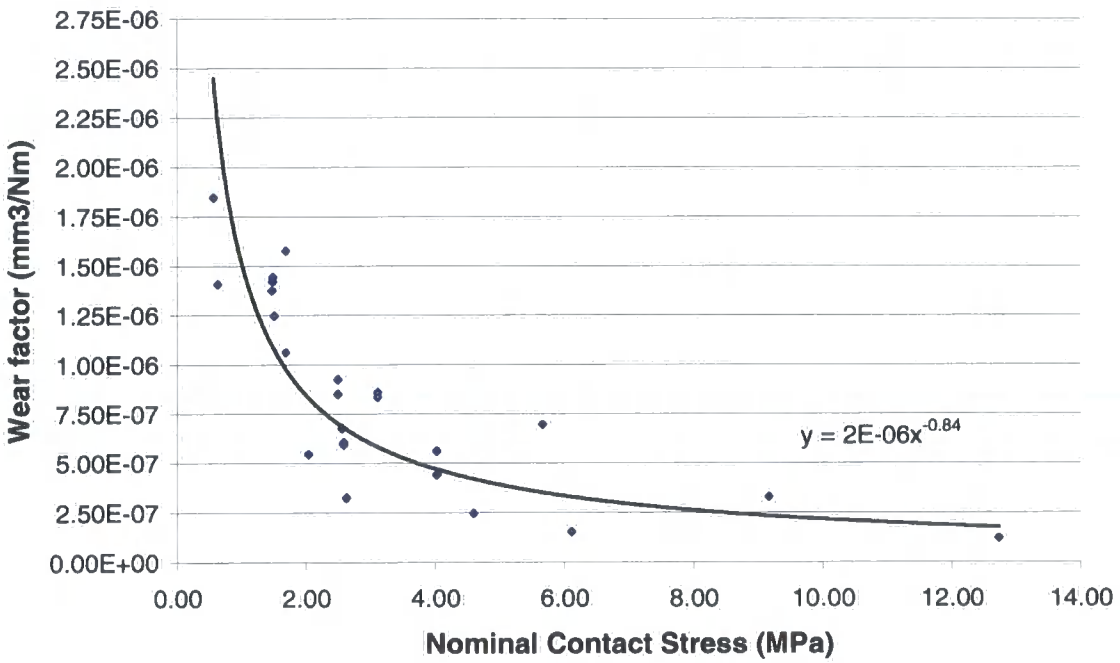

Figure 21. The dependence of Wear Factor on Nominal Contact Stress

4.3.4 Plate Wear

Wear factors for the plates were calculated for completeness. The plate wear factors were found to be negligible, with some plates exhibiting a negative wear factor. This

could possibly indicate a transfer film, although no direct evidence of this was seen. Some light scratching was observed on the wear tracks of all the plates, supporting the significant increase in roughness parameters noted in Section 4.3.5 below. The majority of the wear in each couple, however, was, as expected, found on the pin. The concept of a wear rate for the plates is weak and no further discussion is deemed appropriate.

4.3.5 Surface Study

The plates showed a significant ($p<0.05$) increase in surface roughness (Sa, Srms and PV) between the initial and final values of each parameter as seen in Table 7. All p-values are given to 2 decimal places and are calculated from the raw data. Final mean surface roughnesses were in the range 8.81 to 90.0 nm. Multidirectional scratching was seen on the wear track. Significance was not reached for two of the plates. These were tested under 70N (2.62MPa) and 33N (1.68MPa).

No correlation ($R^2=0.2$) was found between the initial and final values of Sa for the plates, indicating that although most of the plates showed a significant increase in their roughness, the initial and final roughness values are not directly related. Figure 22 shows the final Sa of each plate against the load under which it was tested, while Figure 23 shows the same for the contact stress. It is clear from these graphs that there is no correlation between the final Sa and the conditions of testing ($R^2=0.1$ in both cases).

Final values of the surface parameters for Test D were not applicable since the test terminated when it ran dry. The data were included in the wear results not including the final readings.

		PV /nm			Srms /nm			Sa /nm		
Test	**Plate No.**	**Initial Mean**	**Final Mean**	**p**	**Initial Mean**	**Final Mean**	**p**	**Initial Mean**	**Final Mean**	**p**
A	**1**	73.0	1358.9	0.00	10.86	82.17	0.00	8.89	54.96	0.01
	2	95.3	1337.6	0.00	10.22	84.44	0.01	8.11	55.59	0.03
	3	65.5	1524.9	0.00	8.40	105.56	0.01	6.76	74.32	0.03
	4	83.8	1590.5	0.00	11.97	80.18	0.00	9.75	47.51	0.00
B	**5**	54.4	1179.6	0.00	6.93	98.69	0.00	5.52	77.29	0.00
	6	56.4	502.3	0.00	6.53	23.81	0.00	5.25	15.71	0.00
	7	80.8	1069.7	0.00	9.54	45.43	0.00	7.90	24.80	0.00
	8	61.8	458.6	0.04	8.06	14.20	0.02	6.46	8.81	0.01
C	**1**	62.4	392.2	0.00	7.97	31.68	0.00	6.48	24.43	0.00
	2	82.3	326.7	0.00	9.02	20.39	0.00	7.24	15.18	0.01
	3	69.0	269.8	0.00	8.51	21.41	0.04	6.93	16.99	0.048
	4	70.9	270.4	0.00	8.11	17.74	0.04	6.62	13.45	0.054
E	**1**	86.6	218.0	0.00	9.80	10.92	0.46	8.00	7.64	0.73
	2	110.4	248.9	0.00	9.40	16.08	0.01	7.30	11.80	0.00
	3	89.5	192.9	0.00	9.90	14.12	0.01	7.80	10.95	0.02
	4	81.5	323.6	0.00	9.70	18.27	0.00	7.60	12.66	0.00
F	**1**	133.2	891.8	0.00	16.60	110.70	0.01	13.30	90.00	0.01
	2	131.2	1095.9	0.00	15.70	89.60	0.00	12.70	52.10	0.00
	3	107.8	542.1	0.00	11.90	43.20	0.00	9.90	31.30	0.00
	4	109.7	694.1	0.00	12.50	47.50	0.00	9.70	34.60	0.00

Table 7. Initial and final values of surface parameters PV, Srms and Sa, and the p-value for each pair within each test. Cases for which significance is NOT reached are highlighted.

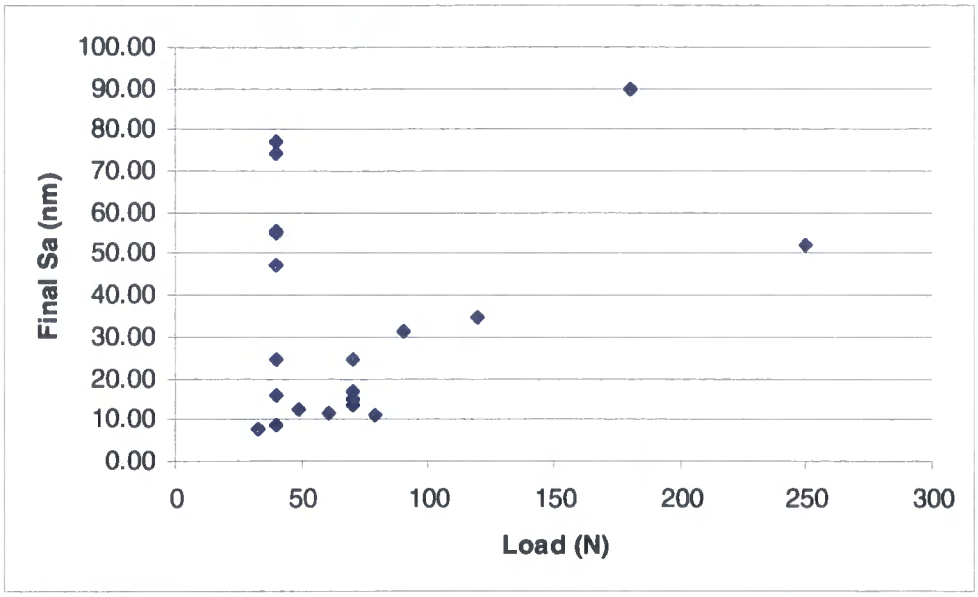

Figure 22. Final Sa of each plate against the load under which it was tested

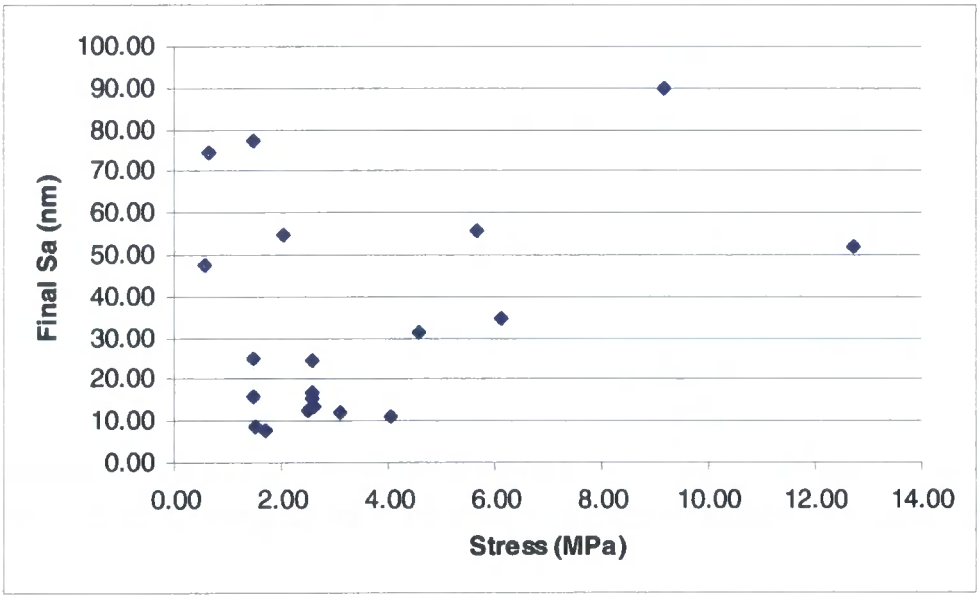

Figure 23. Final Sa of each plate against the nominal contact stress under which it was tested

During the course of testing the machining marks visible on the pin faces were removed, leaving a more polished surface. The mean final Sa was 221-803nm, as can be seen from Table 8. Figure 24 shows the Sa for each pin plotted against the load under which each pin was worn, while Figure 25 shows the same for the contact stress.

It is clear from these two Figures that the final Sa is not related to the either the load or the stress under which the pins were tested (R^2=0.4 and 0.2 respectively).

	PV (nm)	Srms (nm)	Sa (nm)
Test A Durham pin	6277	533	394
Test A Leeds tapered	4121	397	317
Test B pin 1	3038	296	236
Test C pin 1	3751	422	325
Test E pin 5	4404	295	221
Test E pin 6	3823	340	253
Test E pin 7	5589	478	389
Test E pin 8	8139	849	685
Test F pin 3	4836	496	391
Test F pin 4	6415	971	803

Table 8. Mean final values of surface parameters for the UHMWPE pins

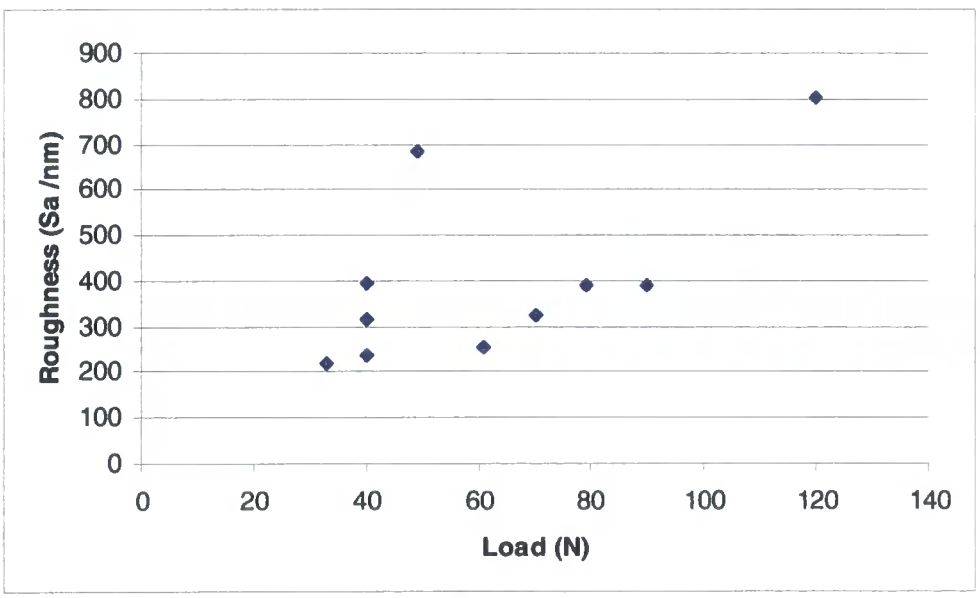

Figure 24. Sa of pins against load under which each pin was worn

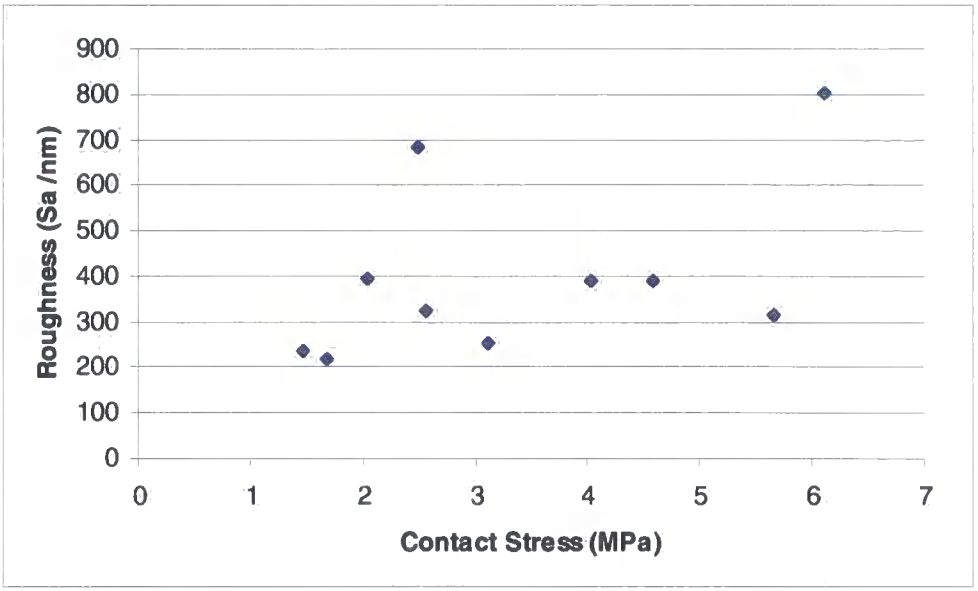

Figure 25. Sa of pins against nominal contact stress under which each pin was worn

For all solid cross-section pins, a nipple became visible at the centre of the pin. This was slightly raised as can be seen in Figure 26 (area of view 181 x 136 μm). In addition some smaller features were seen on the micrographs both at the edges and towards the centre of the pin faces. A typical example is shown in Figure 27 (area of view 181 x 136 μm).

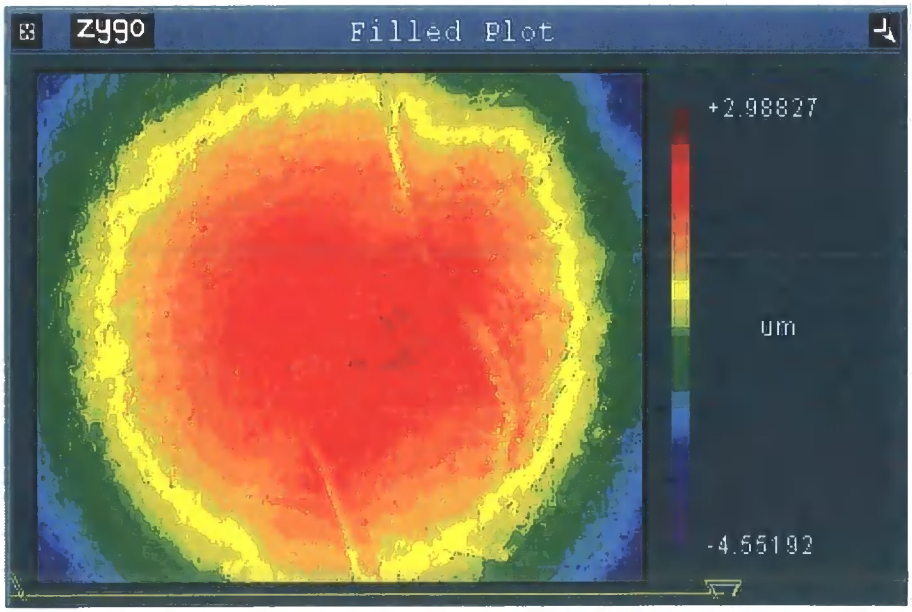

Figure 26. Central nipple on pin 1 of Test B, tested under 40N load and 1.46MPa stress

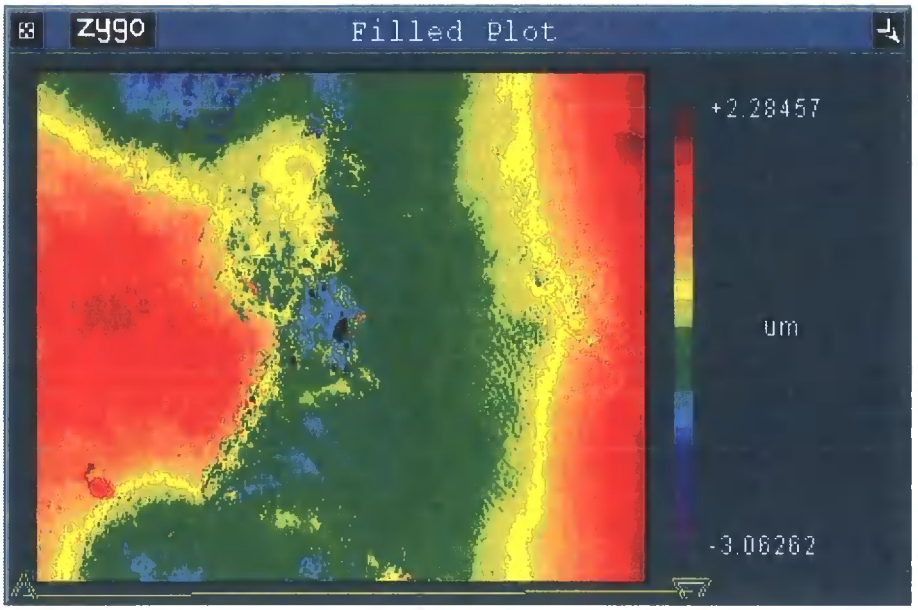

Figure 27. Area of edge of pin 4 from Test F, tested under 120N, 6.11MPa

In addition some multidirectional scratching was noticed in some areas, as seen in Figure 28 (area of view 181 x 136 μm). This image was taken from near the centre of the pin, but is typical of images seen in various areas on many pins.

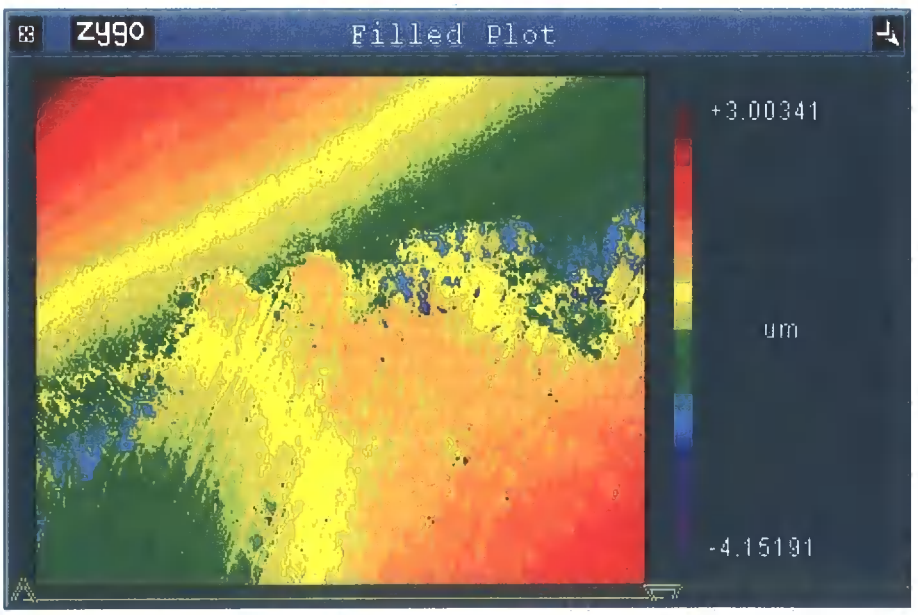

Figure 28. Area of pin 1 Test C, tested under 70N, 2.56MPa showing multidirectional scratching

4.4 Discussion

The wear factors found by Barbour et al[117] were lower than those found in this study by a factor of 100 while those found by Rose et al[118] were higher by a similar order of magnitude. The values found in the Durham Laboratories are, however, comparable with those found clinically. From Dowson and Wallbridge[140] the relationship between volume of wear and clinical wear factor is seen to be $k_{clinical}$=vol/2.376 NWr (neglecting creep). For a volumetric loss of 50mm^3/year on a 22mm diameter Charnley joint, implanted in a 75kg (750N) person, this yields a wear factor of 2.55x10^{-6}mm^3/Nm. This figure was confirmed in a study of over 200 explanted acetabular components[141]. So, whilst the literature contains a wide range of reported wear factors, those from the current work do have clinical relevance.

4.4.1 The effect of pin radius on wear factor

The radius of the pin does not appear to affect the wear factor, at low load and stress, when all other conditions are kept the same. In these tests the nominal face area of each pin is very similar, allowing both load and stress to be kept constant. As such it is expected that the actual contact area will be very similar for all designs of pin[21], and subsequently there is very little difference in the contact of the surfaces on a microscopic scale. However, the results for the higher load and stress test indicate that there may be a larger effect of radius. The wear factor for the highest radius pin was significantly lower than the wear factors on the other pins, which were not significantly different from one another. Further investigation should be undertaken to determine whether there is an effect of radius on the wear factor which is more evident at higher loads.

4.4.2 The effect of applied normal load on wear factor

The wear factor does not seem to be affected by the normal load. For the two cases of constant stress (1.5 and 2.5MPa) the change in applied load causes an opposite trend in the wear factor and in both cases this trend has a very low R^2 value. This is in agreement with the Archard and Lancaster equations[20,22], such that the wear factor is a

constant of proportionality between the volume loss and the product of the load and distance slid for a particular material combination. The Lancaster equation is used to calculate the wear factor and, as such, the load is not expected to have an effect on the wear factor.

4.4.3 The effect of nominal contact stress on wear factor

A decrease in wear factor is seen with increasing nominal contact stress. The relation is found to fit a power-law such that $K=2x10^{-6} \times \sigma^{-0.84}$ with $R^2=0.71$. This indicates that the wear factor becomes less dependent on the contact stress with increasing contact stress. This is consistent with Barbour *et al*[117], but not with Rostoker and Galante[5] or Rose *et al*[118]. Rostoker and Galante find an exponential increase in penetration depth per unit sliding distance with increasing contact pressure, while Rose *et al* find an increasing trend in mass loss with increasing load. While the results are not presented in the same way, they still indicate an increasing trend in the amount of wear with each variable.

4.4.4 Surface Study

The roughness increased along the wear track on the metal components, which is consistent with the slight decrease in mass of the plate over the course of the wear test. The polymeric components became smooth and the concentric machining marks were removed during the test. At the centre of each of the pins with circular face geometry, a nipple became visible. This has been noted in the past by other researchers[142,143].

Interference profilometry is less reliable for the polymeric components since there is some light transmission into the material and not all the incident light is reflected. However, this is intrinsic to the material and hence unavoidable. The scanning parameters are altered to take this into account and while the features of the surface are clearly visible, it is as well to be aware that there is the possibility of greater noise inclusion onto the images.

No correlation was found between the final surface roughness of the pin faces and the conditions of testing (load and stress). Saikko *et al*[130] found a power law relation with

Sa raised to a power less than one. This would suggest a maximum of a 2-fold variation in wear factor over the range of roughnesses seen in this study. Even this variation would not obscure the results found herein, where the wear factors vary by an order of magnitude.

Changes in the surface features of the polymers caused by the articulation are also more difficult to ascertain since the initial surface is machined, and not polished in any way. Thus all surface effects discussed are post wear and are compared with one another not to the initial condition of the polymer surface.

4.5 Conclusions

- Wear factor decreased as nominal contact stress increases for UHMWPE vs Stainless Steel: $K=2x10^{-6}x\sigma^{-0.84}$.
- Pin load did not appear to affect wear factor. This is expected.
- Pin radius did not significantly affect wear factor at low loads and stresses. The wear factor does seem to decrease with increasing average pin radius at the higher stress tested in this study, mainly due to one particularly low result. Further tests would be required to determine whether the effect of radius becomes more pronounced at higher stresses.
- Concentric machining marks on pins were removed during testing.
- Central nipple and multidirectional markings became visible on pin.
- Plates became significantly rougher. This roughness increase did not correlate with testing conditions or initial plate roughness.
- Initial and final plate roughness did not correlate with pin wear factor.

5 Ceramic Clearance Study

5.1 Introduction

The radial clearance of a ball and socket is known to have an effect on the lubrication mechanisms present, as discussed in Chapter 2, Section 2.8.2. The thickness of the lubricant is dependent upon the radial clearance, through the parameter $R_x = R_1R_2/(R_1-R_2)$, where R_1 and R_2 are the radii of the two components respectively. R_x is raised to the power of 0.76 overall in the equation for film thickness, and as such the lubricant thickness is expected to increase with increasing values of R_x, and hence with decreasing radial clearance, although, of course the value of the product R_1R_2 will also change as the exact values of the radii change.

Previous studies however, have been unable to determine an effect of radial clearance experimentally, somewhat because of the extremely low wear rates observed for ceramic-on-ceramic joints. In the study by Clarke *et al*[71] although a wear trend became visible after a long wear test (14 million cycles) there was still too much variation in mass for each joint to enable subtle differences in wear caused by clearance to be seen. Similarly over 5 million cycles Scholes *et al*[115] found no detectable wear gravimetrically for 28mm joints, and as such was unable to confirm an effect of radial clearance. Friction tests indicated a difference in behaviour for different clearances over a range or 23-78μm[129]. When tested with CMC lubricant, 33 and 74μm gave the highest friction values while 23, 40 and 48μm gave lower values.

In this study the effect of the radial clearance was investigated for 32mm alumina ceramic joints and compared with predictions. The joints were initially friction tested and then some of the joints were wear tested. The surfaces were also monitored for any changes in observed features.

5.2 Materials and methods

5.2.1 Materials

5.2.1.1 Bovine Serum Lubricant

The lubricant used was newborn calf serum supplied by Harlan Sera-Lab; batch number 8030901. Chemical analysis of the serum by the supplier showed that the total protein concentration in undiluted serum was 52g/*l*. The serum was diluted to 25% concentration by volume with distilled water and 0.1% sodium azide to reduce bacterial degradation of the lubricant. This resulted in a protein concentration of 13g/*l*. For this test some supplementary serum was supplied by TCS Biosciences Ltd, batch number 97623 with a total protein concentration of 74.4g/*l*. This was diluted to 17.5% to retain the same total protein concentration for the lubricant throughout the test.

5.2.1.2 CMC Fluid Lubricant

Sodium carboxymethylcellulose salt (CMC) was dissolved in distilled water in varying amounts to produce lubricants with viscosities of 0.102, 0.031, 0.010, 0.003 Pa s. Each viscosity was prepared by an iterative process of measuring the viscosity using a Ferrati-Shirley, cone-on-plate viscometer at a shear rate of $3000s^{-1}$. The amount of distilled water or CMC was adjusted as appropriate, to create the desired viscosity. Distilled water with no added CMC (η=0.001Pa s) was used as a 5th lubricant. Aqueous solutions of CMC are shear thinning and were used due to their similar rheological properties to synovial fluid[36].

5.2.1.3 Alumina Ceramic

Alumina ceramic joints of 32mm diameter were supplied by Morgan Advanced Ceramics. These were of HIP Vitox Alumina, and were manufactured in accordance with ISO 6474. The average grain size was 1.2μm, the Poisson's ratio was 0.25, the Young's modulus 407GPa and the density was $3.978Mg/m^3$. The components were 'paired' to provide a series of radial clearances for friction and wear testing. Their roughness was measured on the Zygo NewView 100 non-contacting optical

interferometer both before and after friction and wear testing. The initial roughnesses were found to be between 2.0 and 11.0 nm. The mechanical properties needed for theoretical calculations were taken from a data sheet provided by the manufacturer.

Table 9, shows how the heads and cups were paired together to achieve a range of radial clearances, and the tests carried out on each combination.

Head Ref number	Cup Ref Number	Radial Clearance/μm	Test performed
14	21	35	Wear and Friction
12	18	42	Wear and Friction
17	03	57	Wear and Friction
03	15	64	Wear
15	11	69	Wear
20	08	55	Wear (Control) and Friction
18	17	34	Friction
13	16	42	Friction
09	02	53	Friction
08	10	70	Friction
16	04	73	Friction
06	07	76	Friction
07	04	84	Friction

Table 9. Radial clearances and tests performed for each joint pair.

5.2.2 Methods

5.2.2.1 Friction Study

The components were paired in different combinations (Table 9) to produce a range of clearances. Each joint was placed in the simulator and was tested 3 times with each of distilled water, the 4 viscosities of CMC fluid, and 25% bovine serum. A numerical

average and standard deviation of the friction factor and Sommerfeld number was taken for each lubricant. The average values of friction factor were plotted against those of Sommerfeld parameter to produce a Stribeck plot. The friction and lubrication behaviour of the joint pairs was determined from analysis of the Stribeck plot. The joints surfaces were imaged and analysed, as described in Section 5.2.2.3, before and after friction testing.

Each joint pair was cleaned before each run in the friction simulator. The excess lubricant was removed using a tissue, and then the joint was wiped with a tissue and water, then acetone, to ensure that all the lubricant was removed. In the case of bovine serum lubricant, the joint was additionally wiped with Gigasept, before being wiped with acetone.

5.2.2.2 Wear Study

Five joints and 1 control were placed in the simulator. The heads were mounted on removable tapers which comprised a stainless steel core and thread enabling them to be placed in the simulator. The taper itself was machined from PMMA cast onto a grooved inner stainless steel taper. This was to avoid any metallic transfer on the head taper, which would affect the mass of the ceramic, while allowing a thorough and consistent cleaning of each component. To allow the tapers to be removed, each head, while still attached to the taper, was placed in the freezer, for 30 minutes. The head was then removed using a jig made in-house. The heads and tapers were allowed to return to room temperature before the cleaning protocol was begun.

The components were removed from the rig approximately every 0.5 million cycles and cleaned using the protocol described in Appendix C, Section C.3. The components were weighed 3 times and an average was found; the mean and standard deviation of the component masses are given in Appendix D, Section D.1. Each part of the rig was removed and cleaned by brushing lightly in 1% neutracon solution, then rinsing in distilled water. Once each cell had been reassembled, the 5 test joints were placed into the rig, and the control cell was replaced by a load cell, attached to an oscilloscope. The

loading profile was printed out and checked before the control cell was replaced and the test restarted.

Basic rig maintenance was observed and the rig was serviced and checked before testing began.

5.2.2.3 Surface Study

The surfaces of the cleaned components were monitored for any changes using Non-contact Optical Interferometry (NCOI). Due to the size of the lens, it was only possible to see the polar region of the cup. An image and surface roughness data were obtained using the appropriate applications of the NCOI Software.

The AFM was used to image the heads, on the pole, at 45° and at 90° to the pole, before and after friction testing. A scan of 100microns square was captured, and then some additional scans were done by zooming in on portions of the initial image as necessary. The images were analysed using the analysis tool on the AFM software, and surface information was obtained. The AFM geometry does not allow it to be used to image deep hollows and as such it was not possible to use this technique on the cups.

Some of the components which had been friction tested were subsequently tested in a short wear test. During this test these components were imaged on the pole after 0.6, 1.1 and 1.7 million cycles, and the results are presented in the results section. The wear test was carried out according to the same protocol as the wear test described in Section 5.2.2.2. For the wear test described herein, however, the components were imaged only at the end of the wear test using NCOI.

5.3 Results

5.3.1 Friction results

Each joint with its particular clearance was friction tested at 5 different viscosities of lubricant. The results were thus plotted by radial clearance and by viscosity. Figure 29

shows the Stribeck plot for the smallest clearance and Figure 30 for the largest clearance tested. Both joints can be seen to exhibit a partial fluid film. The joints with smaller clearances moved into fluid film at lower viscosities than the larger clearance joints.

The vertical dotted line represents the λ=3 line, which was calculated theoretically. This was done by working backwards from the equation for λ to obtain the h_{min} needed for fluid film and then going back through the equation for h_{min} to obtain the value of viscosity at which the transition to fluid film occurs. This was converted to a Sommerfeld number. Throughout the calculations, the values of entraining velocity and load were taken to be those under which the friction was measured, i.e. u= 0.017ms^{-1}, L=2000N.

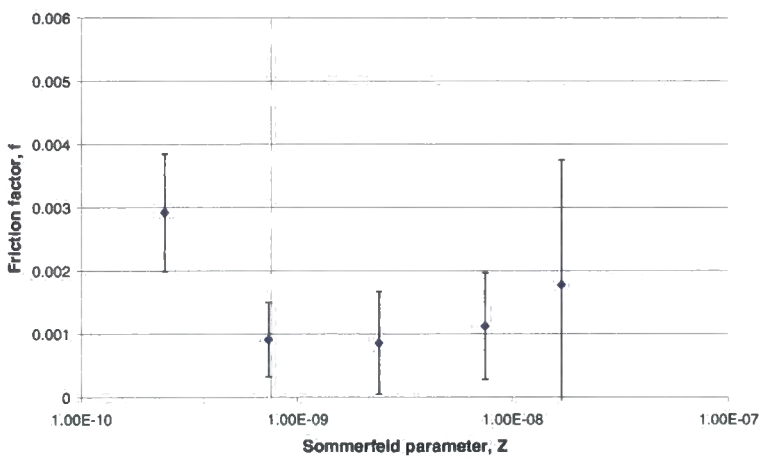

Figure 29. Stribeck plot for 32mm diameter alumina couple with 34micron radial clearance; the dotted line is the theoretical λ=3 line.

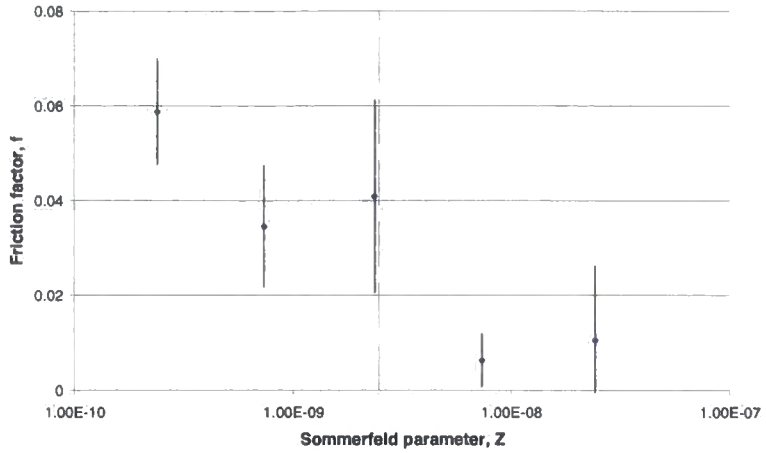

Figure 30. Stribeck plot for 32mm diameter alumina couple with 84 micron radial clearance; the dotted line is the theoretical λ=3 line.

Taking all joint data for a particular viscosity and plotting the friction factor against the radial clearance indicates the effect of the clearance. Figure 31 shows the friction factor for all clearances when tested with 25% bovine serum. The friction factor remained almost constant for all clearances, except for the largest clearance which had a slightly larger friction factor.

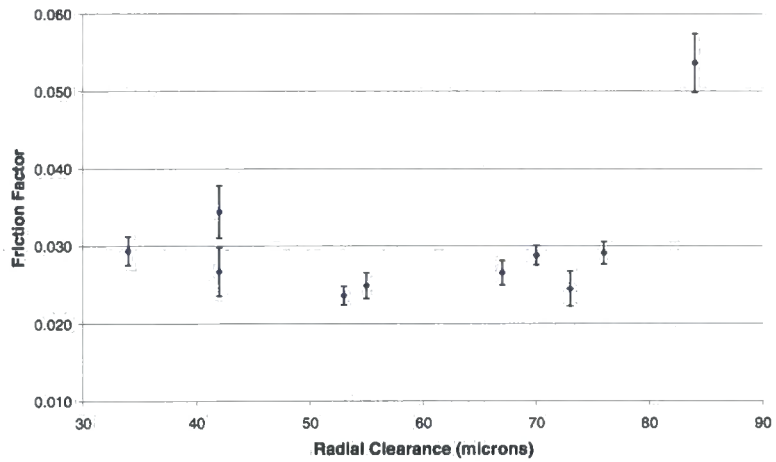

Figure 31. The effect of radial clearance on friction factor when tested with bovine serum lubricant

However, when tested with the lubricants that did not contain proteins, a dependence of friction factor on radial clearance was seen. Figure 32 shows the friction factors for all the clearances when tested with 0.1 Pa s viscosity CMC fluid. The larger clearances are seen to have a slightly higher friction factor than the smaller ones, while the friction

factor itself was lower than when bovine serum was used (0.03 for bovine serum, 0.01 for 0.1Pa s CMC in most cases). Even in the case of the 84μm clearance joint, which showed the highest friction factor, the value found with CMC fluid as a lubricant is lower than that with bovine serum lubricant. The increasing trend for high clearances is more evident with the 0.01Pa s lubricant as seen in Figure 33. The increase in friction factor was greater than for the more viscous lubricant, reaching 0.04.

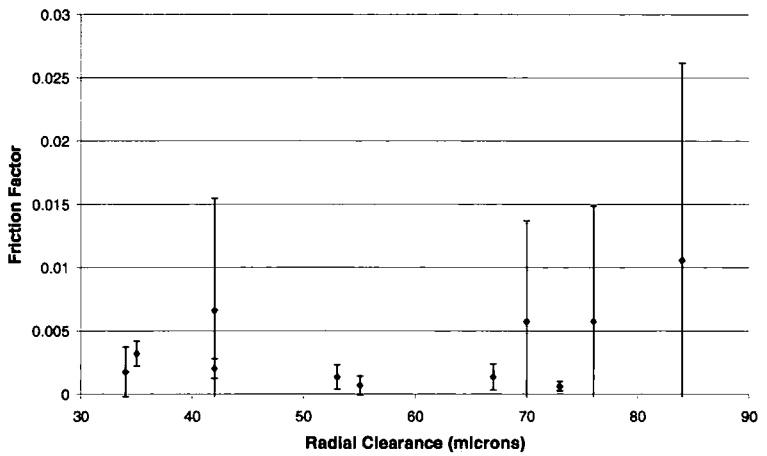

Figure 32. The effect of radial clearance on friction factor when tested with 0.1 Pa s CMC fluid

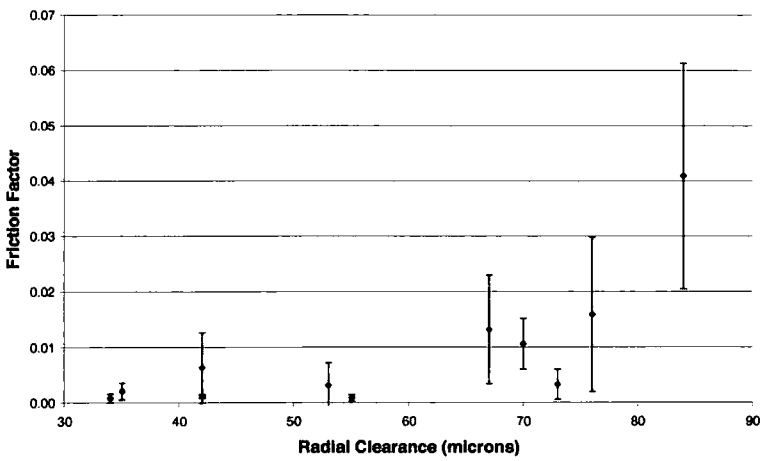

Figure 33. The effect of radial clearance on friction factor when tested with 0.01Pa s CMC fluid

This was even more evident with the joints tested with distilled water as a lubricant as seen in Figure 34. The highest friction factor seen in this case was around 0.06

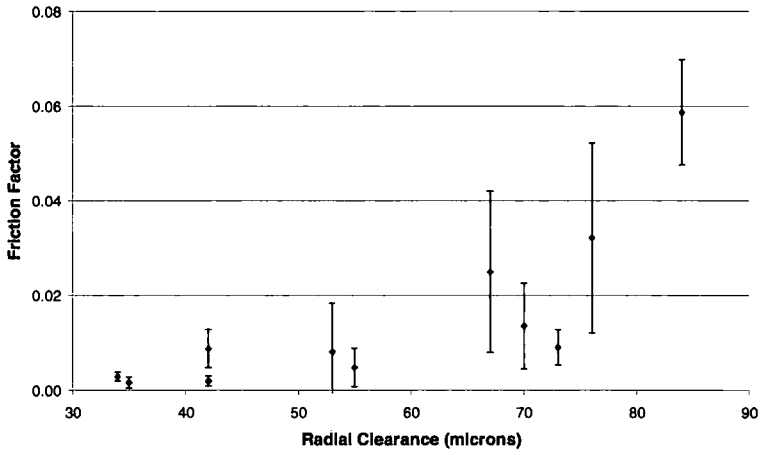

Figure 34. The effect of radial clearance on friction factor when tested with distilled water

5.3.2 Wear results

The mass change of each component was plotted during the course of the simulator wear test. Figure 35 shows the mass change for the heads over the course of the test. Head 4 shows a decrease in mass initially but not thereafter. Beyond this initial jump for head 4, all joints show a variation in mass, but overall the wear rate fluctuated about zero. Figure 36 shows a similar pattern for the cups but in this case Cup 2 shows a large decrease in mass after 1 million cycles, and thereafter follows the other components. The data for head and cup are combined and Figure 37 shows the total mass change per joint.

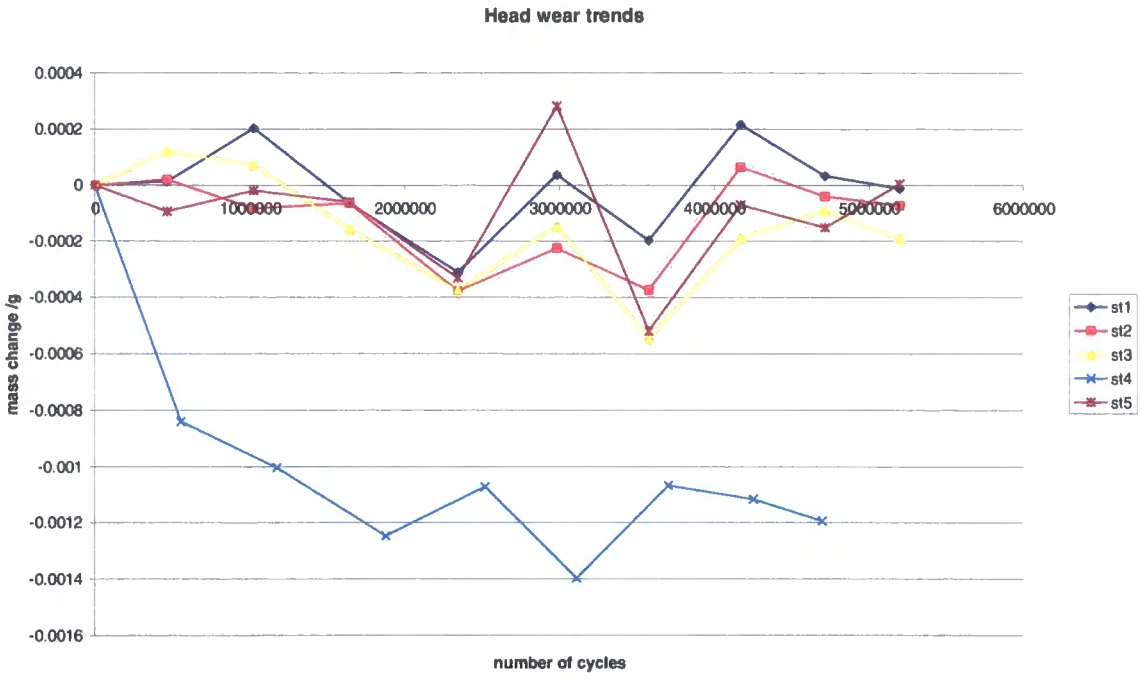

Figure 35. Mass change of femoral components during the course of wear testing

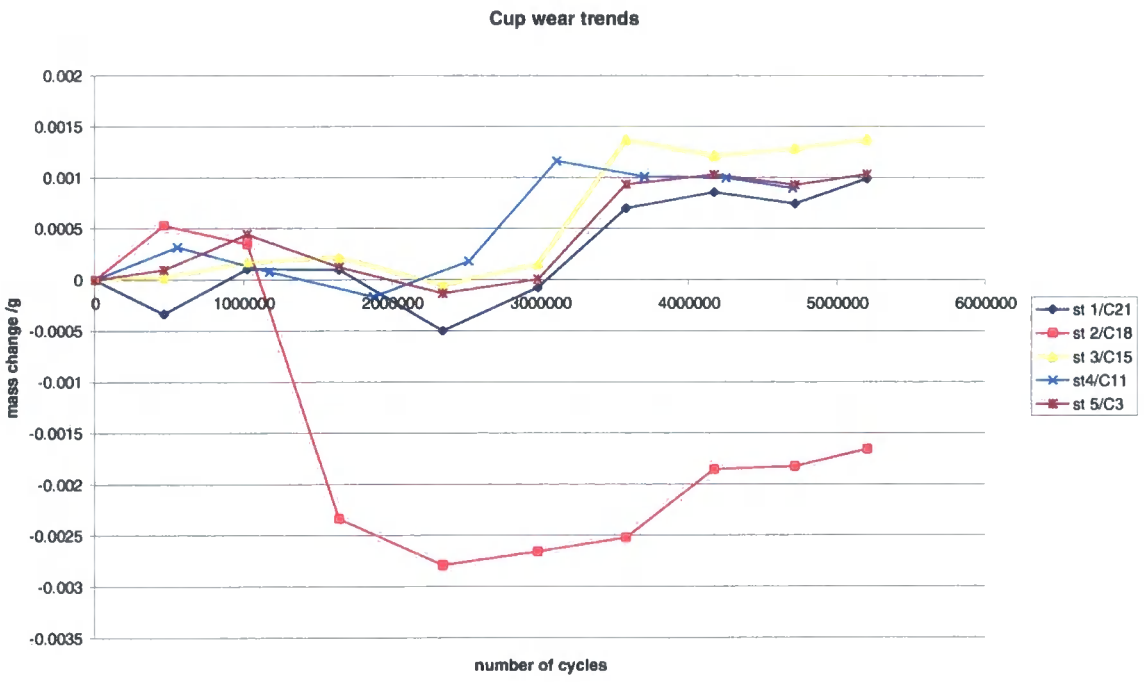

Figure 36. Mass change of acetabular components during wear testing

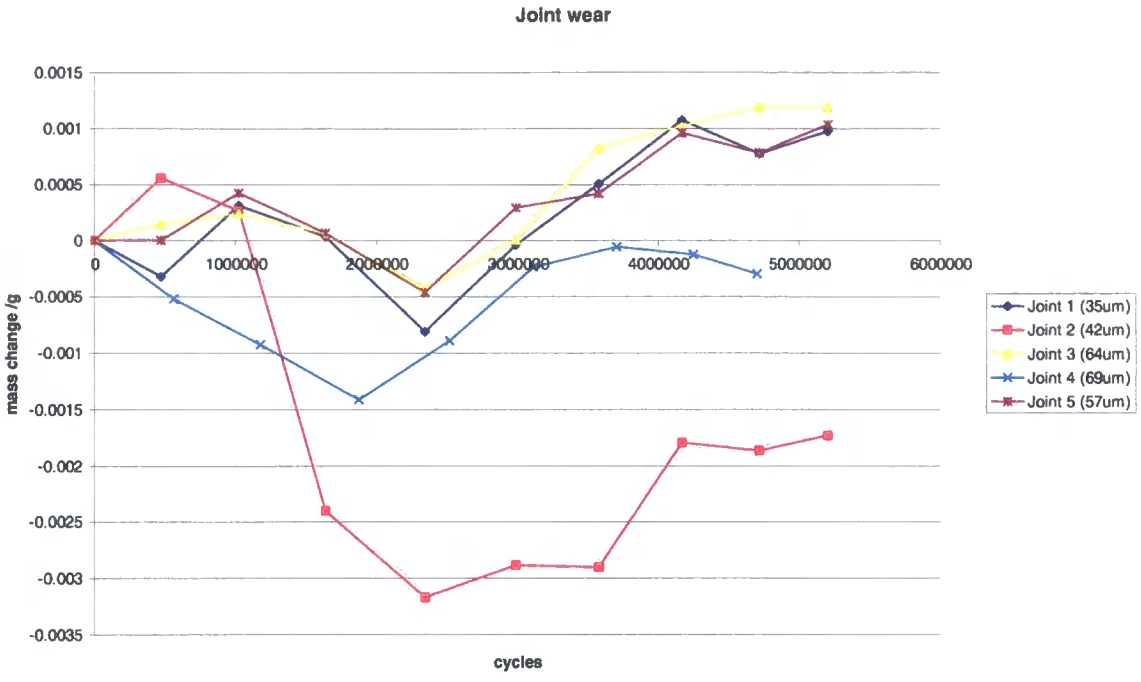

Figure 37. Combined mass change for head and cup pairs over 5 million cycles of wear testing

Overall the mass of the joints (other than Joint 2) did not change much, but fluctuated throughout the test. There was a slight increasing trend on the mass of Joints 1, 3 and 5, indicating the possibility of some transfer which was not removed by the cleaning regime. However, there was no discernible effect of clearance on the wear behaviour of the joints.

5.3.3 Surface study results

The polar regions of the femoral components were imaged by AFM before and during various stages of a wear test. Figure 38 shows an untested component on which multidirectional polishing scratches are clearly visible. Figures 39 and 40 show the initial surface condition at 45° and 90° to the pole respectively. These are typically 10nm deep. After as few as 1500 cycles of testing these scratches were slightly diminished, but also the granular structure of the ceramic became visible (Figure 41). The grain size was typically around 2μm. After 0.6 million cycles, Figure 44, the polishing scratches were almost completely removed and granular pullout was visible. The average depth of the pullout was approximately 10-15nm.

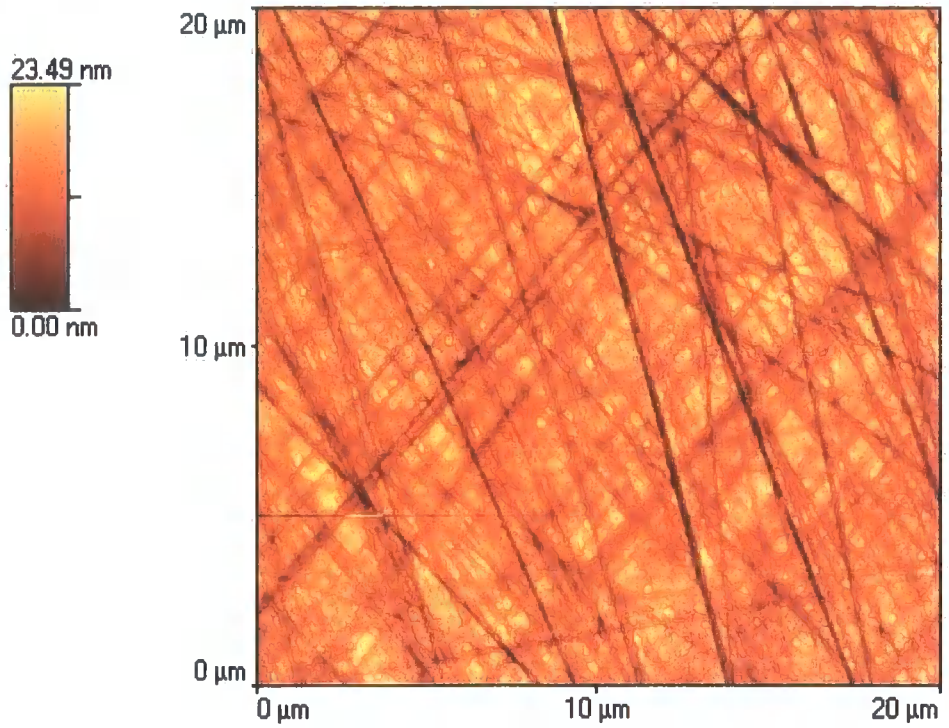

Figure 38. AFM image of the polar region of an untested femoral head.

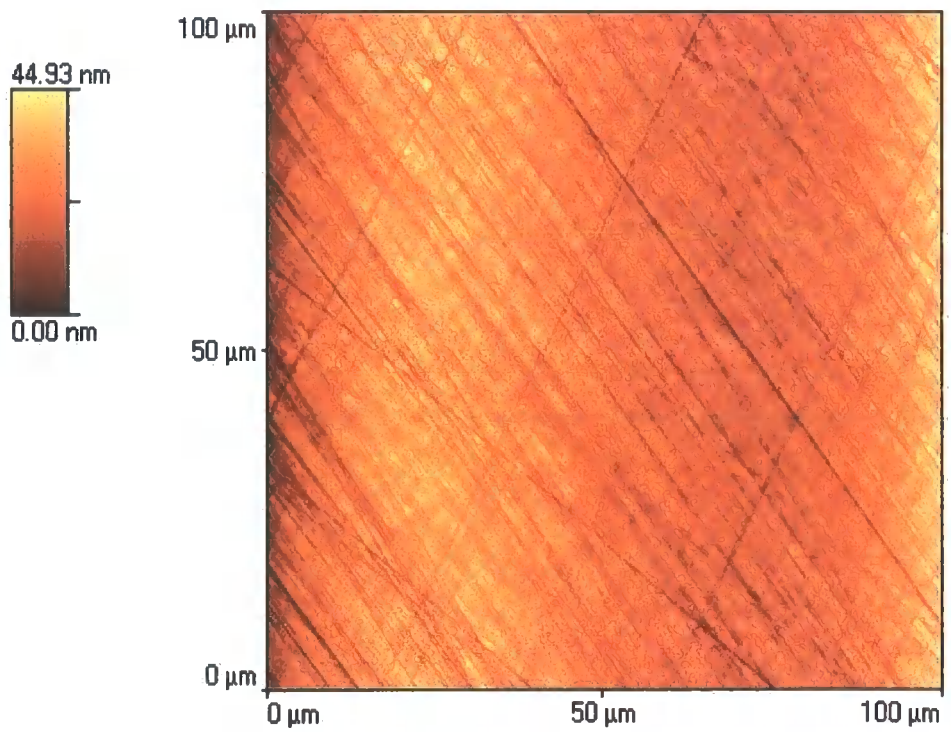

Figure 39. Initial AFM scan of ceramic head at 45° to the pole

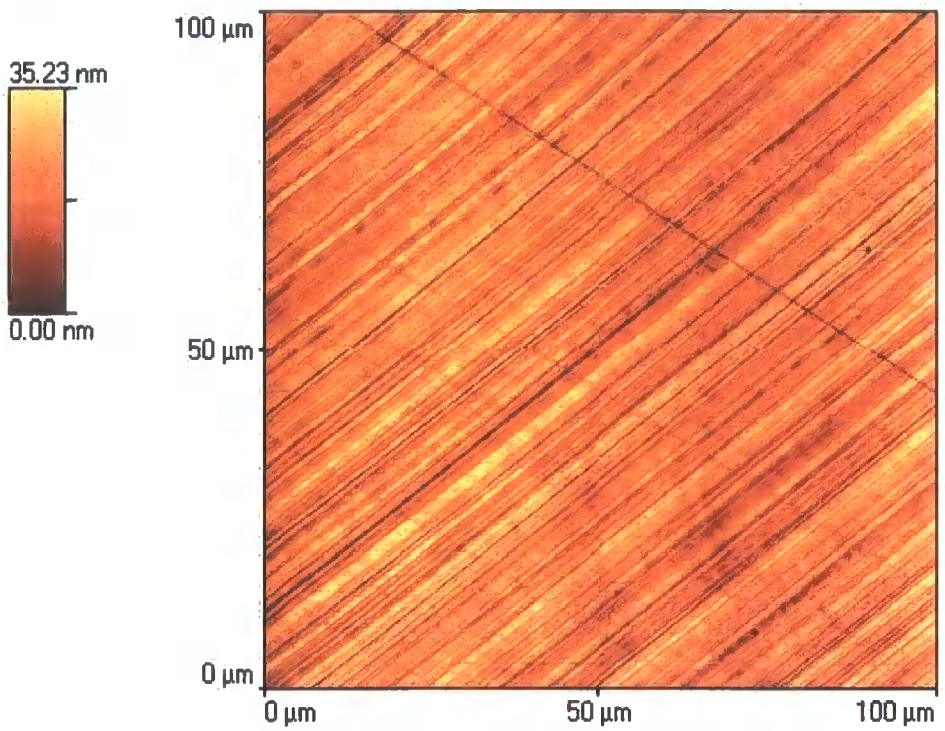

Figure 40. Initial AFM scan of ceramic head at 90° to the pole

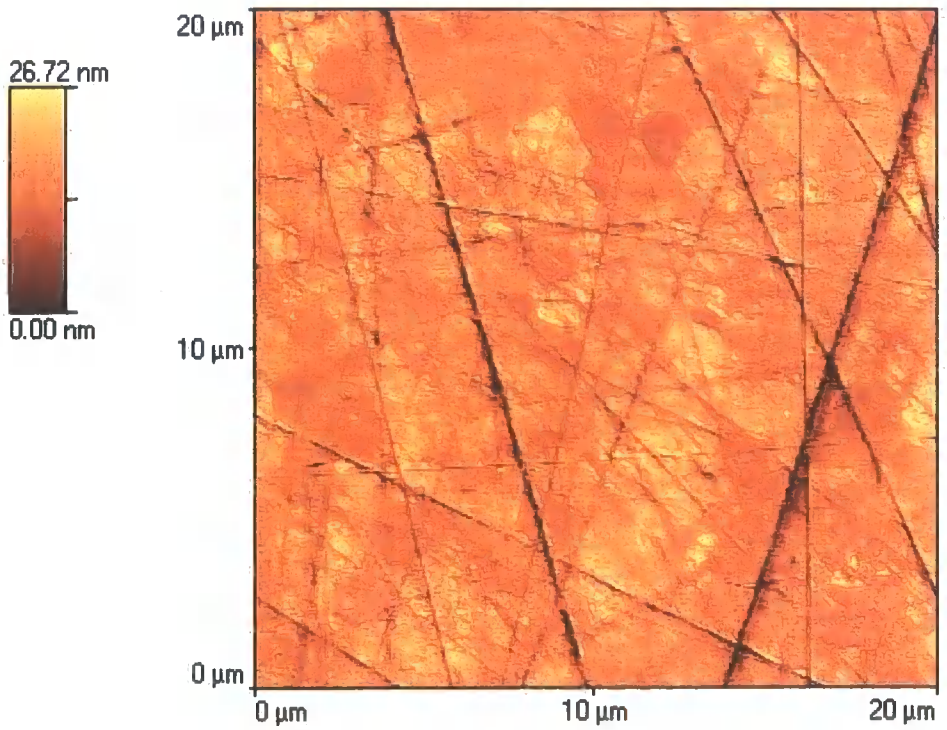

Figure 41. AFM image of the polar region of a femoral head after friction testing (approx. 1500 cycles)

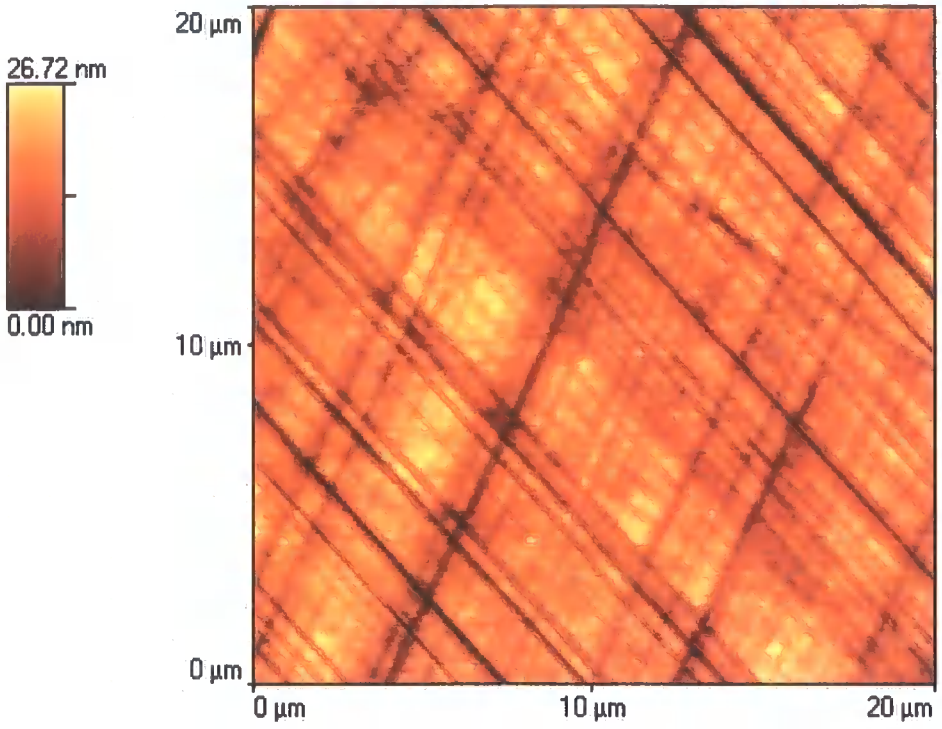

Figure 42. AFM scan after friction testing (approx 1500 cycles) at 45° to the pole

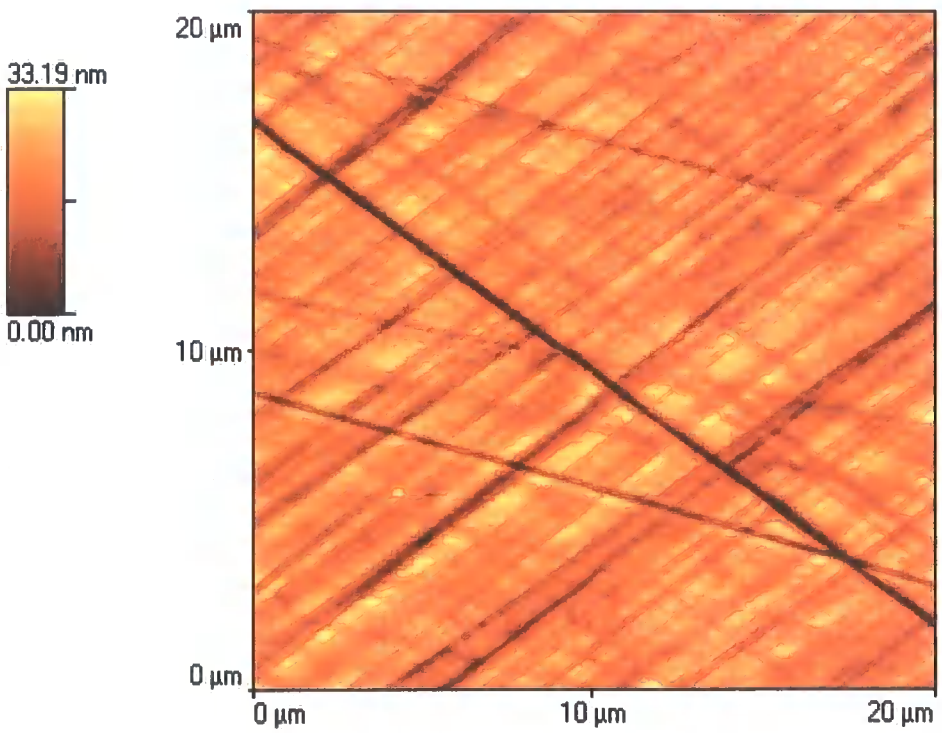

Figure 43. AFM scan of ceramic head after friction testing (1500 cycles) at 90° to the pole

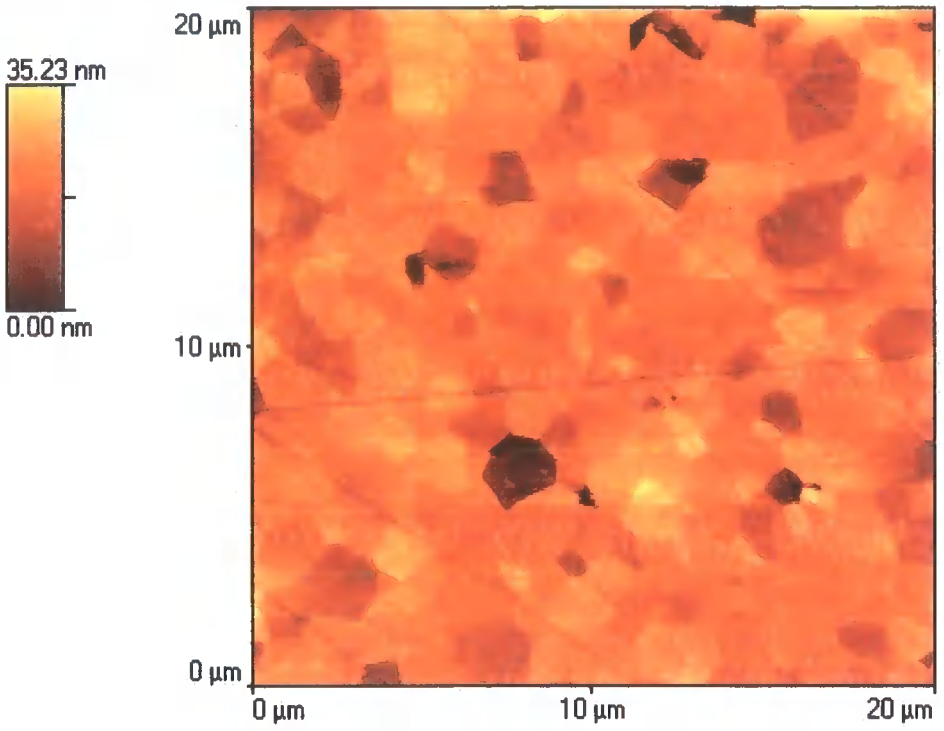

Figure 44. AFM image of polar region of a femoral head after approx 0.6 million cycles of wear testing

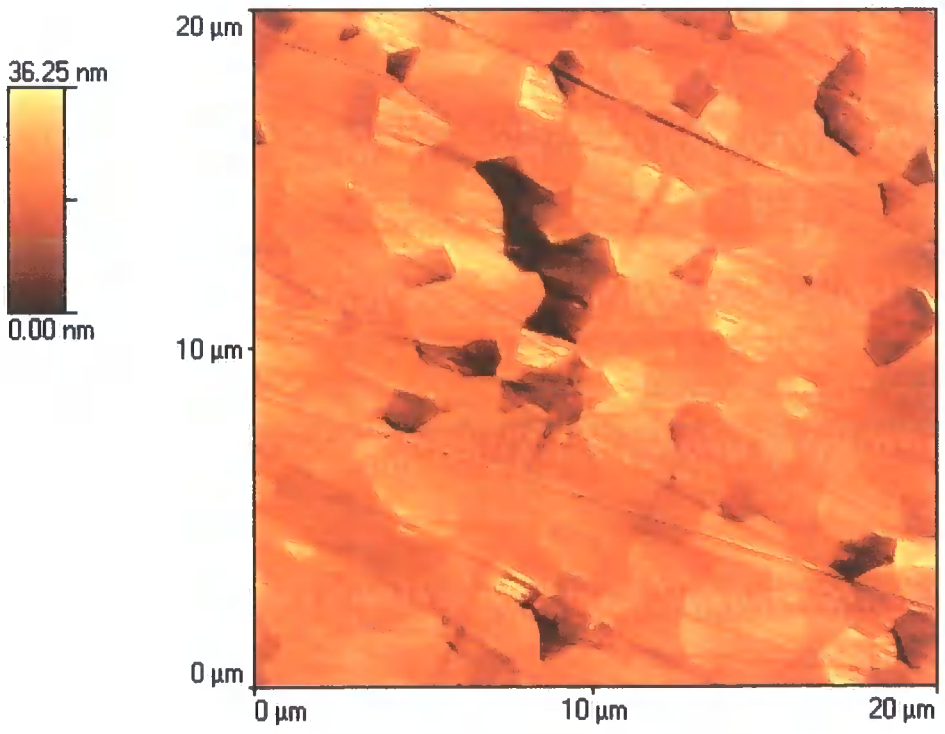

Figure 45. polar region of ceramic head after approximately 1.1 million cycles of wear testing

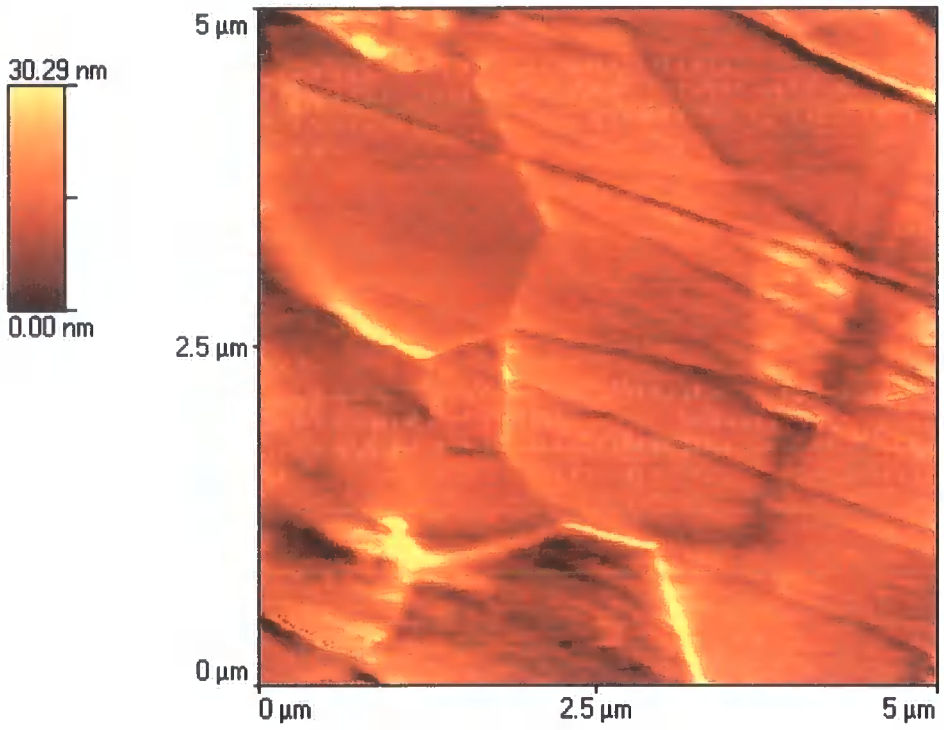

Figure 46. 5 micron squared region of ceramic head after 1.1 million cycles of wear testing

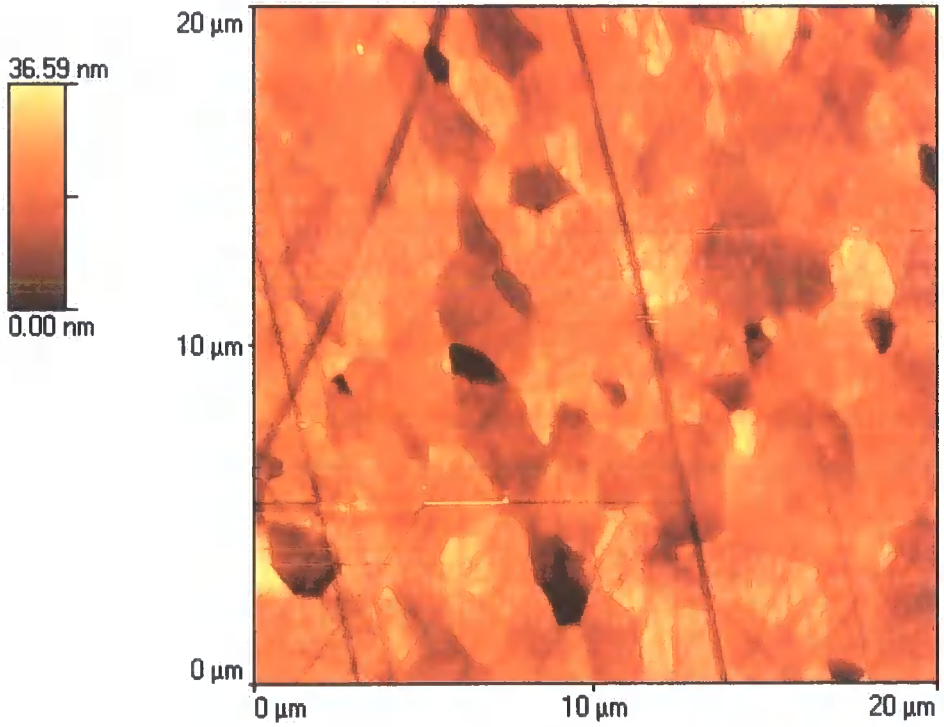

Figure 47. polar region of head after 1.7 million cycles of testing.

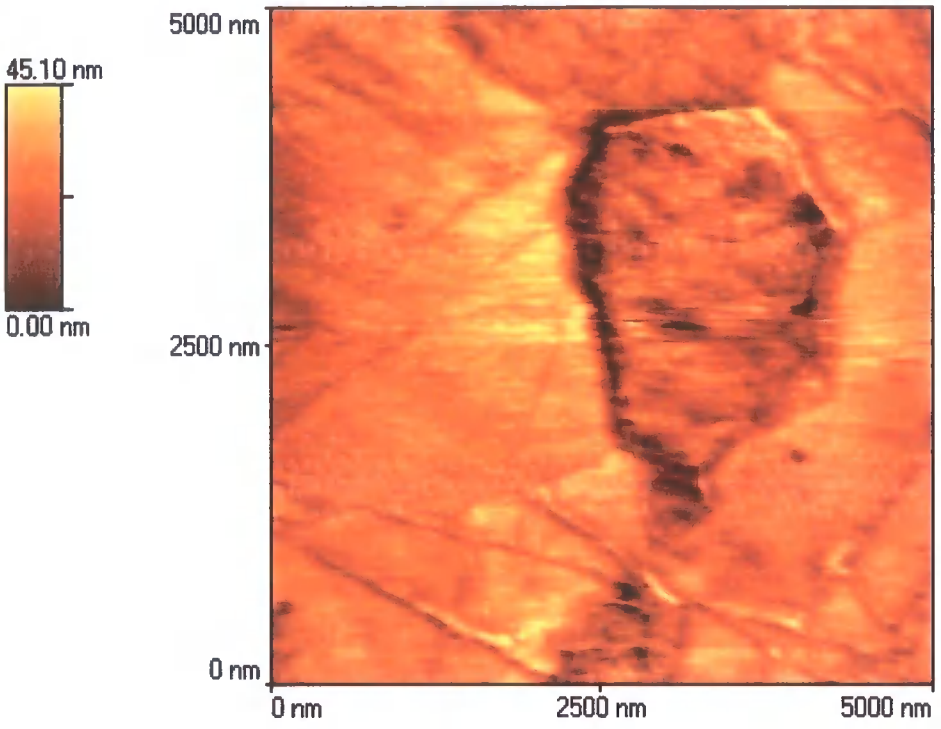

Figure 48. close up of polar region of femoral head after 1.7 million cycles of testing.

5.4 Discussion

5.4.1 Friction study

Stribeck plots for each joint show that at low clearances the joint exhibits fluid film lubrication and that it may operate in the fluid film regime at physiological viscosities. The friction factors for the 34μm clearance joint are lower than 0.003 in all cases. The joints with larger radial clearances also exhibit fluid film lubrication, but not at such low viscosities as the small clearance joints.

When tested with bovine serum lubricant, all joints showed a similar friction factor, regardless of the clearance. This has been seen by other workers on ceramic-on-ceramic joints[144]. The friction factor was around 0.03, except in the case of the highest clearance joint which had a friction factor of 0.055. The friction factors were always higher in the presence of bovine serum. In addition, other tests have shown a similar friction factor in large diameter metal-on-metal joints in this laboratory[103] (See Chapter 7). This coupled with the fact that most of the joints showed a similar friction factor regardless of clearance, indicates that the friction may be induced by shearing of the proteins

themselves. The protein molecules are large in relation to the generated film thickness. This is an indication that the presence of the proteins acts as a boundary lubricant, but increases the friction substantially. Albumin and immunoglobulin-G adsorbed to surfaces can form layers of typically 8 - 12nm[145]. Applying the Hamrock and Dowson equation[34] to a 53 μm clearance joint used in this study, suggests a film thickness of 21nm at the viscosity of bovine serum. Clearly the proteins could interfere with the fluid film lubrication mechanism in such a case.

The effect of the clearance is clearly visible when the friction factor is plotted directly against the radial clearance for each viscosity independently. As expected from theoretical calculations[34], the radial clearance has a more marked effect at low viscosities. The friction increased with increasing clearance. While this was also the case with the higher viscosities, the increase in friction factor appeared only for higher clearances.

At high viscosities, the effect of the clearance on the film thickness was less pronounced, since the viscosity of the lubricant induced a thicker film. At lower viscosities, the effect of changing the clearance was much more pronounced, since the film thickness induced by the lubricant was smaller.

The minimum film thickness was calculated theoretically by $h_{min} = 2.798R_x\left(\frac{u\eta}{E'R_x}\right)^{0.65}\left(\frac{L}{E'R_x^2}\right)^{-0.21}$ [34], where: R_x=equivalent radius, u=entraining velocity, η=viscosity, E'=equivalent modulus of elasticity, L=normal applied load. See also Chapter 2, Section 2.6.3.3.

So for a given experimental arrangement (load, entraining velocity, eccentricity ratio and equivalent elastic modulus), the equivalent radius and the viscosity are the two factors which affect the film thickness. All the joints in this study had the same nominal diameter of 32mm. The equivalent radius takes into account the actual radii of the components in a pair and as such is, in this case, a measure of the radial clearance. From this we can see that the theoretical analysis supports the experimental evidence.

5.4.2 Wear Study

No discernible correlation was seen between wear behaviour and clearance up to 5 million cycles. Much variation was noted around a value after an initial or subsequent jump on some components, notably head 4 and cup 2.

5.4.3 Surface study

Initially the surfaces showed multidirectional polishing scratches. These were typically 10 nm deep. Off pole, the scratches were less random in the orientation. After only a few cycles (approximately 1500) the polishing scratches were diminished and grain structure of the ceramic became visible on AFM images. The typical size of the grain was around 2 μm. This feature was not visible at 45° and 90° to the pole where the original scratches were retained. This is expected since these regions were not in the contact region.

After 0.6 million cycles granular pullout was seen on the ceramic surfaces. The average pullout depth was approximately 10-15nm. This became more apparent as the wear test continued. Looking at the close-up of the grain pullout in Figure 46 we can see that some scratching is still evident over the granular pullout regions.

Although the wear was undetectable using gravimetric techniques, the difference in surface morphology after only a few cycles was undeniable. This indicates that wear really does occur, and has been seen in similar tests with 28mm alumina ceramic joints[86,115]. The polishing scratches were diminished and the grain structure of the ceramic was visible after only 1500 cycles. After 0.6 million cycles, equivalent to 7-8 months in vivo, granular pullout was clearly visible. This is, however, a small mass loss undetectable even after 5 million cycles of testing. There was no detectable difference in the response of the ceramic surface based on joint clearance effects.

5.5 Conclusions

- The ceramic components showed no detectable wear over 5 million cycles of wear testing. As such, any difference in wear rate due to radial clearance was not detectable.
- The radial clearance had a marked effect on the friction and lubrication regime under which the joint worked with CMC lubricant:
    - The friction factor was seen to increase with increasing radial clearance, as predicted by theory.
    - For low viscosities this variation was more marked than for higher viscosities since the film induced by the lubricant was already thicker in the case of the high viscosity fluids.
- The friction factor found in the presence of proteins (bovine serum), was higher than for the same joint tested with CMC fluids. The larger friction factor was thought to be caused by protein molecules being sheared, as indicated by the similarity in friction factor over the range of clearances.
- Although wear was undetectable gravimetrically, some wear did occur, as evidenced by the surface morphology changes that were noticed:
    - The polishing scratches began to be diminished visibly after only 1500 cycles. At this point also, the granular structure of the ceramic was visible, although no deep pullout was noted.
    - Granular pullout was noted after just 0.6 million cycles and continued thereafter.

6 Ceramic Roughness Study

6.1 Introduction

Roughness of the articulating surfaces is known to have an effect on the tribology of bearing surfaces. Predictions of fluid film behaviour are based on λ, the ratio of the film thickness to the combined roughness in a wear couple. Clearly for a component with a larger roughness, asperities would be expected to break through the lubricant film and interact with the asperities of the other surface in the couple. As a result the joint would be expected to operate in the mixed lubrication regime, and some wear would be likely. As such a higher roughness would be predicted to show a higher degree of asperity interactions for the same film thickness and hence show an increased probability for the production of wear particles: a higher wear rate.

This has been investigated experimentally, particularly in the case of the roughness of the harder surface in hard-on-soft combinations[8,130,146,147]. In ceramic components a much lower roughness can be achieved than in metallic or polymeric components and accordingly ceramic on polymer combinations show lower wear rates than metal-on-polymer.

Explanted ceramic-on-ceramic components seen by the author have a typically higher roughness than as-new components and a wear area is clearly visible by eye. However, laboratory tests have shown so little wear as to be beyond detection gravimetrically [71,115]. While this is encouraging for all-ceramic bearings, it does not offer much to further our understanding of wear mechanisms prevailing.

In this study the roughness was deliberately increased on some components in an attempt to understand the effect of this parameter on the tribology of ceramic-on-ceramic THR. One component in each pair was roughened in the hope of gleaning information about the lubrication regimes operating within the joints. Extensive friction testing was carried out to investigate this and roughness was measured after each stage of friction testing. Then a short wear test was carried out to determine whether the

change in roughness would induce any wear on these components while undergoing a normal simulator walking cycle.

6.2 Materials and Methods

6.2.1 Materials

6.2.1.1 Ceramic Components

Ceramic hip components were supplied by Morgan Advanced Ceramics. The material used was HIP Vitox Alumina and was identical to that described and used in Chapter 5. The nominal radius was 28mm, and the exact radius of each component was determined by measurement using a Coordinate Measuring Machine (CMM). After establishing coordinates on the component, six line scans were taken at 30° to one another. A best fit circle was fitted to each line-scan and the average of the radii was taken as the radius for each head or cup. The initial and subsequent roughness of the surfaces was measured on the Zygo NewView100 NCOI. Details of the starting condition of each cup is given in Table 10 and for each head in Table 11.

Cup	Average Diameter (mm)	Standard deviation in diameter	Initial PV (µm)	Initial Srms (µm)	Initial Sa (µm)	Initial Ssk
10	28.054	0.002	0.416	0.008	0.007	-1.874
18	28.068	0.001	0.359	0.008	0.006	-1.493
20	28.054	0.003	0.607	0.009	0.007	-2.012
22	28.037	0.002	0.668	0.009	0.007	-6.729
29	28.071	0.002	0.393	0.008	0.006	-1.668

Table 10. Diameter and initial surface parameters for ceramic cups

Head	Average Diameter (mm)	Standard deviation in diameter	Initial PV (μm)	Initial Srms (μm)	Initial Sa (μm)	Initial Ssk
06	27.990	0.001	0.226	0.009	0.007	-0.138
08	27.990	0.000	0.162	0.01	0.008	-0.059
23	27.991	0.001	0.283	0.01	0.008	-0.174
26	27.991	0.001	0.352	0.009	0.007	-1.01
28	27.994	0.001	0.309	0.009	0.007	-1.005

Table 11. Diameter and initial surface parameters for ceramic heads

Two heads and two cups were worn together in the wear simulator with a small amount of 6μm diamond paste [Buehler] for 2 hours, to increase the roughness in the polar contact region of these components. The new surface parameters for these components are given in Table 12.

Roughened Component	PV (μm)	Srms (μm)	Sa (μm)	Ssk
Cup 10	26.903	0.407	0.271	-7.234
Cup 22	0.521	0.028	0.022	-0.578
Head 06	0.691	0.025	0.018	-1.231
Head 26	0.551	0.023	0.016	-1.999

Table 12. Roughness parameters for roughened components

6.2.1.2 Lubricant

Solutions of sodium carboxymethyl cellulose[36] in distilled water were used in various concentrations to achieve lubricants of different viscosity for friction testing as described in detail in section 5.2.1.2. The viscosities used were 0.1, 0.03, 0.01 and 0.003 Pa s, measured at a shear rate of $3000s^{-1}$. In addition distilled water was used (0.001 Pa s). No proteins were present in the study.

For the wear test the viscosity of the CMC used was 0.0046 Pa s for all joints throughout the test.

6.2.2 Methods

6.2.2.1 Roughness determination

The roughness parameters were found on the pole of each component using the Zygo NewView100 NCOI. Five scans of the surface were taken each of an area 363 μm x 273 μm, and the results for various surface parameters were averaged. The rms roughnesses were used to calculate the combined roughness of each pair of components and to predict the tribological behaviour[34,35]. The value of λ [46] was found for every possible combination of components using a spreadsheet in Microsoft Excel. These predictions were used to determine which components should be tested. PV, Sa, and Ssk values were also recorded from the same scans as the Srms.

6.2.2.2 Friction Testing

The roughness on the pole of each component was determined before each test. A number of combinations were selected to ensure a range of predicted λ values with each component only being tested against one other component in each round of testing. Three friction tests were carried out on each joint pair with each viscosity of lubricant using Friction Simulator I and an average of the three results was found. After the set of joints were tested the roughness was determined again and the procedure was repeated.

After all friction testing had been completed, one (not roughened) pair of components was tested in the absence of any lubricant.

6.2.2.3 Wear testing

After all friction testing was completed, the component roughnesses were found and entered into the spreadsheet to determine the predicted values of λ for each combination of components. A set of 5 joints was selected for wear testing and no control was used. Each component was cleaned and weighed according to the protocol described in Appendix C, Section C.3, and the mean and standard deviation of these data are given in

Appendix D, Section D.2. At the viscosity of the lubricant (CMC solution, viscosity 0.0046 Pa s) the range of predicted λ for the chosen joints was 0.25-5.06. The test ran to 2.3 million cycles. The values of λ were calculated as described in Section 5.3.1.

6.3 Results

6.3.1 Friction testing

A Stribeck curve was plotted for each joint combination tested. Figure 49 shows typical Stribeck plots for two of the smoothest joints tested. Four higher-roughness joints are shown in Figure 50. In both cases, the dotted lines are the predicted positions of λ=3 and are colour coded to match the data set to which they belong.

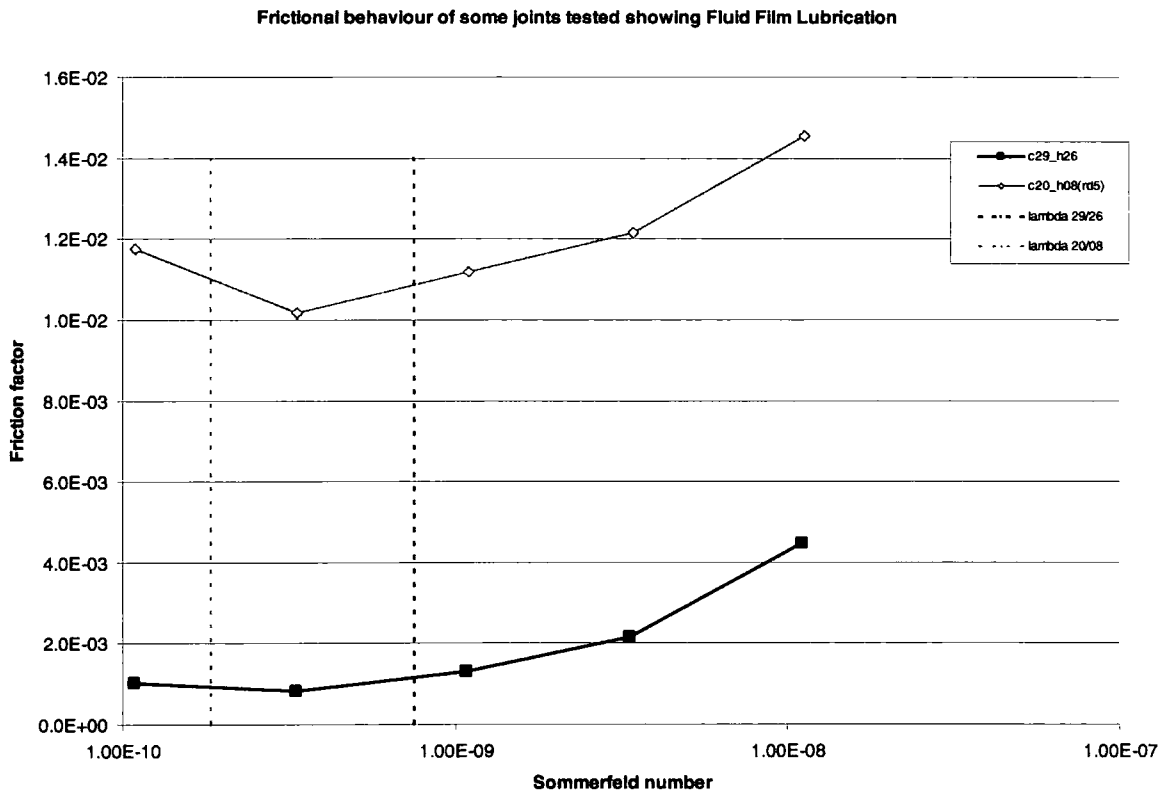

Figure 49. Stribeck curve for two joints with low combined roughness; the dotted lines are λ=3.

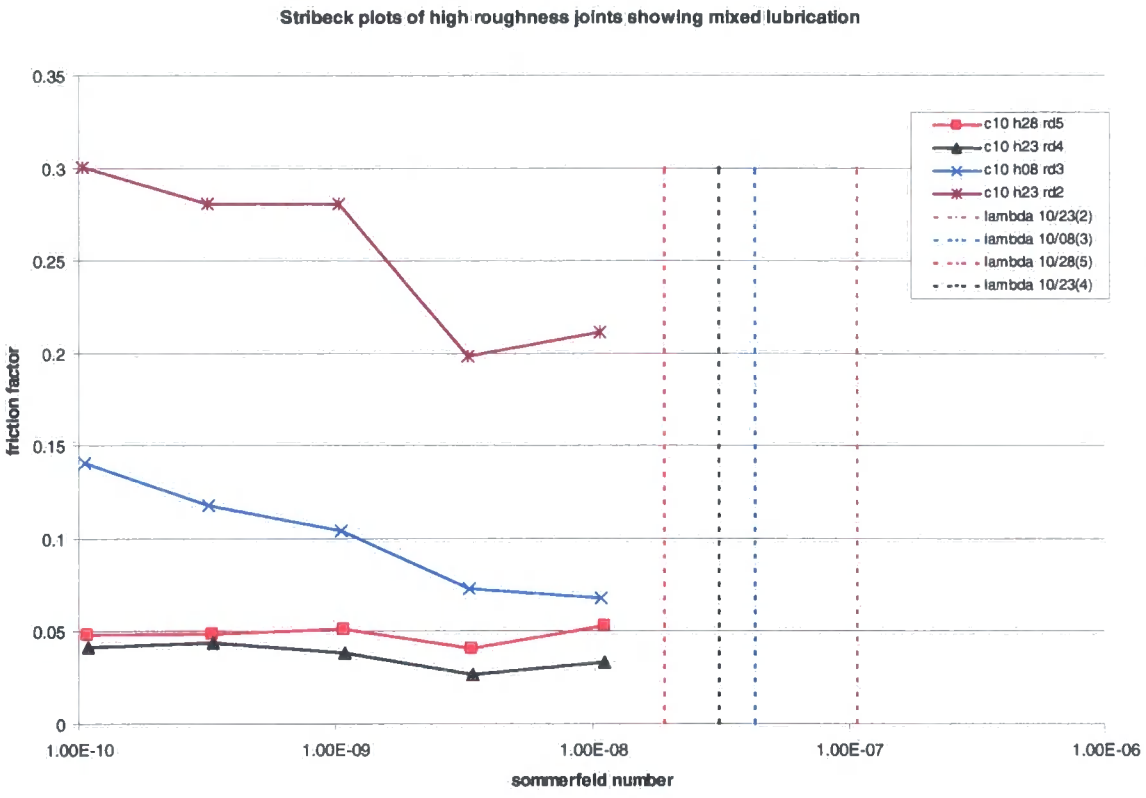

Figure 50. Stribeck plot for four rough joints tested in this study; the dotted lines are λ=3

The friction factors were then further plotted against the combined root mean squared roughness (Srms) of the head and cup for each individual viscosity. The points which are represented by squares are predicted to be within fluid film by the theoretical calculations.

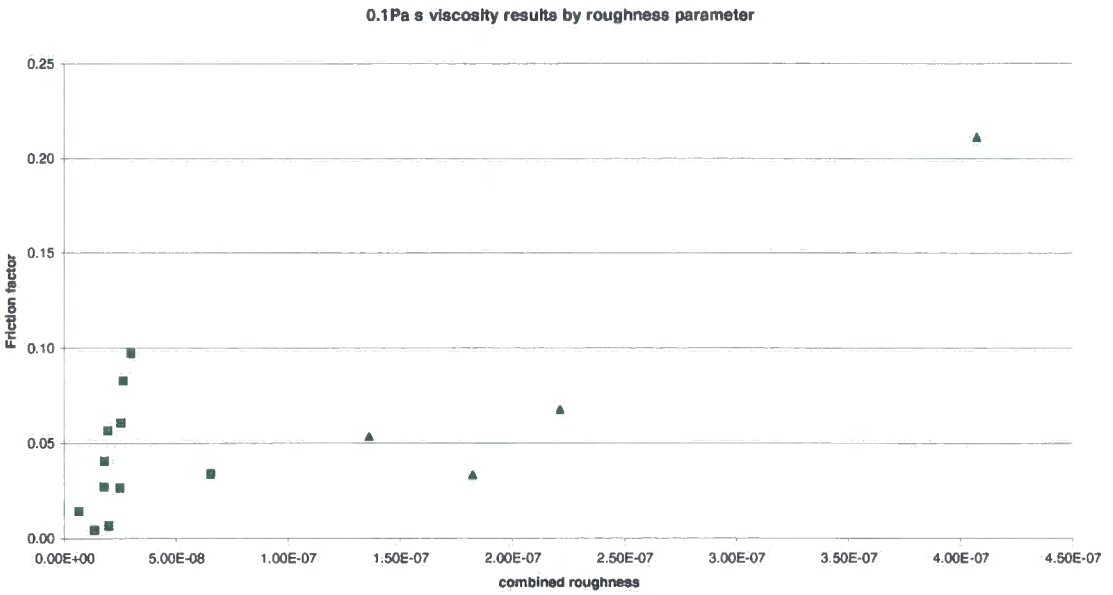

Figure 51. Friction factor at 0.1Pa s viscosity vs combined Sms for all component combinations tested

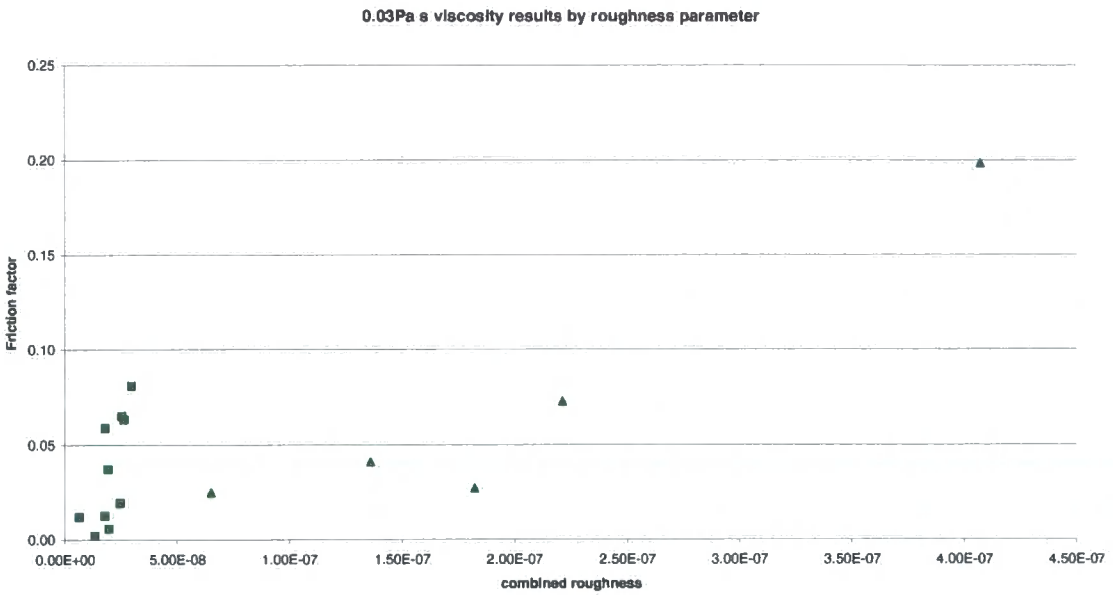

Figure 52. Friction factor at 0.03Pa s viscosity vs combined Sms for all component combinations tested

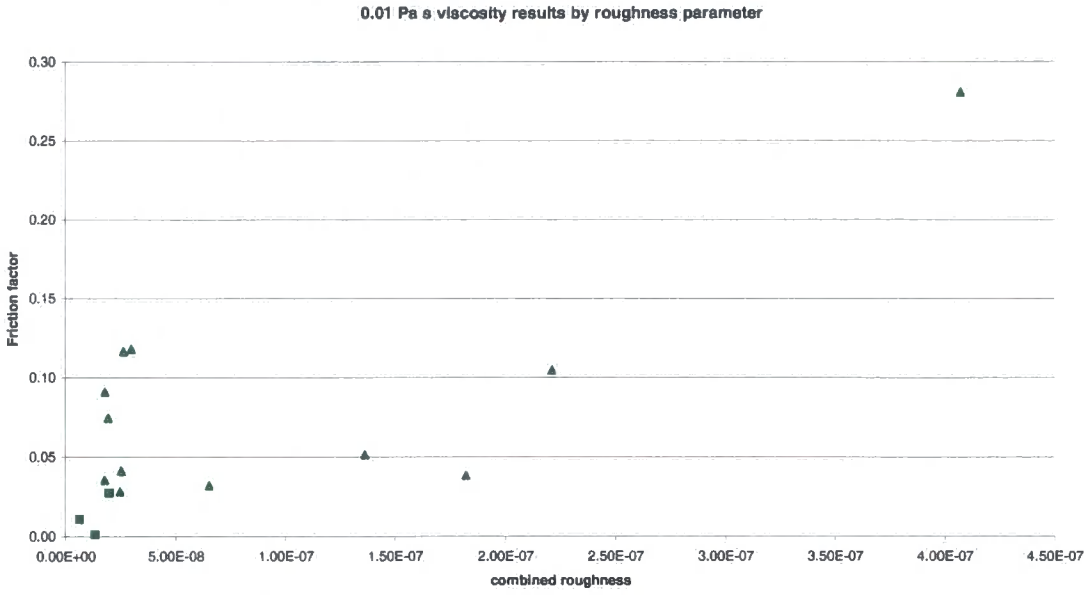

Figure 53. Friction factor at 0.01Pa s viscosity vs combined Srms for all component combinations tested

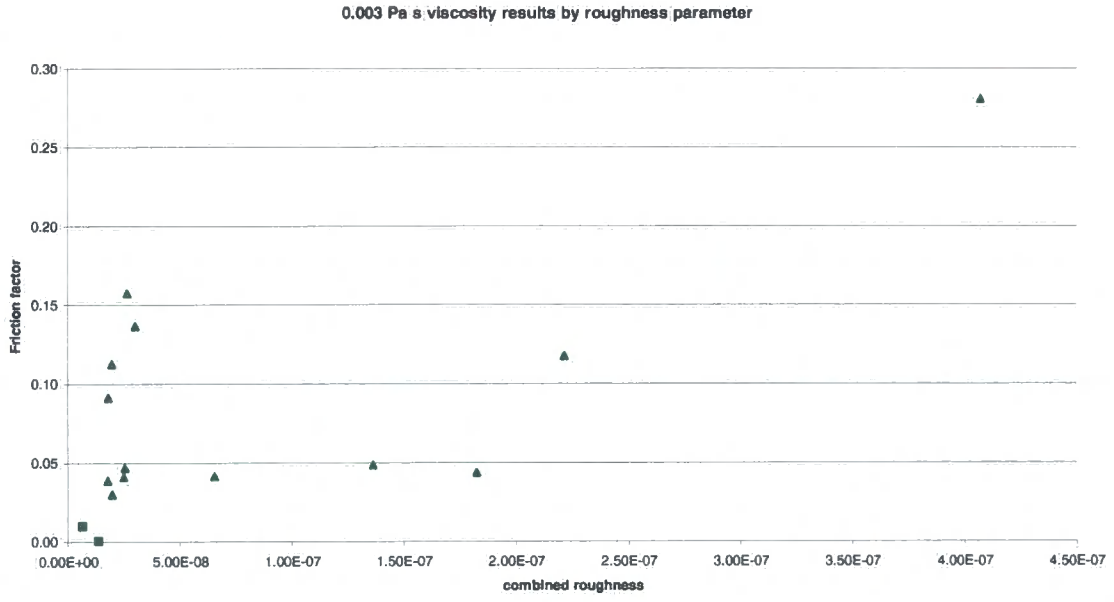

Figure 54. Friction factor at 0.003Pa s viscosity vs combined Srms for all component combinations tested

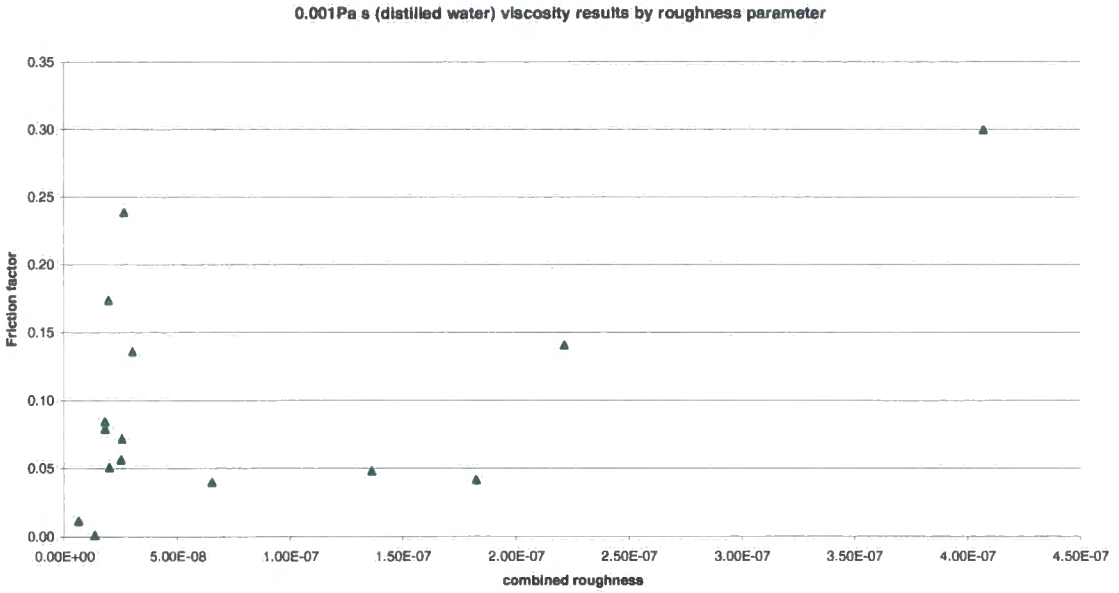

Figure 55. Friction factor at 0.001Pa s viscosity (distilled water) vs combined Srms for all component combinations tested

From the above figures, there appeared to be two distinct trends emerging. Therefore, the results were separated at the natural discontinuity ($5x10^{-8}$m) and plotted on separate graphs. The two charts for distilled water lubricant are shown below. Many more 'smooth' combinations (combined roughness $<5x10^{-8}$m - Figure 56) were tested than 'rough' ones (combined roughness $>5x10^{-8}$m - Figure 57), and the smoother combinations showed more scatter than the rougher ones. However, the two trends did remain visible when plotted in this manner.

The results were similarly split for all the viscosities, and the relevant coefficients are given in Table 13.

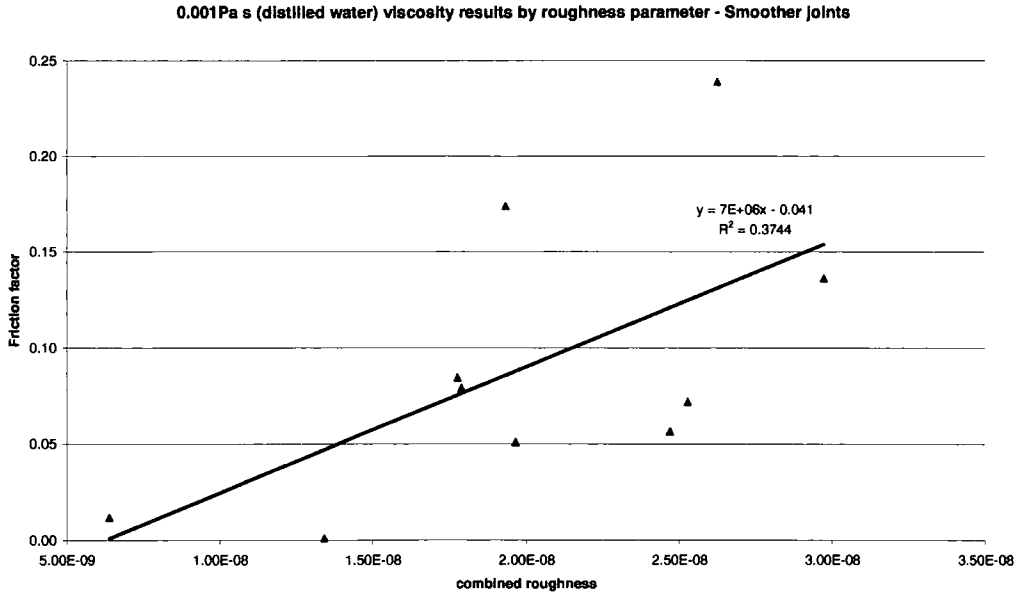

Figure 56. Friction results for distilled water lubricant for joints with combined roughness lower than $5x10^{-8}$m

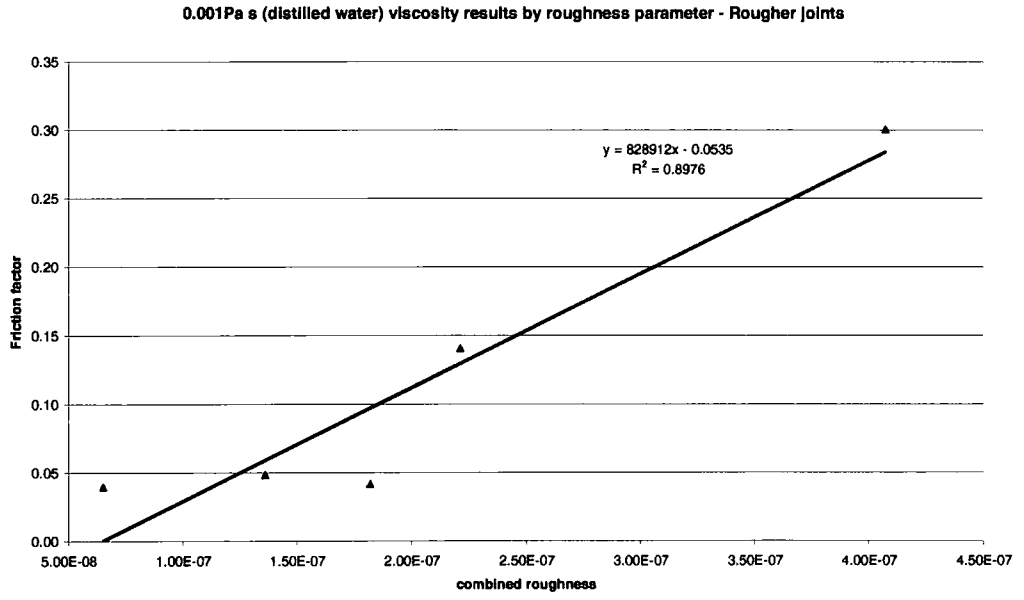

Figure 57. Friction results for distilled water lubricant for joints with combined roughness greater than $5x10^{-8}$ m.

	Lubricant Viscosity (Pa s)				
Rough joints	**0.1**	**0.03**	**0.01**	**0.003**	**0.001**
slope	5.42E+05	5.37E+05	7.72E+05	7.57E+05	8.29E+05
y intercept	-0.03	-0.04	-0.05	-0.05	-0.05
R^2	0.86	0.89	0.90	0.90	0.90
Smooth joints					
slope	3.51E+06	2.95E+06	4.07E+06	5.26E+06	6.56E+06
y intercept:	-0.03	-0.02	-0.03	-0.04	-0.04
R^2	0.57	0.49	0.43	0.44	0.37

Table 13. Regression statistics for each lubricant viscosity

Also, the friction factor was plotted against PV and Sa for the 0.1Pa s viscosity data. These showed similar trends to those seen for the Srms, as seen in Figure 58 (PV) and Figure 59 (Sa) and were thus not investigated further.

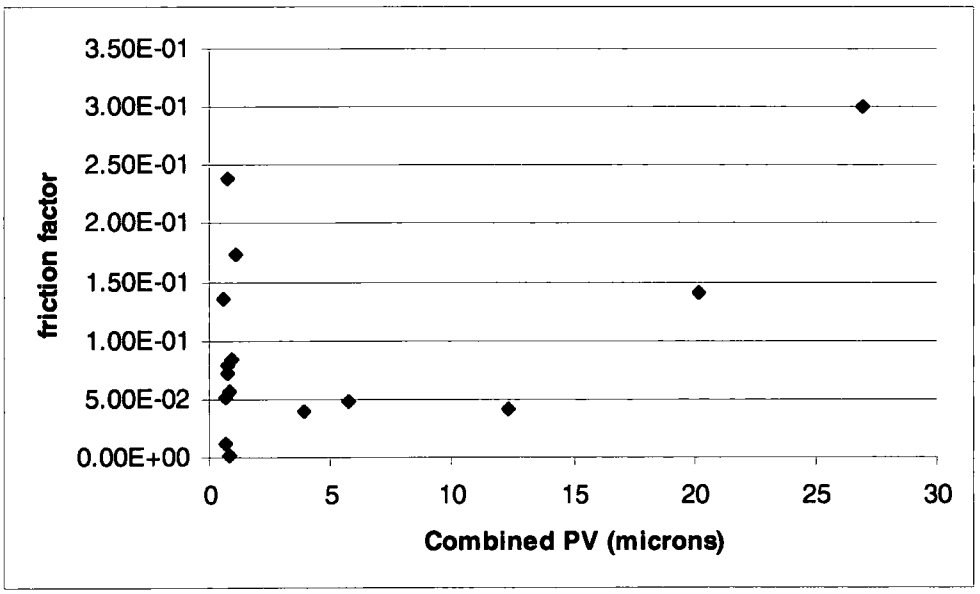

Figure 58. Friction factor at 0.1Pa s viscosity vs combined PV for all component combinations tested

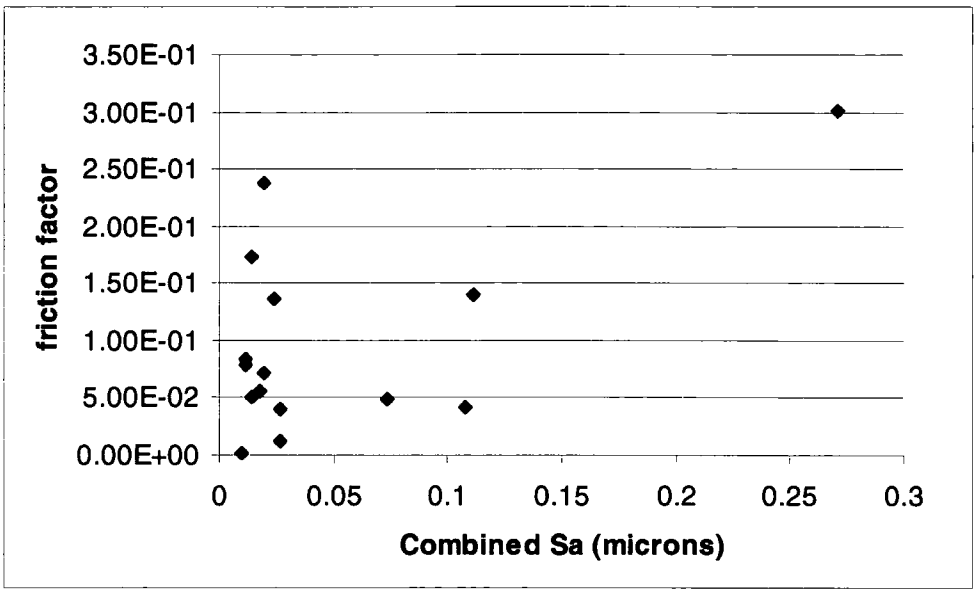

Figure 59. Friction factor at 0.1Pa s viscosity vs combined Sa roughness for all configurations tested

In addition, the Ssk was plotted individually for the heads (Figure 60) and cups (Figure 61), since root mean square combination of Ssk results in a loss of the negative/positive aspects of the skewness. For highly negative values of head skewness, the friction factor is lower than for those closer to zero. No trend is apparent for the cup skewness results, however.

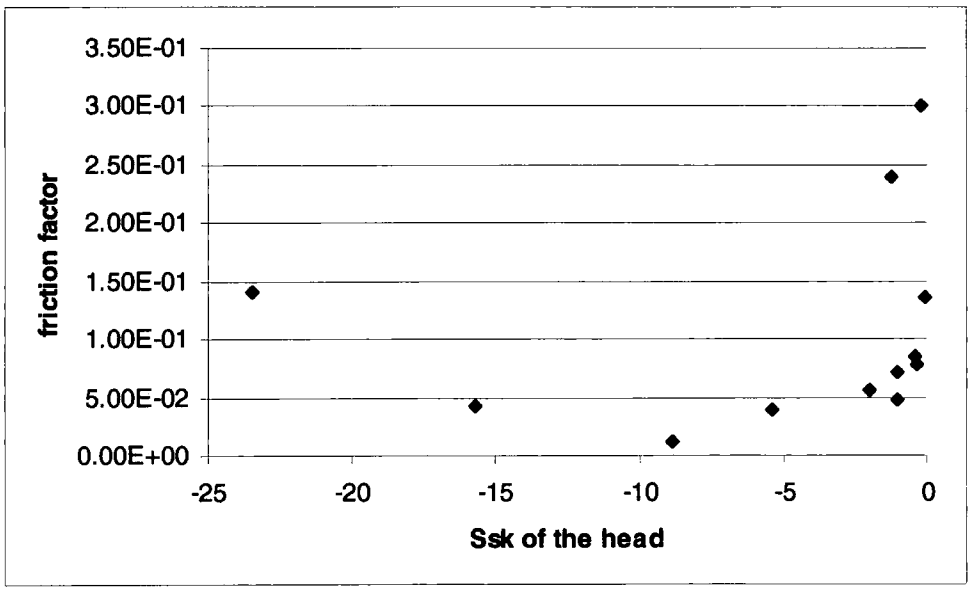

Figure 60. Friction factor at 0.1Pa s viscosity vs the Ssk of the head for each test

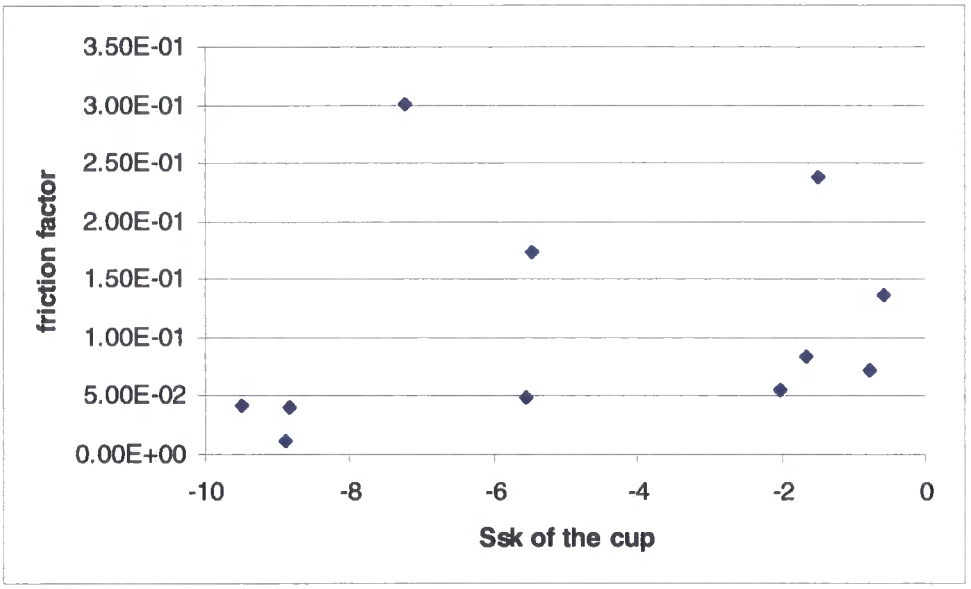

Figure 61. Friction factor at 0.1Pa s viscosity vs the Ssk of the cup for each test

The component tested dry was tested 3 times as is normal practice with friction tests. The results are given in Table 14. The value of the friction factor was initially very high at 0.65 but this reduced to 0.41 in the second run and reduced again to 0.24 in the third run.

	run1	run2	run3
Cup 29 vs Head 23	0.65	0.41	0.24

Table 14. Friction factors for single joint tested in the absence of lubricant

The values of the roughness parameters of the head and cup, before and after the friction test are given in Table 15. The changes in the roughness parameters were not statistically significant.

Cup	PV (μm)	Srms (μm)	Sa (μm)	Ssk	Head	PV (μm)	Srms (μm)	Sa (μm)	Ssk
initial	0.171	0.004	0.003	-2.58	**initial**	0.546	0.004	0.003	-13.37
final	0.203	0.003	0.002	-7.54	**final**	0.392	0.005	0.004	-6.275

Table 15. Roughness parameters before and after friction test in absence of lubricant

6.3.2 Wear test

The roughness of each component was measured at each interval of the wear test. The combined results for each joint are given in Table 16.

	Combined roughness of head and cup (nm)				
Million Cycles	**Joint 1**	**Joint 2**	**Joint 3**	**Joint 4**	**Joint 5**
0	136	29.4	10.3	15.8	5.83
0.5	99.5	42.5	19.6	24.2	8.96
1	76.6	60.1	20.3	77.2	18.9
1.7	30.1	43.4	15.5	25.4	14.5
2.2	32.7	36.3	15.2	24.7	12.2

Table 16. Combined measured Srms roughness for each joint at each stage of the wear test

Using these combined roughness values a prediction of the λ parameter is found for each joint at each stage of the test and these predictions are given in Table 17.

	Predicted λ for each joint at 0.0046Pa s				
Million Cycles	**Joint 1**	**Joint 2**	**Joint 3**	**Joint 4**	**Joint 5**
0	0.25	1.46	3.29	1.86	5.06
0.5	0.35	1.01	1.73	1.22	3.29
1	0.45	0.71	1.67	0.38	1.56
1.7	1.15	0.99	2.19	1.16	2.04
2.2	1.05	1.18	2.24	1.19	2.43

Table 17. Predicted values of λ for each joint at each stage of the wear test

The wear results for each head can be seen in Figure 62, and the results for each cup in Figure 63. The overall wear for each joint is shown in Figure 64.

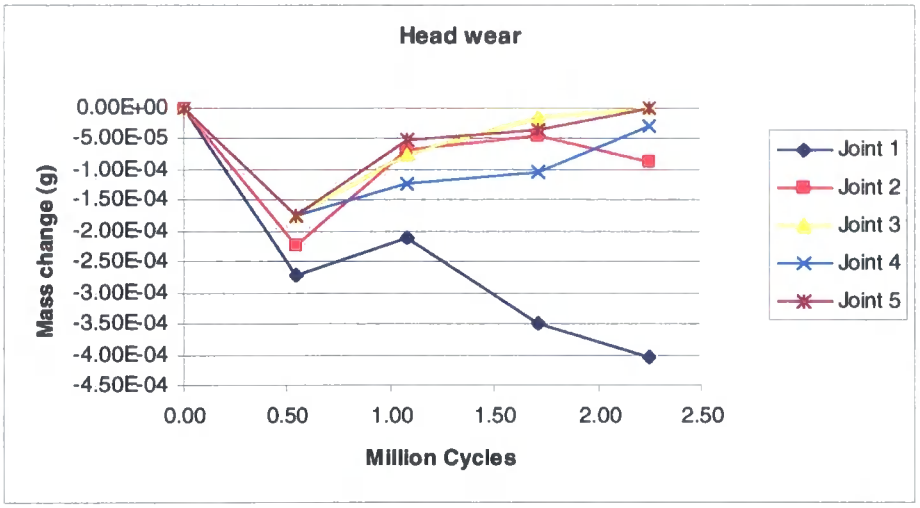

Figure 62. Mass change in ceramic heads over the course of wear test

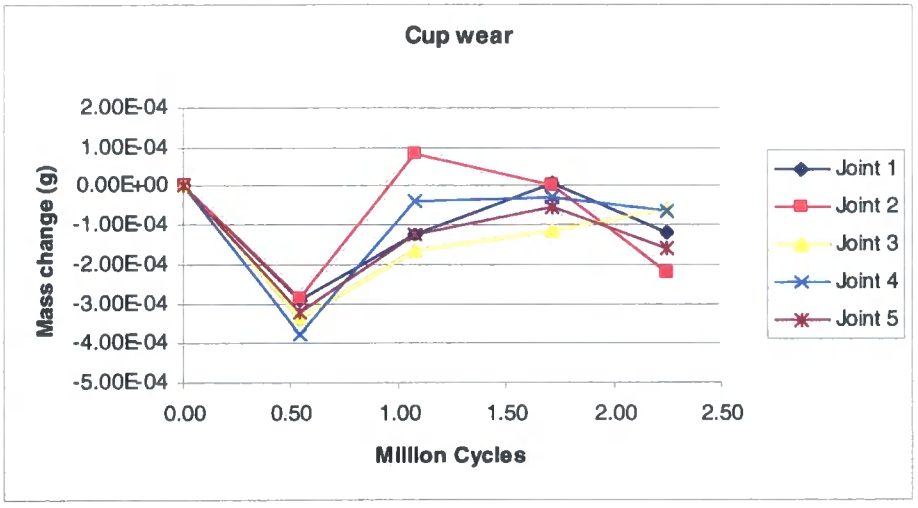

Figure 63. Mass change in ceramic cups during the course of wear testing

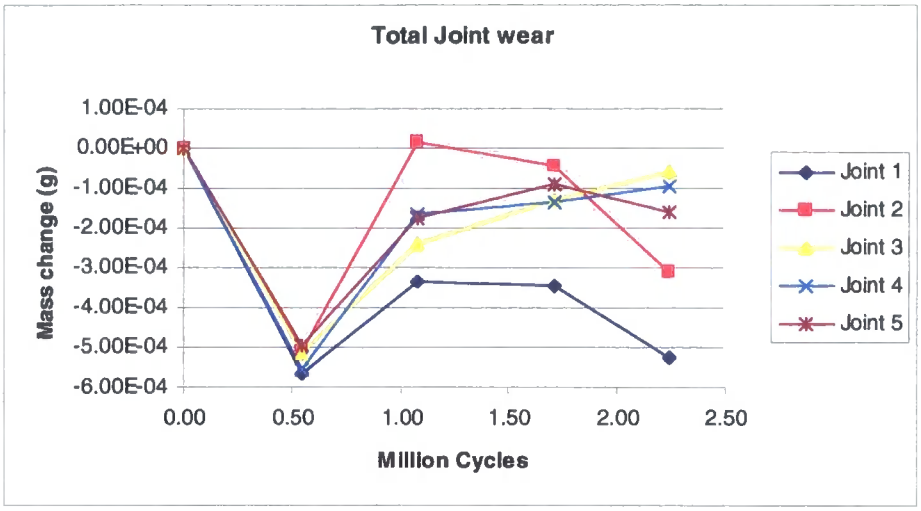

Figure 64. Overall mass change for each joint during the course of wear testing

6.3.3 Surface study

Surface profiles for a selection of components throughout the test are given in the figures on the following pages. All images show an area of 363µm x 272 µm. Images were typical of ceramic surfaces with some multidirectional scratching on polished components and pitting on roughened components. Some directional scratching was visible after both friction and wear testing on smooth components, while the roughened components mostly retained their pitted appearance with some scratching evident in some cases.

The Srms of each component before and after each round of friction testing is shown in Table 18, along with the values for the component it was tested against in each round. Significant increases and decreases are highlighted in pink and blue respectively, while the components which had been roughened are shaded in grey. The significant increases or decreases did not appear to be associated with a particular type of counterface or the number of tests undergone by the component.

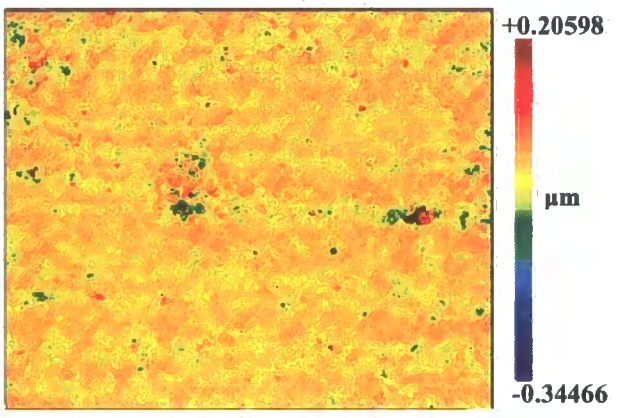

(a)

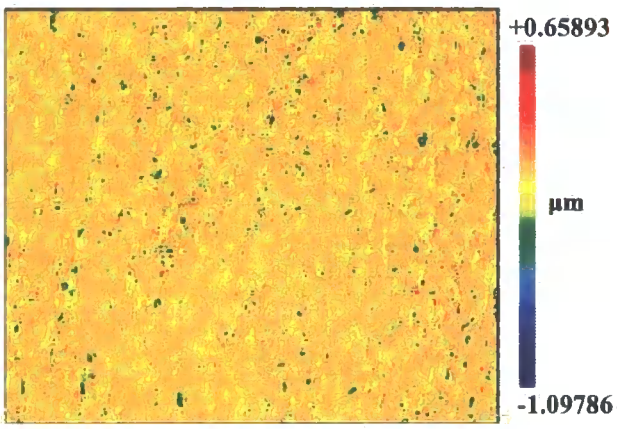

(b)

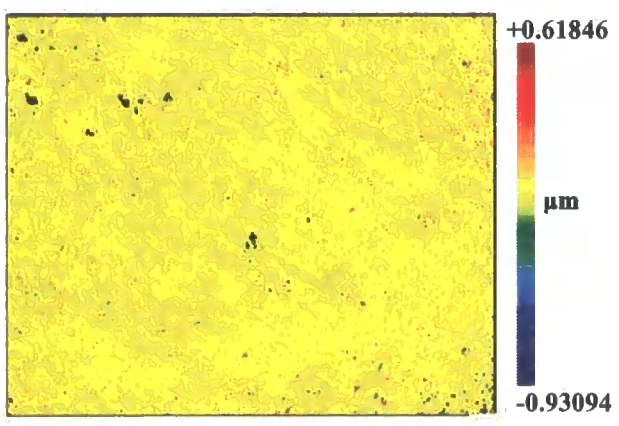

(c)

Figure 65. Surface profiles of Cup 10 (roughened component) roughened before testing(a), after friction testing (b), and after the wear test (c).

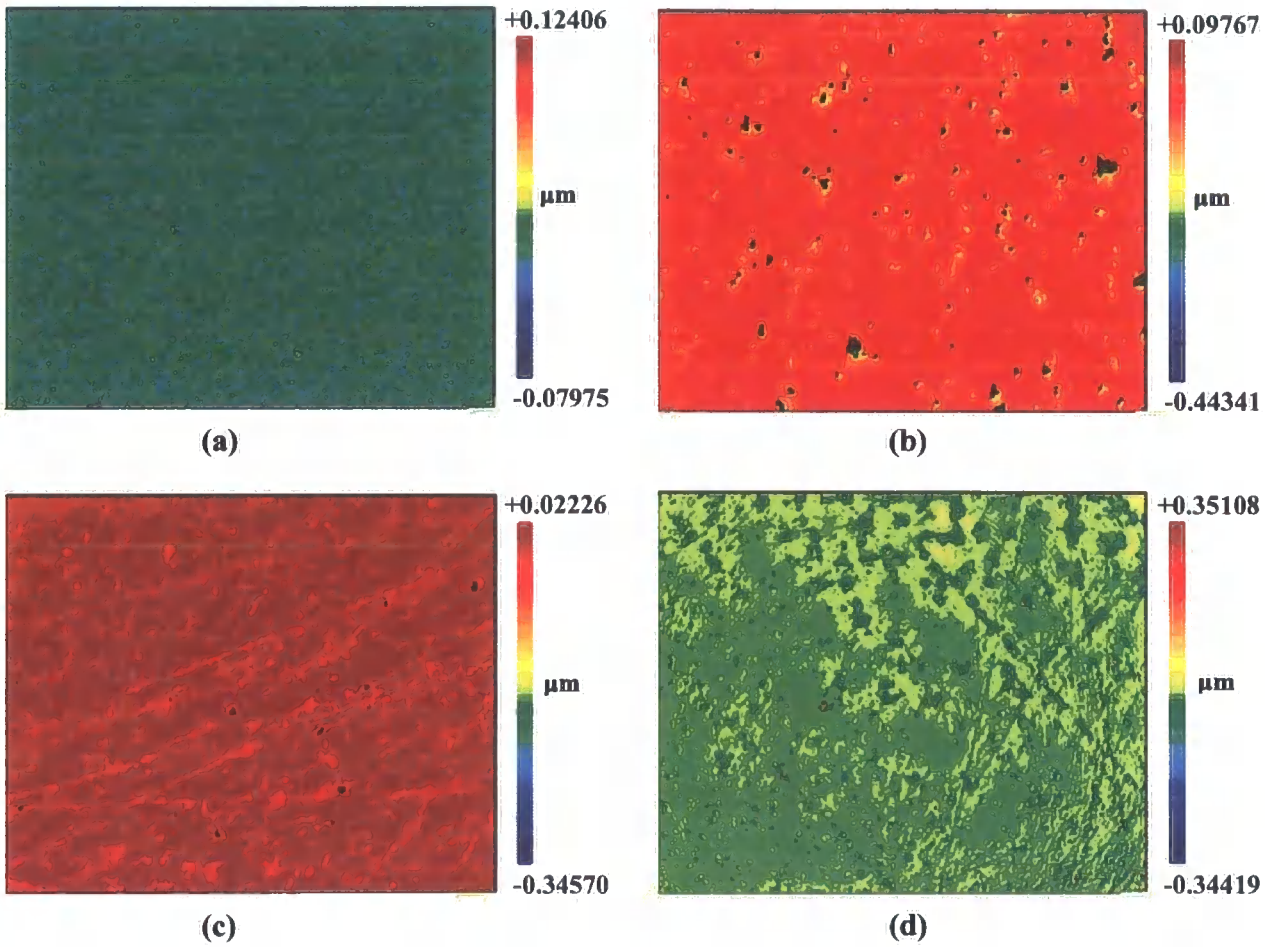

Figure 66. Surface profile of a ceramic head 6 (roughened component) before roughening (a), after roughening (b), after the friction test (c), and after the wear test (d).

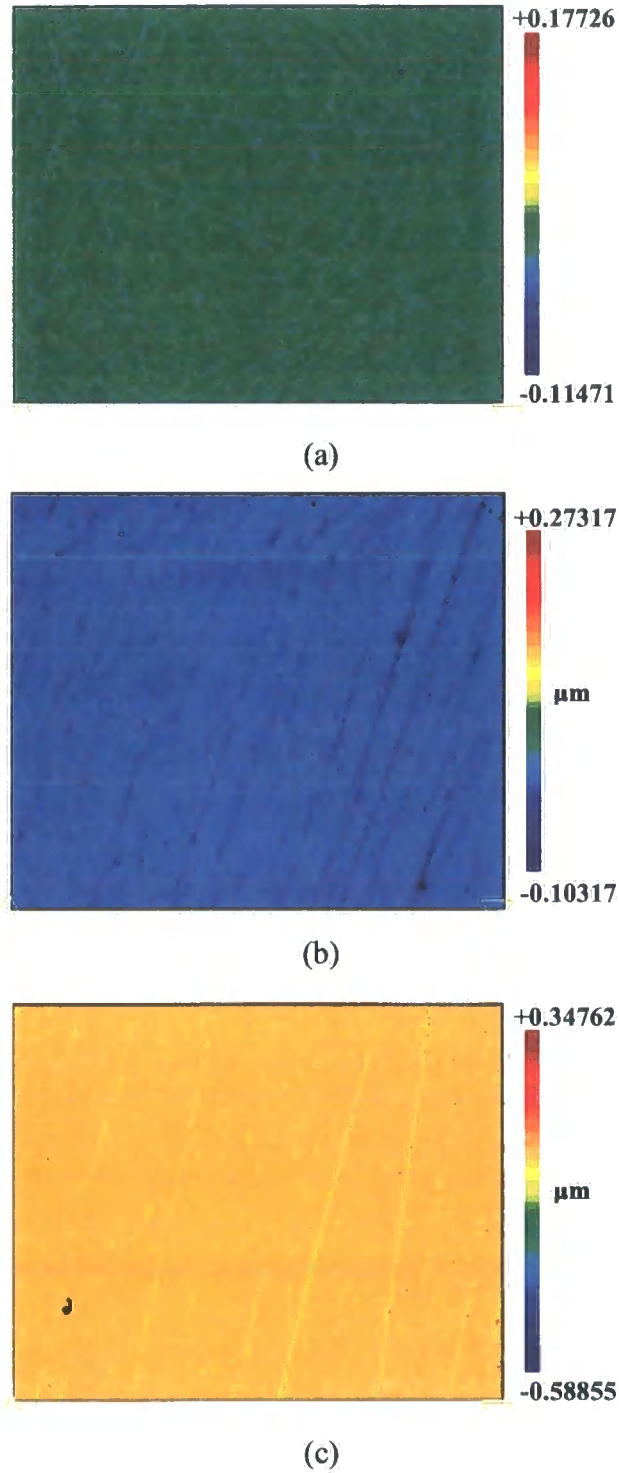

Figure 67. Surface profiles of cup 20 (non-roughened component) before testing(a), after friction testing (b), and after the wear test (c).

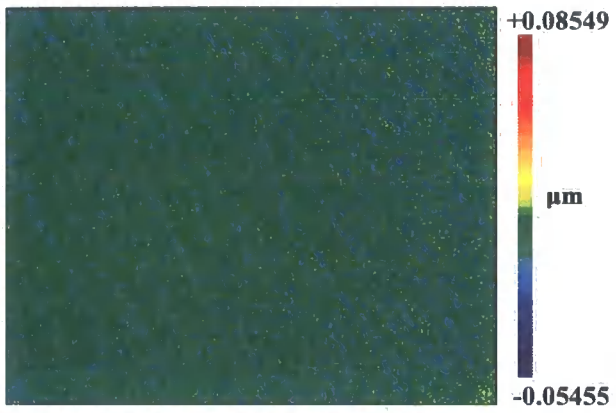

(a)

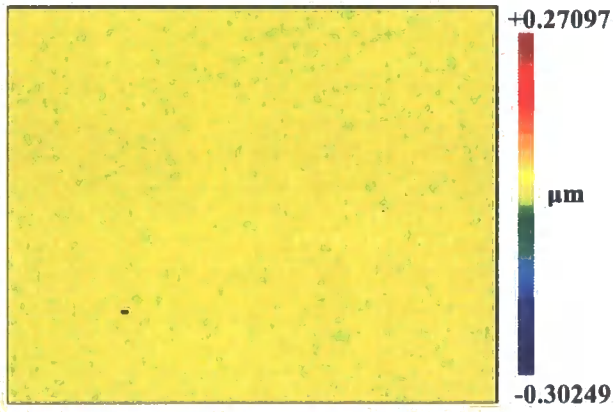

(b)

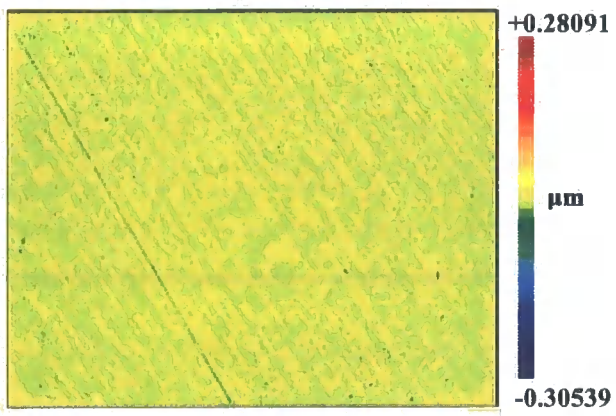

(c)

Figure 68. Surface profiles of Head 8 (non-roughened component) before testing(a), after friction testing (b), and after the wear test (c).

Component behaviour					behaviour of other component in fr. Test.			
	Number of friction tests	Initial mean S_{rms} (µm)	Final mean S_{rms} (µm)	p	Other component	Initial mean S_{rms} (µm)	Final mean S_{rms} (µm)	p
head 08	0-1	0.0098	0.0073	0.082067	cup 22	0.0284	0.0236	0.055355
	1-2	0.0073	0.0046	0.053896	Cup 10	0.221	0.1824	0.823994
	2-3	0.0046	0.0054	0.241982	Cup 22	0.0648	0.0292	0.000175
	3-4	0.0054	0.0046	0.01613	Cup 20	0.0042	0.005	0.099301
head 06	0-1	0.0246	0.0159	0.08349	Cup 18	0.0082	0.0070	0.295472
	1-2	0.0159	0.0192	0.160264	Cup 29	0.0076	0.0064	0.508621
	2-3	0.0192	0.0096	0.151669	Cup 20	0.0048	0.0042	0.426317
head 26	0-1	0.0234	0.0184	0.018541	Cup 20	0.0086	0.0048	0.041255
	1-2	0.0184	0.012	0.001833	Cup 18	0.0070	0.0088	0.269161
	2-3	0.012	0.0136	0.099301	Cup 29	0.0064	0.0042	0.260431
cup 22	0-1	0.0284	0.0236	0.055355	head 08	0.0098	0.0073	0.082067
	1-2	0.0236	0.0164	0.009333	Head 28	0.009	0.003	9.12E-07
	2-3	0.0164	0.0648	8.73E-06	Head 23	0.0078	0.0046	0.11508
	3-4	0.0648	0.0292	0.000175	Head 08	0.0046	0.0054	0.241982
cup 10	0-1	0.4074	0.221	0.174345	Head 23	0.0098	0.0078	0.177808
	1-2	0.221	0.1824	0.823994	Head 08	0.0073	0.0046	0.053896
	2-3	0.1824	0.136	0.263407	Head 23	0.0046	0.0046	1
	3-4	0.136	0.1144	0.119651	Head 28	0.003	0.0052	0.0109
cup 18	0-1	0.0082	0.0070	0.295472	head 6	0.0246	0.0159	0.08349
	1-2	0.0070	0.0088	0.269161	Head 26	0.0184	0.012	0.001833
cup 20	0-1	0.0086	0.0048	0.041255	Head 26	0.0234	0.0184	0.018541
	1-2	0.0048	0.0042	0.426317	Head 06	0.0192	0.0096	0.151669
	2-3	0.0042	0.005	0.099301	Head 08	0.0054	0.0046	0.01613
cup 29	0-1	0.0076	0.0064	0.508621	Head 06	0.0159	0.0192	0.160264
	1-2	0.0064	0.0042	0.260431	Head 26	0.012	0.0136	0.099301
head 23	0-1	0.0098	0.0078	0.177808	Cup 10	0.4074	0.221	0.174345
	1-2	0.0078	0.0046	0.11508	Cup 22	0.0164	0.0648	8.73E-06
	2-3	0.0046	0.0046	1	Cup 10	0.1824	0.136	0.263407
head 28	0-1	0.009	0.0030	9.12E-07	Cup 22	0.0236	0.0164	0.009333
	1-2	0.003	0.0052	0.0109	Cup 10	0.136	0.1144	0.119651

Table 18. Summary of RMS roughness parameters for all joint during the course of Friction Testing: grey shading indicates roughened components, blue and pink indicate a significant decrease and increase in Srms respectively

6.4 Discussion

6.4.1 Wear study

The mass change in the individual components was in the region of 0.5mg. No wear trend was determined with respect to the roughness of the component. However, as can be seen in Figure 62, head 1 showed a larger mass change than the other heads. This head was worn against Cup 10, which was initially the roughest component in the study although it did not remain the roughest component throughout (Table 18), nor was the predicted λ for this joint the lowest throughout the wear test. However, the predicted λ is lower than 1.15 at all times, indicating that the joint is likely to operate well within the mixed lubrication regime.

The larger mass loss on the head did not have an effect on the wear trend of the joint overall (Figure 64) although this joint does have the highest mass loss.

6.4.2 Friction study

The smoother joints had low friction and showed an increasing trend in friction factor. This indicates that the joints were operating in fluid film lubrication with some of the lubricants tested. The rougher joints operated in a mixed lubrication regime over the entire range of the viscosities tested.

However, friction factor plotted against combined roughness may indicate two trends: one at low combined roughness values and one at higher values. When the results were split at the natural discontinuity in the data (combined roughness around $5x10^{-8}$), the two increasing trends were seen more clearly. Table 13 shows the regression statistics for each of the two groups. The correlation of the smoother data is much lower than that for the rougher combinations, indicating a more dispersed data set.

This discontinuity in the results may be indicative of a difference in contact mechanism or lubrication regime. The natural split in the results roughly coincided with the combinations which were predicted to operate under fluid film lubrication at 0.1Pa s (the square data points in Figure 51). Therefore it is logical to postulate that the joints

operated close to fluid film over the entire range of viscosities. However, it should be noted that all the rough combinations bar one involved an articulation with Cup 10, the roughest component throughout friction testing. The other combination involved Cup 22 (which was the other cup to be roughened) in its final friction test. This was the test in which its roughness was highest, although during the test the surface roughness decreased significantly. Cup 10 never showed a significant change in roughness and only once induced a significant change in roughness (an increase) on its counterface.

The general increase in friction factor from lowest to highest viscosity graphs is indicative of the mostly mixed lubrication regime these joints were seen to work under. This is also true of the combined Sa and PV of the components. Plotting the friction factor against the Ssk of the heads and cups also revealed no correlation between the two. However, it is important to note that the Ssk was negative for all components throughout the friction testing, indicating a surface characterised mostly by valleys, not peaks. This is a favourable condition for lubrication.

6.4.3 Surface observations

The surface of the roughened components was optically (although not microscopically) different from the surfaces later seen by the author on some explanted joints. The explanted joints typically showed a distinct wear patch discernible by a well-defined area of unpolished surface, the boundary of which was visible by eye. This was not seen on the roughened components. The polar roughness increased due to the roughening procedure, but the distinct and well defined wear patch was not seen. This indicates that the method of roughening of these components was not completely indicative of failed ceramic hip prostheses. However, the surface features of the roughened components as seen using NCOI is similar to that seen on explanted ceramic surfaces, and is typical of ceramic surfaces.

The surface roughness changed after every friction test and also at each stage during the wear test. However, the roughness sometimes increased and sometimes decreased with no apparent pattern or cause. As can be seen in Table 18 the roughness changes are not always significant, and there is no easily apparent pattern regarding the roughness of the counterface.

6.5 Conclusions

- As the roughness increased, the friction factor increased. However, at a combined roughness of around $5x10^{-8}$ m there was a discontinuity in the data and the friction factor fell dramatically. Beyond this point the friction factor continued to increase with increasing roughness.
- Rougher joints operated further within the mixed lubrication condition than smoother ones
- The wear remained very low and a direct effect of roughness was not detected, although the joint containing the initially roughest component showed more mass loss than the other joints.
- Over the range of roughnesses generated in the study and using the methods used herein, the effect of the roughness on joint tribology is not enough to induce wear in the ceramic joints. The roughness however, did affect the lubrication regime the joints operated under.
- The surfaces were not entirely representative of explanted ceramic joint surfaces.

7 Tribology of metal-on-metal hip resurfacing device

7.1 Introduction

Early, small diameter (<32mm), metal-on-metal hip joints were prone to premature failure [98], although some specimens are known to have been in place successfully for up to 20 years [100,101]. This suggests there being a favourable tribological condition in some cases, although not in the majority of cases for early designs of metal-on-metal joints.

New generation, larger diameter metal-on-metal hip joints have been more successful in the mid term [83,148] although longer term results are not yet available. Theory points to the diameter being a major contributing factor to the better performance of these joints, since a larger diameter would promote better lubrication conditions as discussed in Chapter 2, Section 2.8.2.

However, van Kampen *et al*'s work [104] showed that the joints were not initially fully fluid film lubricated. Since clinically the joints perform fairly well, it follows that this may just be an initial phenomenon and the lubrication mechanisms may change as the joint "runs in" in the body.

This project was undertaken to investigate the effect of wearing-in on the tribology of the Birmingham Hip Resurfacing arthroplasty device (BHR). Friction and wear tests were carried out and surface roughness data were collected at various intervals. Friction studies gave an insight into the lubrication modes operating within the device and as such, the effects of running-in could be studied on the friction, lubrication and surface condition.

7.2 Materials and methods

7.2.1 Materials

7.2.1.1 Prostheses

Six Birmingham Hip Resurfacing prostheses were supplied by Midland Medical Technologies, now Smith & Nephew (Bromsgrove). These were all 50mm nominal diameter with diametral clearances of 150-200μm as seen in Table 19. The material was as-cast CoCrMo alloy with a density of 0.0085 g/mm^3 and a carbon content of 0.266%.

Joint	Head Diameter /mm	Cup Diameter /mm	Diametral Clearance /μm
1	49.85	50.05	200
2	49.85	50.02	170
3	49.86	50.01	150
4	49.85	50.01	160
5	49.86	50.01	150
Control	49.84	50.01	170

Table 19. Diameters and clearances for metal-on-metal joints

7.2.1.2 Lubricant

All friction and wear tests were carried out in bovine serum (batch no. 97623, TCS Biosciences, total protein content 74.4 g/*l*) filtered through a 0.2 μm filter and diluted to 25%, resulting in a protein concentration of 18.6g/*l*. To this was added 0.2% sodium azide and 20 mM EDTA to help resist biodegradation of the lubricant and calcium deposit formation respectively. For the friction study, CMC was added to the lubricant in varying amounts as a viscosity enhancer[36], to achieve a range of 5 viscosities for testing: 0.0012 (no CMC), 0.0042, 0.011, 0.036 and 0.098 Pa s.

7.2.2 Methods

7.2.2.1 Friction Study

A single joint (Joint 1) was tested before the wear test, and after each million cycles of the wear test, in Hip Function Friction Simulator II as described in Section 3.2. The joints were placed in the friction simulator in an inverted position with respect to the orientation *in vivo*. The cup holder was angled at 33° to simulate the condition *in vivo*, and the head and cup were placed in the friction simulator such that the direction of flexion-extension of the wear simulator coincided with the direction of motion in the friction simulator. This ensured that the friction was being measured over the correct contact area.

Each joint was tested 3 times with each fluid viscosity and an average and standard deviation was calculated. The maximum and minimum loads were 2000N and 100N respectively as described in Section 3.2.

In each case the joint pair was cleaned before each individual run in the friction simulator. After the run, the excess lubricant was removed using a tissue, and then the joint was wiped with Gigasept, then acetone, to ensure that all the lubricant was removed, before the joint was retested with another viscosity of lubricant.

7.2.2.2 Wear study

The components were placed in the wear simulator in the anatomical position. The cups were angled at 33° to simulate the condition *in vivo*. Each joint was mounted into an individual closed cell with 500ml of lubricant. Approximately each 0.5 million cycles the joints were removed, cleaned and weighed according to the protocol described in Appendix C, Section C.4, and the cell components were also cleaned. The maximum and minimum loads were 2975N and 100N respectively and the loading profile (See Section 3.4, Figure 14) was checked before the joints were replaced in the simulator. Regular rig maintenance was carried out. The test ran for 3 million cycles in total.

7.2.2.3 Surface study

At the start and end of the test and approximately every 0.5 million cycles, the surface roughnesses of the contact region of each component were measured using the Zygo NewView100 non-contacting interference profilometer (NCOI). Ten measurements were taken on the polar region of the contact area of each component and 5 on the periphery of the heads. The peripheral regions of the contact area on the cups could not be measured, due to the lens geometry. From each measurement, a value of each Sa, Srms, PV and Ssk were obtained and an average and standard deviation was calculated. T-tests were also run on these values to determine any significant differences as a result of testing. The joint that was friction tested throughout the wear test was always imaged on the Zygo before friction testing.

7.3 Results

7.3.1 Friction Study

Figure 69 shows the Stribeck curves for Joint 1 before wear testing and after each million cycles up to 3 million. Before wear testing the joint had a friction factor which was around 0.08, which is much lower than the 0.15-0.2 seen for small diameter metal-on-metal joints[39,116]. After 1 million cycles, the familiar mixed lubrication Stribeck curve began to form with the friction factor falling to 0.03 at the highest viscosity. The synovial fluid from a patient with rheumatoid arthritis is around 0.005 Pa s[36], which corresponds to a Sommerfeld number of 1.7×10^{-9} which lies slightly to the left of the 3rd point on each curve in Figure 69. At this viscosity, the friction factor within the joint was found to be 0.083 initially, falling to around 0.055 at 1 million cycles. At 2 million cycles this fell again to around 0.015 and some fluid film lubrication behaviour was seen. This seemed to be stable at 3 million cycles.

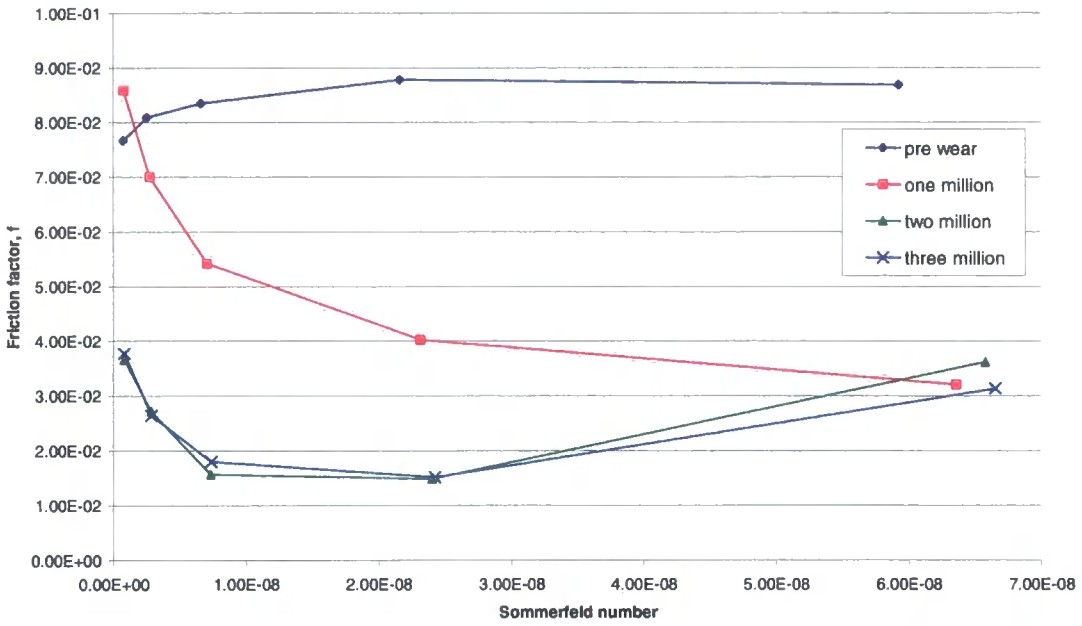

Figure 69. Stribeck plot for Joint 1 throughout wear testing

7.3.2 Wear study

The volume loss on each prosthesis is summarised in Figure 70 and the wear rates calculated by regression analysis are given in Table 20 and Figure 71. During the testing it became apparent that Joint 2 was showing much higher wear than the other joints. The rig was checked and there was found to be no problem with the load, and the gimbals and bushes all operated freely. Therefore, at 1.5 million cycles this joint and Joint 3 were swapped within the simulator and hence tested in a different station for 0.5 million cycles. Both of these joints continued to show the same wear rate over this period as they had previously and were hence returned to their original stations within the simulator for the remainder of the test.

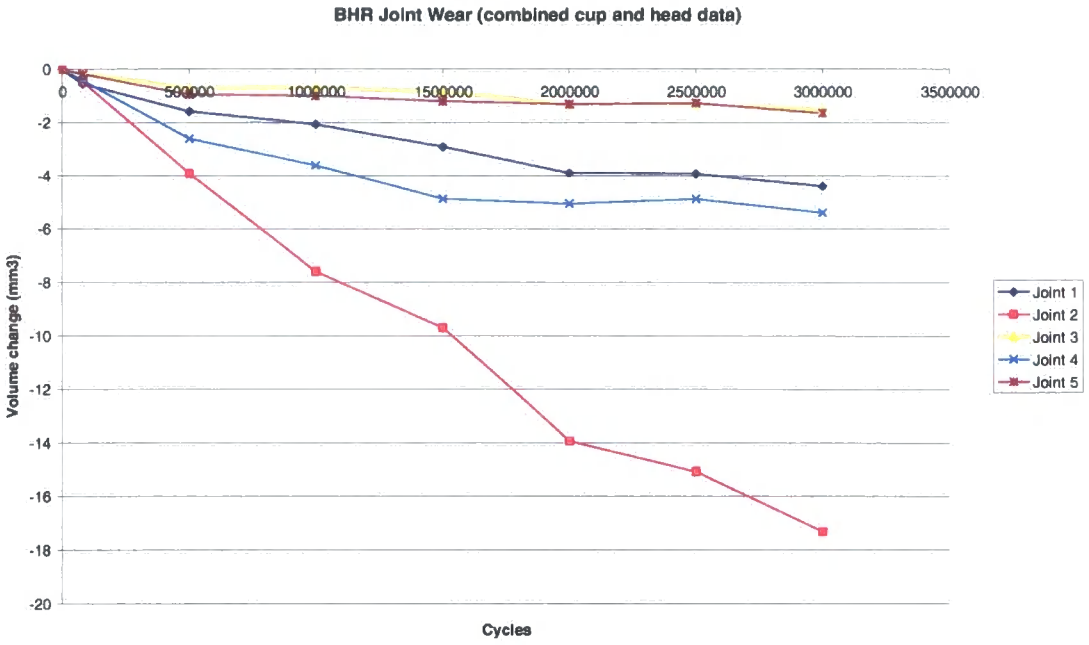

Figure 70. Volume change on prostheses during wear test

	0-1 million cycles	1-2 million cycles	2-3 million cycles	Overall wear rate
Joint 1	2.05	1.84	0.49	1.46
Joint 2	7.57	6.36	3.39	5.77
Joint 3	0.68	0.64	0.19	0.50
Joint 4	3.59	1.44	0.35	1.79
Joint 5	0.99	0.32	0.33	0.55
Average	2.98	2.12	0.95	2.02
N	4	3	3	8

Table 20. Wear results for each joint given in mm^3/million cycles.

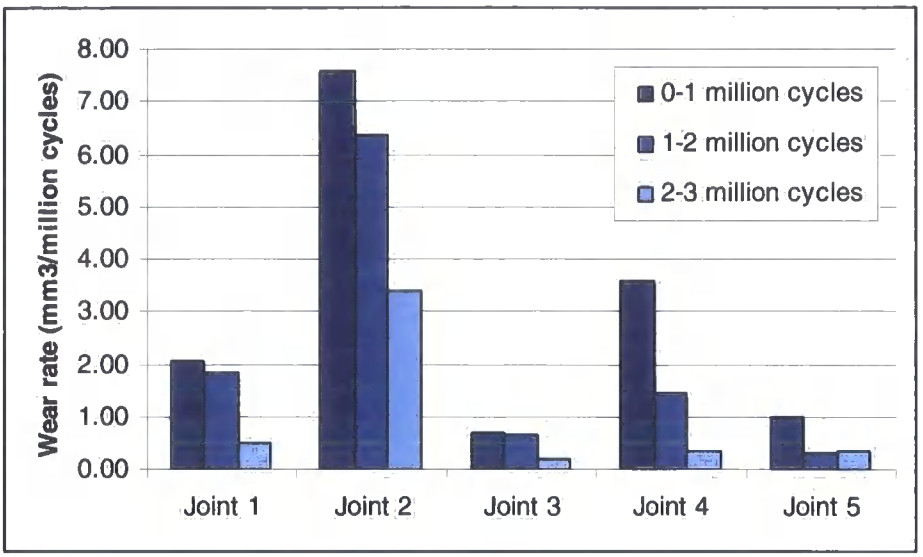

Figure 71. Wear results for each joint for portions of the wear cycle, given in mm3/million cycles

For most of the joints, the wear rates became progressively lower during each successive million cycles of the wear test.

7.3.3 Surface Study

Typical surface images for the components are given on the following pages. All images represent an area size of 363x272 microns and the Z-scale is indicated on each image.

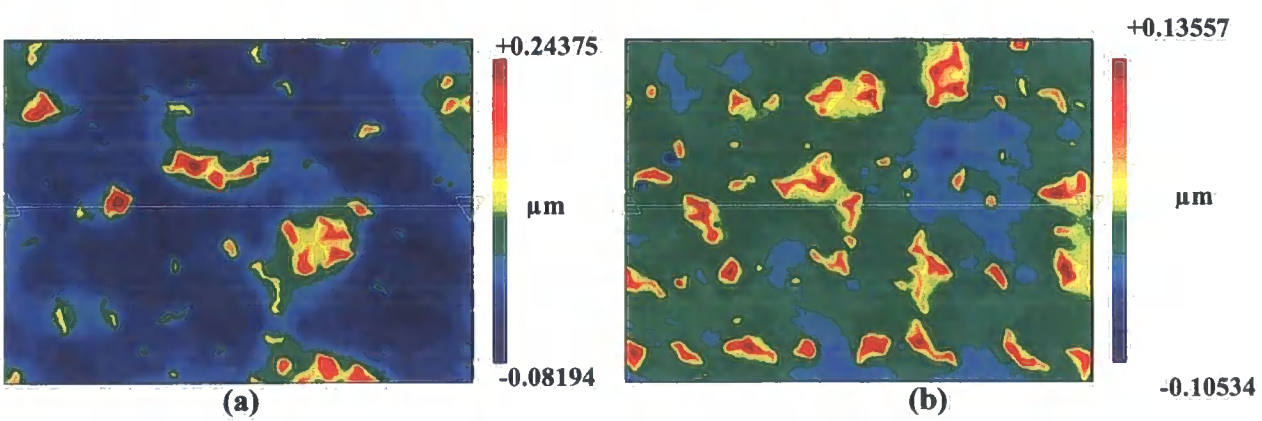

Figure 72. Initial surface images for (a) Head 1 and (b) Cup 1 showing presence of carbides

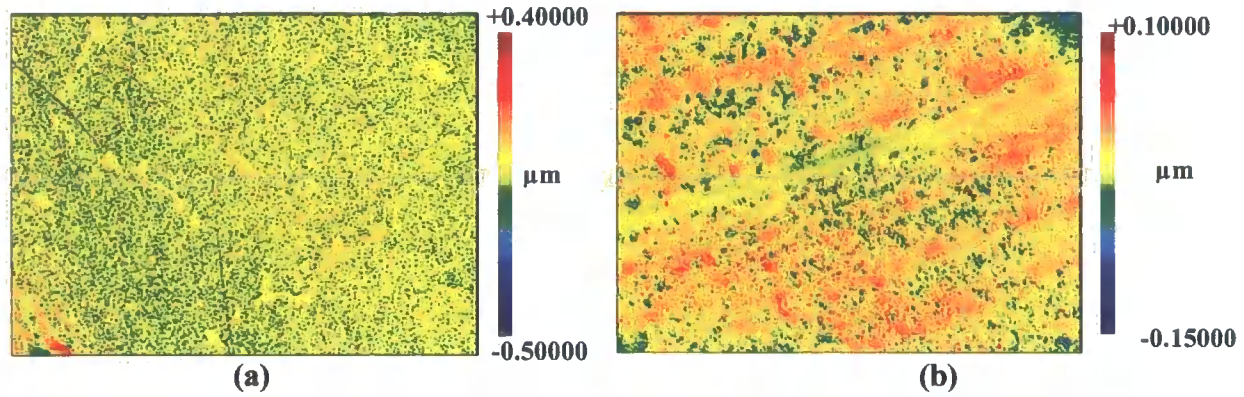

Figure 73. Surface profile of (a) Head 3 and (b) Cup 3 after 1 million cycles of testing

Initially the surfaces showed the presence of carbides as an array of protruding features. These were present on all heads and cups and typical images are seen in Figure 72. However, as the test progressed this feature diminished as seen from Figure 73 although evidence of the carbide features did remain in some cases up to 3 million cycles (Figure 74). Some components, showed smearing of the carbide feature (Figure 75) which was in some cases still apparent at 3 million cycles.

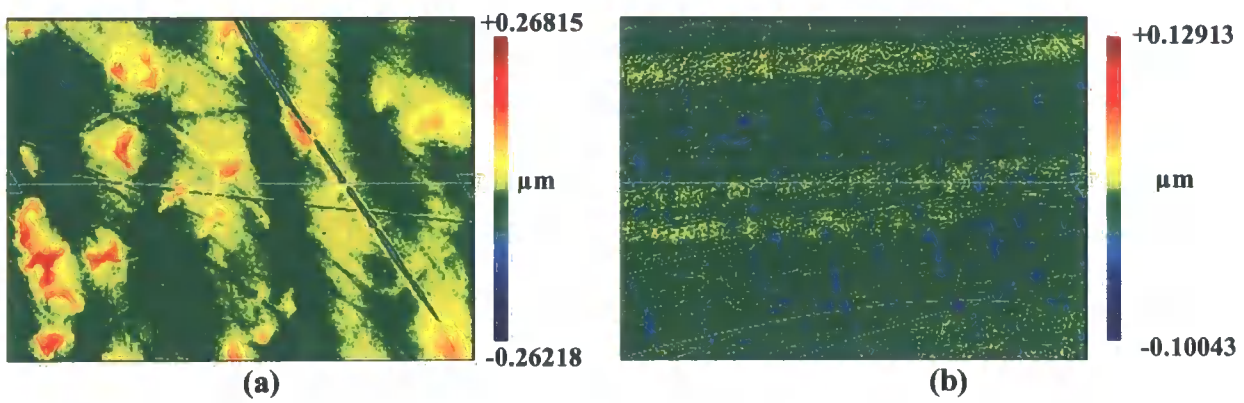

Figure 74. Surfaces of (a) Head 3 and (b) Cup 3 at 3 million cycles showing evidence of carbides

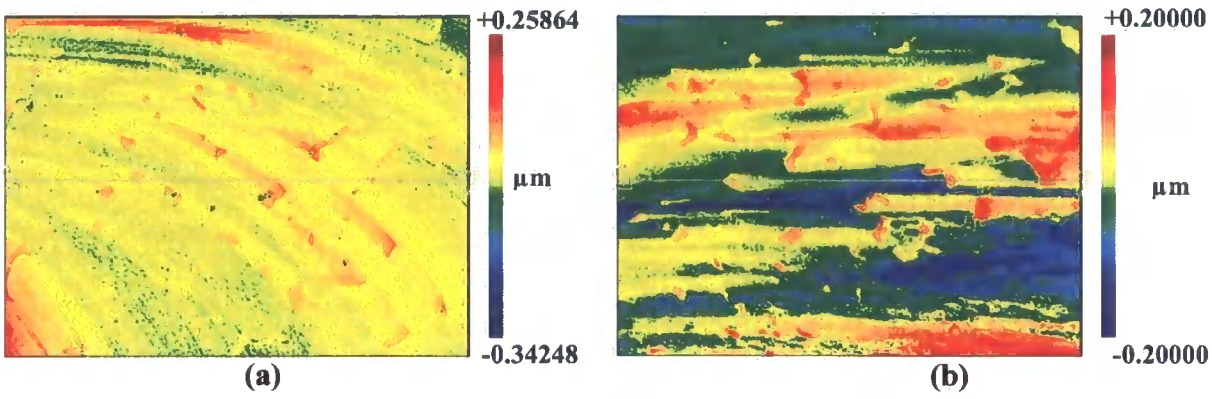

Figure 75. Surfaces of (a) Head 2 and (b) Cup 2 after 1 million cycles of wear showing smearing of carbides.

In the following Figures, the z-scale is kept the same for ease of comparison. The topography of Head 1 became progressively smoother throughout the course of testing (Figure 76). Head 2 also showed diminishing of the carbide features, but surface scratches were more in evidence (Figure 75). Cup topography followed a similar trend although to a slightly lesser extent.

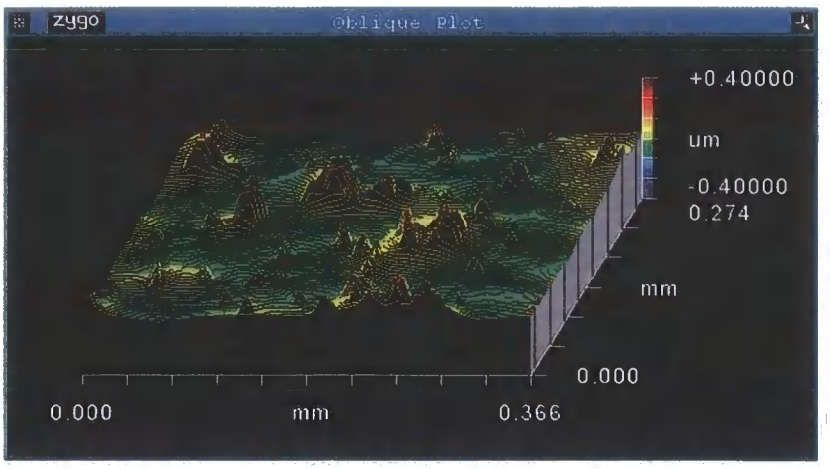

a)

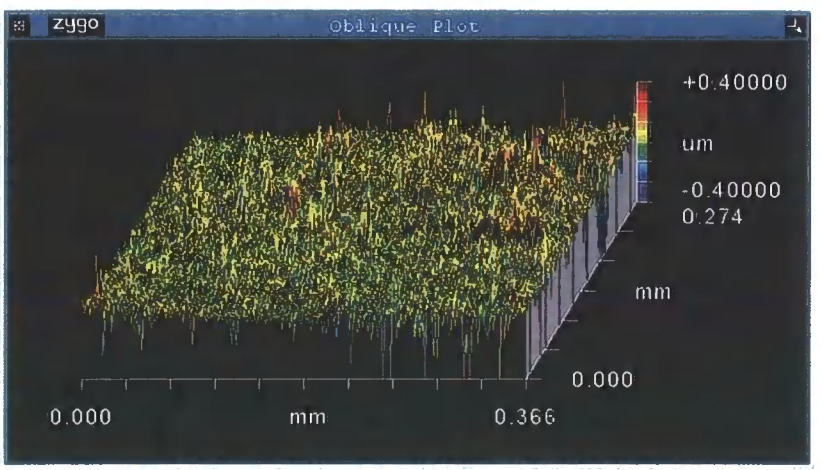

b)

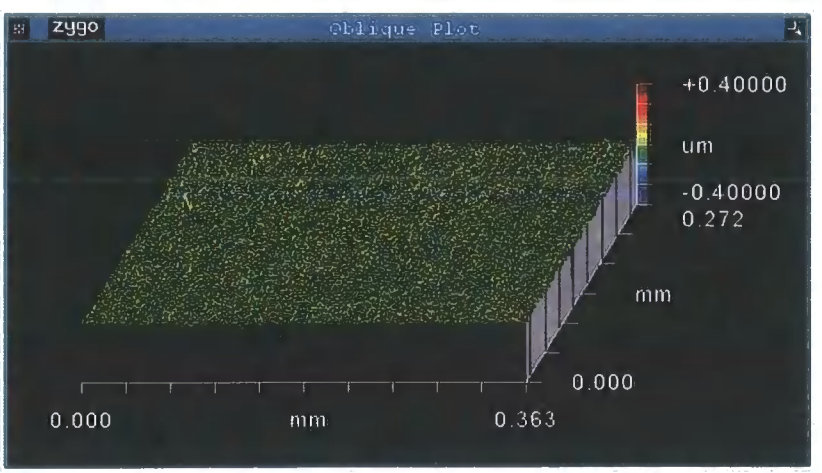

c)

Figure 76. Surface topography of Head 1; a) initial b) after 1 million cycles c) after 3 million cycles

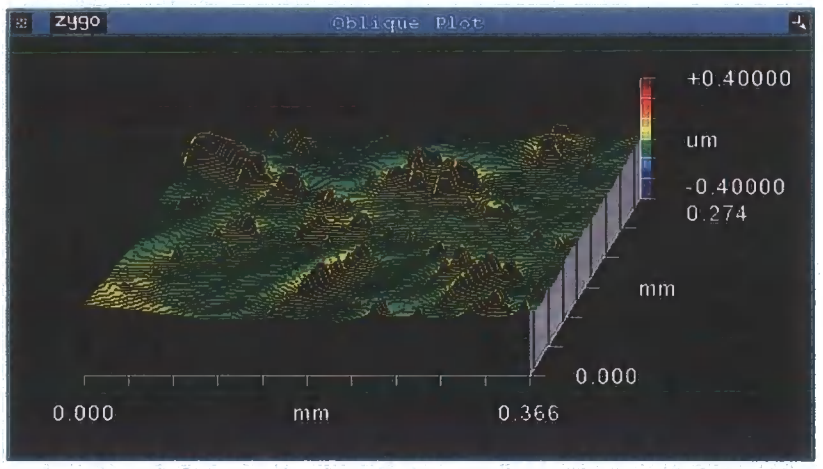

a)

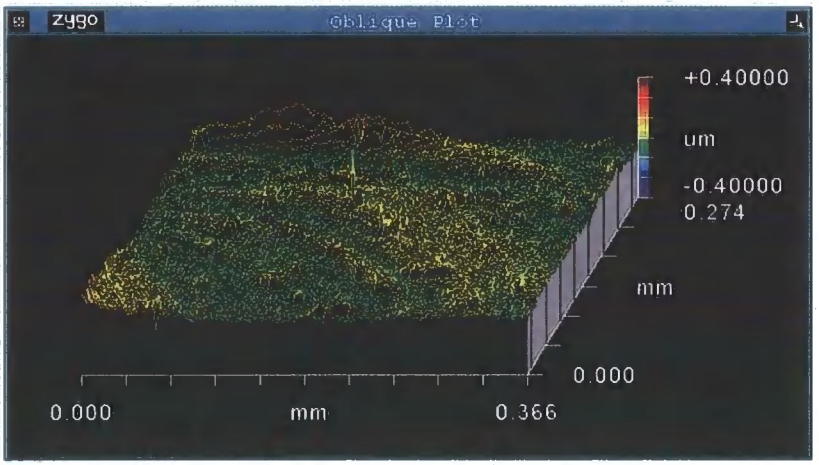

b)

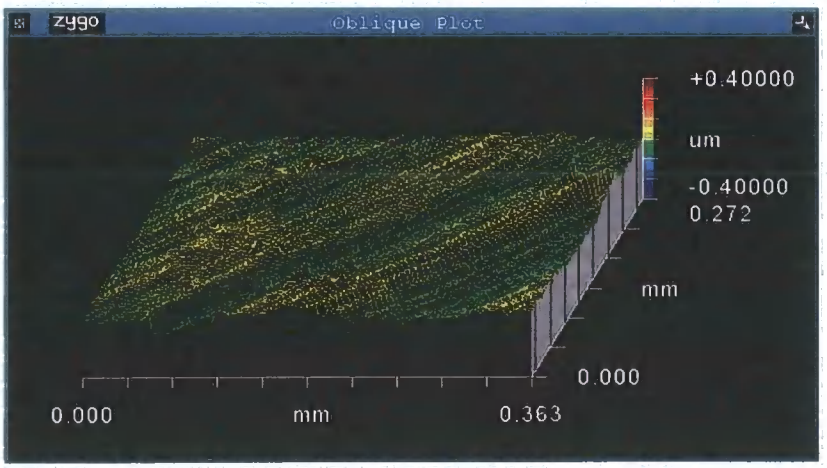

c)

Figure 77. Surface topography of Head 2; a) initial b) after 1 million cycles c) after 3 million cycles

A white deposit was seen on some components and this was investigated on the SEM. In the image (Figure 78) the deposit appears as dark areas. Elemental analysis was done on both light and dark areas of the image (i.e. both the metal and the deposit) and the results are seen in Figure 79 and Figure 80 respectively. A large spike for carbon is seen on the deposit indicating that it is organic in nature.

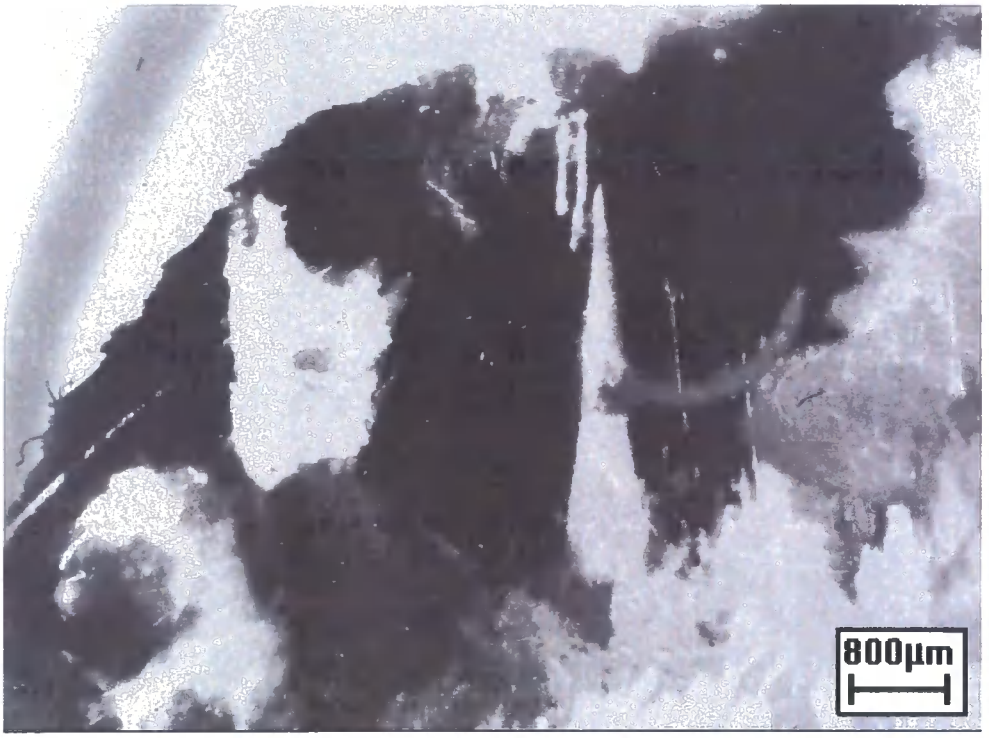

Figure 78. SEM image showing areas of deposit, which appears dark in the image

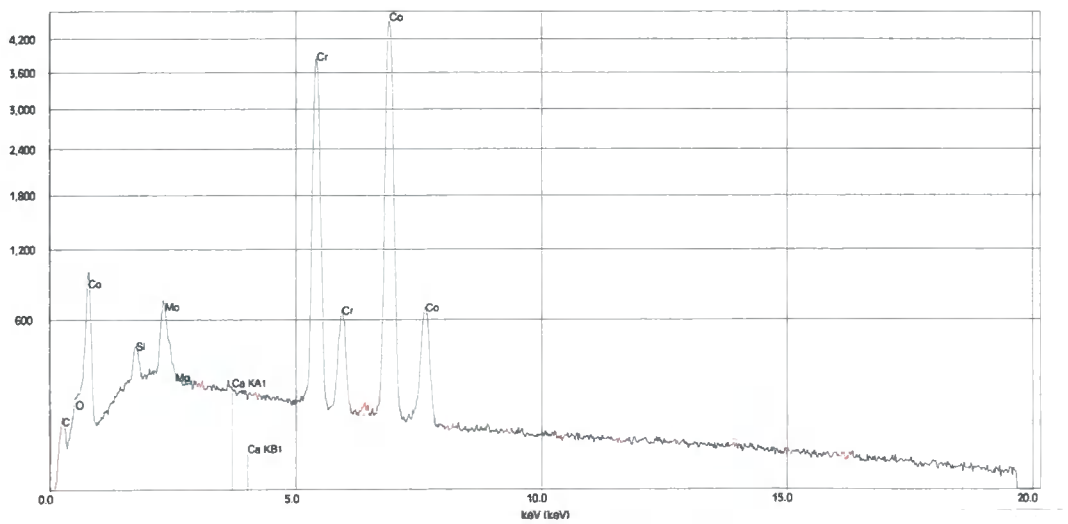

Figure 79 . Elemental analysis of component

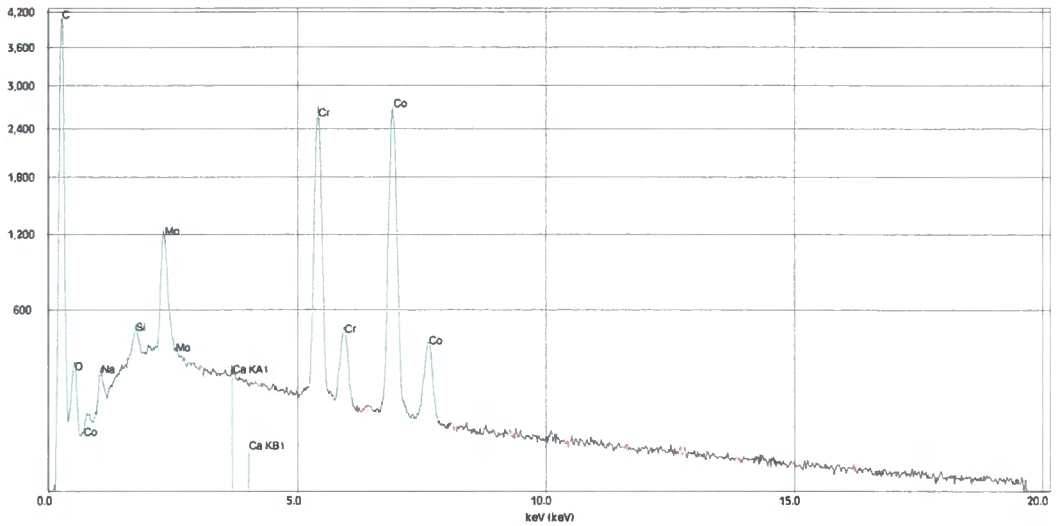

Figure 80. Elemental analysis of deposit on component.

The initial and final surface data for each component is given in the following tables. Where significance is reached, this is highlighted in pink for increases and blue for decreases.

Component	Initial Srms (μm)	Final Srms (μm)
Head 1	0.045	0.017
Head 2	0.035	0.040
Head 3	0.040	0.029
Head 4	0.054	0.028
Head 5	0.042	0.073
Cup 1	0.058	0.011
Cup 2	0.034	0.020
Cup 3	0.040	0.022
Cup 4	0.025	0.018
Cup 5	0.033	0.018

Table 21. Initial and final Srms values for each individual component; highlighted results are statistically significant decreases

Component	Initial PV (μm)	Final PV (μm)
Head 1	0.370	0.544
Head 2	0.335	0.548
Head 3	0.358	0.622
Head 4	0.450	0.488
Head 5	0.417	0.942
Cup 1	0.396	0.415
Cup 2	0.285	0.265
Cup 3	0.311	0.452
Cup 4	0.317	0.288
Cup 5	0.293	0.347

Table 22. Initial and final PV values for each individual component; highlighted results are statistically significant increases

Component	Initial S_{sk}	Final S_{sk}
Head 1	1.935	-1.117
Head 2	1.856	-0.035
Head 3	1.586	-1.641
Head 4	1.649	-0.743
Head 5	1.644	-0.342
Cup 1	2.025	-4.389
Cup 2	1.390	0.339
Cup 3	1.795	0.273
Cup 4	1.755	0.272
Cup 5	2.045	0.058

Table 23. Initial and final Ssk values for each individual component; all joints showed a statistically significant decrease.

7.4 Discussion

7.4.1 Wear

The total average wear rate was 2.02 mm^3/million cycles. However, the joints showed a higher wear rate initially (0-1 million cycles) of 2.98 mm^3/million cycles, which then reduced to 2.12 mm^3/million cycles over the next million cycles and reduced further to 0.95 in the last million cycles of the test. A higher initial wear rate is common, particularly with metal-on-metal articulations[70,149,150]. It is also not uncommon to see large variations in the wear rates between different components[70,149] as seen here with Joint 2. The wear rate from this study compares well with both published clinical (Table 24) and simulator (Table 25) results by other workers. The wear rates in Table 25 are normalised per 1000N for a more direct comparison.

As can be seen, the results of this study fit fairly well with the results of other large diameter bearings. If we assume similar wear on the head and cup in Scholes *et al*'s study[70] all the large diameter bearings still show slightly higher wear than the conventional metal-on-metal joints, although Clarke *et al*'s study on the Metasul[71] shows wear comparable to the large diameter bearings. All these joints show much lower wear than conventional metal-on-UHMWPE articulations, which typically show a wear rate of 35-50mm^3/million cycles[135,151].

Joint Type	Wear rate (mm^3/year)			Time *in vivo*
	Head	Cup	Total	
McKee-Farrar	2.04			1-25 years [152]
Muller	2.97			8-13 years [152]
McKee-Farrar	2.24	1.4	3.64	8-23 years [153]

Table 24. Clinical wear rates of metal-on-metal joints

Joint type	Wear rate ($mm^3/10^6$ cycles) per 1000 N			No. of cycles (millions) & Reference
	Running-in	Steady state	Total	
28 mm ϕ CoCrMo			0.36	2 [149]
28 mm ϕ CoCrMo (cups only)	0.30	0.07		0.5 & 4.5 [70]
Metasul	1.34	0.488		Cycles not stated [71]
Wright Medical (45mm)				
Wrought	0.19-5.7	0.11		0.5 & 2.5 [72]
Cast & heat treated	0.95-3.8	0.29		0.5 & 2.5 [72]
40mm Cormet	0.97	0.20		1 & 2 [60]
56mm Cormet	2.85	0.20		1 & 2 [154]
50mm This study	1.00	0.51		1 & 2
			0.68	3

Table 25. Simulator wear rates of metal-on-metal joints

7.4.2 Friction and Lubrication

The Stribeck plots for the joint tested throughout the wear test are given in Figure 69. Before wear testing, the joint had an almost constant friction factor in the region of 0.08. This is much lower than the 0.18 reported for other metal-on-metal articulations[116]. However, as the wear test continued the shape of the Stribeck curve changed to indicate a more favourable lubrication regime. After 2 million cycles the Stribeck curve looked like a classical fluid film lubrication curve indicating that at the higher viscosities the joint was operating in fluid film conditions. The friction factor fell to a minimum value of around 0.03 which has been seen on this type of joint in this laboratory before[104].

7.4.3 Surface topography

Initially the surfaces of all cups and heads clearly showed the presence of carbides protruding from the surface, which is typical of this material[61]. By 1 million cycles these were diminished, a fact supported by the significant reduction in the skewness. The surfaces became more negatively skewed, which is indicative of diminishing peaks or increasing valleys. The PV showed a significant increase on many components. Looking at this in combination with the skewness, it becomes clear that the roughness was manifest as valleys rather than peaks, which is a more favourable condition for lubrication. The roughness also decreased significantly in most cases. These data were supported by the friction results, which showed a shift towards fluid film lubrication as the test progressed, and also by the lower wear factor seen in the later stages of testing.

Smearing of the carbides was seen on some joints (Figure 75); this was still evident at 3 million cycles in some cases. This would also contribute to the reduction in the skewness.

Joint 2, which showed the highest wear, showed evidence of diminishing features during the course of testing (Figure 77), but not to such a large extent as the other joints, such as Joint 1 (Figure 76). The evidence of deeper scratching on Head 2 supports the higher initial wear rate seen on that joint, while improvement in the surface topography is consistent with the decrease in wear factor.

A whitish deposit was seen on the surface of the joints (Figure 78). SEM x-ray spectral analysis showed that the deposit had a high carbon content indicating its organic nature. It is likely that this deposit was a layer of denatured protein adhering to the surface. This has been noted before by other workers on explanted McKee-Farrar metal-on-metal joints[105]. Therefore, while the presence of the deposit may be protecting the surfaces somewhat in this study, a similar process may be occurring *in vivo*.

7.5 Conclusions

- Wear rates of BHR surface replacement were comparable to those found by other workers for metal-on-metal joints, both for both small and large diameter.
- Joint tribology and surface condition improved with "running-in" of the joint
- Friction factors were very low for metal-on-metal combinations
- Surface became more negatively skewed – favourable for lubrication
- Surface changes were consistent with the changes seen in friction results and with the reduction of the wear factor as the test progressed

8 Concluding Discussion

The studies herein considered the effect of various factors on the tribology of biomedical materials. First, the effects of load and stress on the wear of UHMWPE-on-stainless steel contact were investigated in a pin on plate test. While load had no effect on the wear factor, as expected, the contact stress did affect the wear factor especially at lower stresses, according to the relation $K=2x10^{-6} x \sigma^{-0.84}$.

The metal-on-metal hip wear test was conducted under a higher maximum load than the ceramic-on-ceramic tests. While a higher load was shown in the pin on plate test to have no effect on wear factor, it is usual to present wear as a wear rate rather than a wear factor for simulator studies[8,70-72]. Hence in the simulator studies the wear was presented as mm^3/million cycles, rather than mm^3/Nm, and the load was therefore not incorporated into the wear result, as in the case of the pin on plate work. As such it was prudent to draw up a comparative table to take into account the maximum load of simulator tests from the literature before discussing the performance of the joint in relation to other designs (Table 25).

The effects of radial clearance and roughness in ceramic-on-ceramic contacts were investigated. Wear tests alone were not sufficient to shed any light on the effect of either of these factors on ceramic-on-ceramic hip joints. Even over 5 million cycles the wear was undetectable gravimetrically. The large variations in the mass of components masked any overall wear and hence also any effect of either roughness or clearance. Longer wear tests would perhaps have allowed a wear trend to become evident; however, from the experiences of Clarke *et al* [71] it seems unlikely that this would have yielded any more information on the effects of the factors under investigation, namely clearance and roughness.

Friction studies, however, were able to give more insight into the effects of both clearance and roughness. The rough joints clearly operated in mixed lubrication (Figures 49 and 50) and this was supported by theoretical calculations of h_{min}[34] and λ[46]. The changes in the surface roughness of these joints also confirm that some surface contact is occurring. Changes in the surfaces of the smooth ceramics (in the clearance

test) also suggest that some surface contact did take place, since granular pullout was clearly visible on the AFM scans (e.g. Figure 44), which is in accordance with similar studies performed on 28mm ceramic joints[86,115,128,129].

The metal-on-metal joints investigated, however, did show detectable wear. Neither running-in nor steady state wear correlated with the clearance in the joints, as seen in Table 26, which shows the correlation values for the wear rates and diametral clearance, for all the wear rates given in Chapter 7. This is not just a statistical effect: Joint 2 had the highest wear and had a clearance in the middle of the range. Higher wear has been seen, however, on metal-on-metal joints with higher clearance in previous studies[70,126] and direct measurements of surface separation have also shown a higher degree of separation for smaller clearances[127].

Joint	Diametral Clearance /μm	Wear rates mm^3/million cycles			
		0-1 million cycles	1-2 million cycles	2-3 million cycles	Overall Wear
1	200	2.05	1.84	0.49	1.46
2	170	7.57	6.36	3.39	5.77
3	150	0.68	0.64	0.19	0.50
4	160	3.59	1.44	0.35	1.79
5	150	0.99	0.32	0.33	0.55
Correlation		0.10	0.28	0.16	0.18
N		5	5	5	5

Table 26. Correlation of wear rate with diametral clearance for metal-on-metal resurfacing joints

The clearances in the metal-on-metal study overlapped with the range of clearances investigated in the ceramic clearance study. Considering the effect of clearance on the lubrication in that study, it is somewhat surprising that no effect was seen, especially since the effect was more marked at lower viscosities. There were a number of differences that could account for this, however. Firstly, the resurfacing prostheses had a much higher radius, which favours better lubrication, and may mask the clearance

effect. Also, the metal-on-metal joints were tested in bovine serum, while the friction study of the radial clearance in the ceramic-on-ceramic joints was conducted in the absence of proteins. The presence of the proteins is thought to protect the surface, and this may make the effect of clearance less pronounced.

The presence of proteins in the ceramic clearance wear test, was likely to have protected the surfaces from wear to some extent, although clearly there was a change in the surface over the course of the test. It is unlikely however, that detectable wear rates would have been seen in this test had it been conducted in the absence of proteins. The ceramic roughness wear test used CMC solution as the lubricant, and the wear rates were still not discernible.

From Figure 81 it is evident that the control components in the metal-on-metal test showed a varying but measurable change in mass during the course of testing of the order of 0.0002-0.0006g. Figure 82 shows the mass change of the control for the ceramic clearance test. Apart from the large jump between 1-1.5 million cycles (seen on all components at this point), the control specimens showed a change in mass of the order of 0.002g.

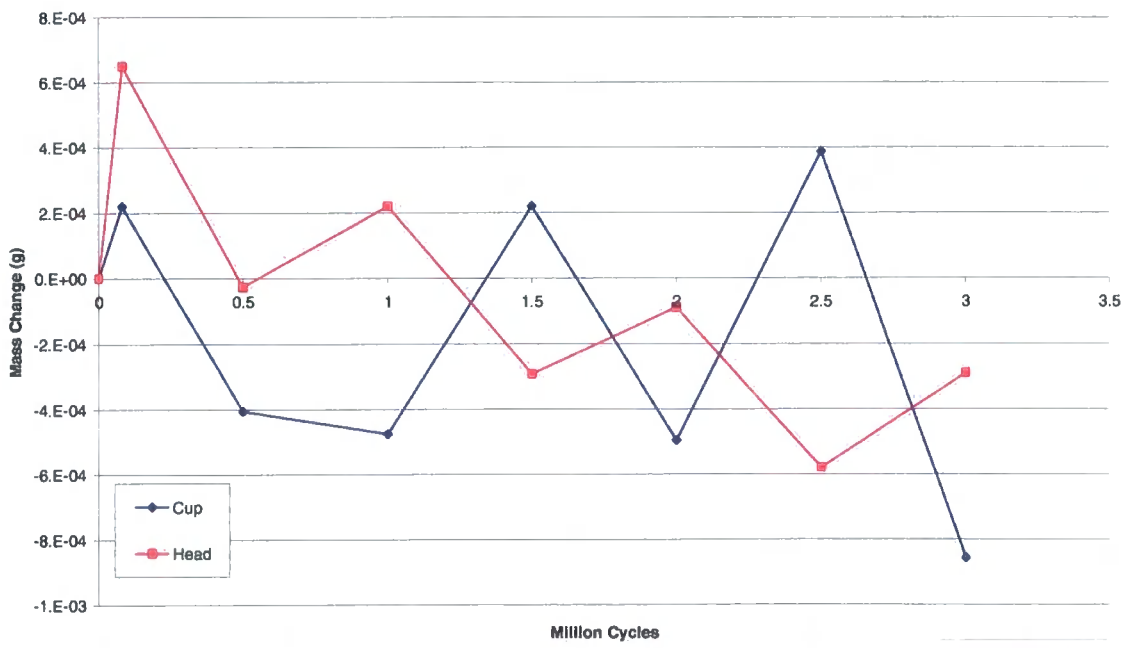

Figure 81. The change in mass of the control specimens during the metal-on-metal resurfacing test

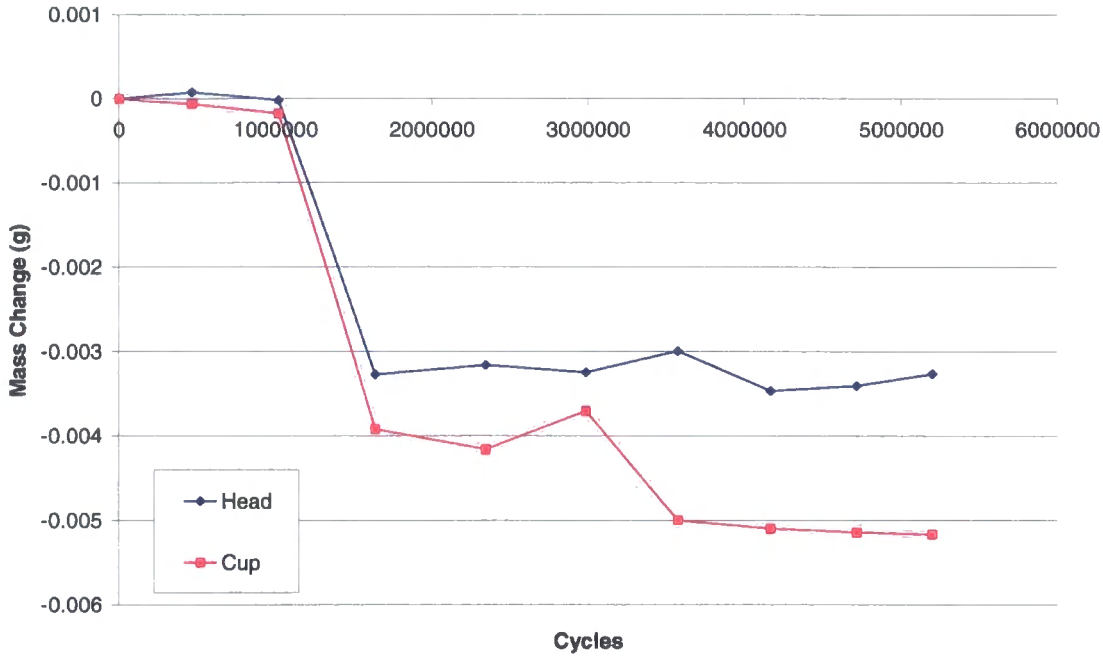

Figure 82. Changes in mass of control components for ceramic clearance testing.

Comparing this with the wear graphs for each of the ceramic-on-ceramic tests (Figures 37 and 64), where variation is 0.0008g and 0.0006g respectively it is seen that this is smaller than the variation in the ceramic control but of the order of the changes in the metallic one. Therefore the mass change on the ceramics was of the order of the mass change on the control component, making the detection of actual wear difficult. This adds further credence to the wear existing on those components, but being beyond the detection limit of the test protocol.

When friction-tested with bovine serum, the ceramic-on-ceramic joints gave a friction factor of approximately 0.025-0.03 regardless of the clearance (Figure 31) with only one exception. From Figure 69 it can be seen that post running-in the friction factors for the metal-on-metal joint were also in this region, particularly for the lowest viscosities which would be most comparable to the lubricant used in the ceramic-on-ceramic test. A friction factor of 0.02-0.03 has been seen in this laboratory for large diameter metal-on-metal joints[104] and 28mm ceramic-on-ceramic joints[128]. This further supplements the suggestion that the friction seen in this case is generated by the shearing of the

proteins present in the lubricant, since the value of the friction factor is the same in both cases, even though the material and joint dimensions differ.

9 Overall Conclusions

- The wear factor in stainless steel-on-UHMWPE contacts was found to decrease as nominal contact stress increased, according to the relation: $K=2x10^{-6}x\sigma^{-0.84}$
- The wear for ceramic-on-ceramic components was undetectable. The variation in the mass of the components in both ceramic studies is of a similar magnitude to the variation in mass on the CoCrMo control components. However, surface topography studies did show a change in surface condition throughout testing.
- Pre-wear friction studies gave more insight into the effect of radial clearance and roughness on the tribology of ceramic-on-ceramic hip joints:
    - Friction factor increased with increasing radial clearance and the effect was more marked at lower viscosities as expected from theoretical calculations
    - Friction factor increased with increasing roughness. There was a discontinuity in the data at a combined roughness of $5x10^{-8}$ m at which point the friction factor dropped dramatically. After this point the friction factor continued to rise
    - Rougher joints operated further within the mixed lubrication regime than smoother ones
- The tribology of the BHR resurfacing prosthesis improved as the wear test progressed:
    - Friction studies indicated a progressive shift towards fluid film lubrication throughout the wear test
    - Wear rates decreased as the wear test progressed
- The friction factors found in tests using bovine serum lubricant were in the same range (0.025-0.03), both for 32mm ceramic-on-ceramic joints and for 50mm metal-on-metal joints. This supports the theory that the friction in this case is caused by shearing of proteins adsorbed to the surface of the joints.

Suggestions for future work

The work carried out during the author's course of study, and included herein has, as is common in science, left many unanswered questions. Further work based on these studies could help to shed more light on some of these.

For example, it would be interesting to repeat the ceramic roughness friction study with particular attention to the combined roughnesses of around $5x10^{-8}$m and higher. While carrying on the wear tests to a higher number of cycles may seem like a logical next step, Clarke *et al*'s experience with a 14.4 million cycle wear test indicates that this may not be a sensible way to proceed with ceramic joints. However, the friction studies herein have proven to show the effects of the various investigated factors on lubrication, even when wear is undetectable. Therefore extended friction studies into factors affecting tribology for ceramic-on-ceramic joints is perhaps prudent before any wear tests are carried out. When a wear test is carried out on ceramic-on-ceramic joints, this should be a long-term wear test in excess of 5 million cycles.

In addition, if the roughness of ceramic joints is to be investigated in future, the author suggests that explanted ceramic joints be studied carefully in order to attempt to match the surface condition as closely as possible. Alternatively, if available, explanted ceramic joints could be used in the study, although thorough non-destructive testing should be undertaken first in order to gain as much knowledge as possible from them.

Furthermore, it would be interesting to investigate further the effect of the pin radius on the wear of UHMWPE on stainless steel, especially at higher load/stress combinations. There is a practical limit to the range of radii that can be manufactured due to the thin walls of the annular pins at larger radii. Using sets of pins with either higher or lower contact area than those used in this study could be a way of increasing the range of load/stress values considered.

References

1. Wright V. The structure, friction and wear of natural joints. In: Dumbleton JH, ed. *Tribology of natural and artificial joints*. Amsterdam: Elsevier Scientific Publishing Company, 1981:23-46.

2. Paul JP. Forces transmitted by joints in the human body. *Proceedings of the Institution of Mechanical Engineers Part J 1966;181-3J:8-15.*

3. Gray H, Carter HV. *Gray's Anatomy.* Bath: Paragon, 1858 (2002).

4. Luttgens K, Hamilton N. *Kinesiology: the scientific basis of human motion.* Madison, WI, 1997.

5. Rostoker W, Galante JO. Contact Pressure Dependence of Wear Rates of Ultra High Molecular Weight Polyethylene. *Journal of Biomedical Materials Research 1979;13:957-64.*

6. English TA, Kilvington M. In vivo records of hip loads using a femoral implant with telemetric output (a preliminary report). *Journal of Biomedical Engineering 1979;1-2:111-5.*

7. Bergmann G, Graichen F, Rohlmann A. Hip joint loading during walking and running measured in two patients. *Journal of Biomechanics 1993;26-8:969-90.*

8. Bowsher JG, Shelton JC. A hip simulator study of the influence of patient activity level on the wear of crosslinked polyethylene under smooth and roughened femoral conditions. *Wear 2001;250:167-79.*

9. Robbins SL. *Pathologic Basis of Disease.* Philadelphia: W. B. Saunders Company, 1974.

10. Berry DJ, Harmsen WS, Cabanela ME, Morrey BF. Twenty-five-year survivorship of two thousand consecutive primary Charnley total hip replacements: factors affecting survivorship of acetablar and femoral components. *Journal of Bone and Joint Surgery 2002;84-A-2:171-7.*

11. Revell PA, Al-Saffar N, Kobayashi A. Biological reaction to debris in relation to joint prostheses. *Proceedings of the Institution of Mechanical Engineers Part H-Journal of Engineering in Medicine 1997;211-H2:187 - 97.*

12. Howie DW, Vernon-Roberts B, Oakeshott R, Manthey B. A Rat Model of Resorption of Bone at the Cement-Bone Interface in the Presence of Polyethylene Wear Particles. *Journal of Bone and Joint Surgery 1988;70-A-2:257-63.*

13. Ingham E, Fisher J. Biological reactions to wear debris in total joint replacement. *Proceedings of the Institution of Mechanical Engineers Part H- Journal of Engineering in Medicine 2000;214-H1:21-37.*

14. Schmalzried TP, Jasty M, Harris WH. Periprosthetic Bone Loss in Total Hip Arthroplasty. *Journal of Bone and Joint Surgery 1992;74-A-6:849 - 63.*

15. Elfick APD, Smith SL, Green SM, Unsworth A. The quantitative assessment of UHMWPE wear debris produced in hip simulator testing: the influence of head material and roughness, motion and loading. *Wear 2001;249:517-27.*

16. The Swedish Total Hip Replacement Register. Annual Report 2003 - The Swedish national hip arthroplasty register. 2004.

17. The Swedish Total Hip Replacement Register. Prognosis of Total Hip Replacement. *2000.*

18. Warashina H, Sakano S, Kitamura S, Yamauchi K-I, Yamaguchi J, Ishiguro N, Hasegawa Y. Biological reaction to alumina, zirconia, titanium and polyethylene particles implanted onto murine calvaria. *Biomaterials 2003;24-21:3655-61.*

19. Rabinowicz E. *Friction and Wear of Materials.* New York: John Wiley and Sons, Inc, 1965.

20. Lancaster JK. Dry bearings: a survey of materials and factors affecting their performance. *Tribology 1973;6:219-51.*

21. Greenwood JA, Williamson JBP. Contact of nominally flat surfaces. *Proceedings of the Royal Society 1966;A295:300-19.*

22. Archard JF. Contact and Rubbing of Flat Surfaces. *Journal of Applied Physics 1953;24-8:981-8.*

23. Buckley DH. *Surface effects in adhesion, friction, wear and lubrication.* Vol. 5Amsterdam: Elsevier Scientific Publishing Company, 1981.

24. Tsao A, Mintz L, McRae CR, Stulberg D, Wright T. Failure of the Porous-Coated Anatomic Prosthesis in Total Knee Arthroplasty Due to Severe Polyethylene Wear. *Journal of Bone and Joint Surgery 1993;75-A-1:19-26.*

25. Black J. *Orthopaedic Biomaterials in Research and Practice.* Churchill Livingstone, 1988.

26. Unsworth A. The effects of lubrication in hip joint prostheses. *Physics in Medicine and Biology 1978;23-2:253-68.*

27. Gore TA, Higginson GR, Kornberg RE. Some evidence of squeeze-film lubrication in hip prostheses. *Engineering in Medicine 1981;10-2:89-95.*

28. Hutchings IM. *Tribology: Friction and Wear of Engineering Materials.* London: Edward Arnold, 1992.

29. Higginson GR, Unsworth A. The lubrication of natural joints. In: Dumbleton JH, ed. *Tribology of natural and artificial joints.* Amsterdam: Elsevier Scientific Publishing Company, 1981:47-73.

30. Jin ZM, Dowson D, Fisher J. Fluid film lubrication in natural hip joints. In: Dowson D, Taylor C, Godet M, Dalmaz G, Childs THC, eds. *Thin Films in Tribology: proceedings of the 19th Leeds-Lyon symposium on tribology*: Elsevier Scientific Publishing Company, 1993:545-55.

31. Unsworth A. Tribology of human and artificial joints. *Proceedings of the Institution of Mechanical Engineers Part H- Journal of Engineering in Medicine 1991;205:163-72.*

32. Hills BA. Boundary lubrication in vivo. *Proceedings of the Institution of Mechanical Engineers Part H- Journal of Engineering in Medicine 2000;214-H1:83-94.*

33. Spikes HA. Mixed Lubrication - An Overview. *10th International Colloquium 'Tribology - Solving Friction and Wear Problems'.* Ostfildern: Technische Akademie Esslingen, 1996:1712 - 35.

34. Hamrock BJ, Dowson D. Elastohydrodynamic Lubrication of Elliptical Contacts for Materials of Low Elastic Modulus I - Fully Flooded Conjunction. *Journal of Lubrication Technology 1978;100:236 - 45.*

35. Jin ZM, Dowson D, Fisher J. Analysis of fluid film lubrication in artificial hip joint replacements with surfaces of high elastic modulus. *Proceedings of the Institution of Mechanical Engineers Part H- Journal of Engineering in Medicine 1997;211-H3:247-56.*

36. Cooke AF, Dowson D, Wright V. The rheology of synovial fluid and some potential synthetic lubricants for degenerate synovial joints. *Engineering in Medicine 1978;7-2:66-72.*

37. Joyce TJ, Monk D, Scholes SC, Unsworth A. A multi-directional wear screening device and preliminary results of UHMWPE articulating against stainless steel. *Bio-Medical Materials and Engineering 2000;10-3-4:241-9.*

38. Clarke IC, Chan FW, Essner A, Good VD, Kaddick C, Lappalainen R, Laurent M, McKellop HA, McGarry W, Schroeder D, Selenius M, Shen MC, Ueno M, Wang A, Yao J. Multi-laboratory simulator studies on effects of serum proteins on PTFE cup wear. *Wear 2001;250:188-98.*

39. Scholes SC, Unsworth A, Hall RM, Scott R. The effects of material combination and lubricant on the friction of total hip prostheses. *Wear 2000;241-2:209-13.*

40. Mazzucco D, Spector M. Effects of contact area and stress on the volumetric wear of ultrahigh molecular weight polyethylene. *Wear 2003;254-5-6:514-22.*

41. Good VD, Clarke IC, Gustafson GA, Downs B, Anissian L, Sorensen K. Wear of ultra-high molecular weight polyethylene and polytetrafluoroethylene in a hip simulator. *2000;71-4:365-9.*

42. Vassiliou K, Elfick APD, Scholes SC, Unsworth A. The effect of "running in" on the tribology of metal-on-metal hip resurfacing device. *Society for Biomaterials.* Memphis, Tennessee, USA, 2005:83.

43. Vassiliou K, Unsworth A. Is the wear factor in total joint replacements dependent on the nominal contact stress in ultra-high molecular weight polyethylene contacts? *Proceedings of the Institution of Mechanical Engineers Part H- Journal of Engineering in Medicine 2004;218-H2:101-8.*

44. Stribeck R. Die wesenlichen Eigenchaften der Gleit - und Rollen-lager. *Zeitschrift d. Vereins Seutscher Ingenieure 1902;46:1341.*

45. Unsworth A, Pearcy MJ, White EFT, White G. Soft layer lubrication of artificial hip joints. *Proceedings of the Institution of Mechanical Engineers - International Conference Volume on Tribology 1987;219:715-24.*

46. Johnson KL, Greenwood JA, Poon SY. A simple theory of asperity contact in elastohydrodynamic lubrication. *Wear 1972;19:91-108.*

47. Johnson KL. Normal contact of elastic solids: Hertz theory. In: *Contact mechanics.* Cambridge: Cambridge University Press, 1985:84-106.

48. Timoshenko S, Goodier JN. *Theory of Elasticity.* 2nd ed. New York: McGraw-Hill Book Company, Inc., 1951 (1934).

49. Fisher J, Dowson D. Tribology of artificial joints. *Proceedings of the Institution of Mechanical Engineers Part H- Journal of Engineering in Medicine 1991;205:73-9.*

50. Berzen J. Standardization of UHMW-PE for use as implant material. In: Willer H-G, Buchhorn GH, Eyerer P, eds. *Ultra-High Molecular Weight Polyehtylene in Orthopedic Surgery*: Hogrefe & Huber Publishers, 1991:50-4.

51. Barbour PSM, Stone MH, Fisher J. A study of the wear resistance of three types of clinically applied UHMWPE for total replacement hip prostheses. *Biomaterials 1999;20-22:2101-6.*

52. Ratner BD, Hoffman AS, Schoen FJ, Lemons JE, eds. *Biomaterials Science: an Introduction to the Materials in Medicine.* Academic Press, 1996.

53. Skinner HB. Ceramic bearing surfaces. *Clinical Orthopaedics and Related Research 1999;369:83-91.*

54. Hench LL, Wilson J, eds. *An introduction to Bioceramics.* Vol. 1: World Scientific, 1993.

55. Affatato S, Testoni M, Cacciari GL, Toni A. Mixed-oxides prosthetic ceramic ball heads. Part 2: effect of the ZrO2 fraction on the wear of ceramic on ceramic joints. *Biomaterials 1999;20-20:1925-9.*

56. Cherif K, Gueroult B, Rigaud M. Wear behaviour of alumina toughened zirconia materials. *Wear 1996;199-2:113-21.*

57. Firkins PJ, Tipper JL, Ingham E, Farrar R, Fisher J. Wear and debris analysis of low and high carbon content cobalt chrom alloys for use in metal on metal total hip replacements. *44th Annual Meeting of the Orthopaedic Research Society.* New Orleans, Louisiana, 1998:370.

58. Scholes SC, Unsworth A. Pin-on-plate studies on the effect of rotation on the wear of metal-on-metal samples. *Journal of Materials Science-Materials in Medicine 2001;12-4:299-303.*

59. Tipper JL, Firkins PJ, Ingham E, Fisher J, Stone MH, Farrar R. Quantitative analysis of the wear and wear debris from low and high carbon content cobalt chrome alloys used in metal on metal hip replacements. *Journal of Materials Science Materials in Medicine 1999;10-6:353-62.*

60. Bowsher JG, Nevelos JE, Pickard J, Shelton JC. Do heat treatments influence the wear of large diameter metal-on-metal hip joints? An in vitro study under normal and

adverse gait conditions. *49th Meeting of the Orthopaedic Research Society.* Vol. 28. New Orleans, Louisiana, 2003, 2003:Poster: 1398.

61. Cawley J, Metcalf JEP, Jones AH, Band TJ, Skupien DS. A tribological study of cobalt chromium molybdenum alloys used in metal-on-metal resurfacing hip arthroplasty. *Wear 2003;255-7-12:999-1006.*

62. McKellop HA, Shen F-w, Lu B, Campbell P, Salovey R. Development of an extremely wear-resistant ultra high molecular weight polyethylene for total hip replacements. *Journal of Orthopaedic Research 1999;17-2:157-67.*

63. Joyce TJ, Unsworth A. The design of a finger wear simulator and preliminary results. *Proceedings of the Institution of Mechanical Engineers Part H- Journal of Engineering in Medicine 2000;215:519-26.*

64. Good VD. Polyethylene selection in TKA: does it make a difference? *Emerging orthopaedic technologies: where surgeon and scientist meet.* Flims, Switzerland, 2005:Session V, Paper 1.

65. Charnley J. Arthroplasty of the Hip - a new operation. *The Lancet 1961:1129 -32.*

66. Layrolle P, van der Valk C, Dalmeijer R, van Blitterswijk CA, de Groot K. histomorphometrical study of biomimetic apatite coating implanted in femurs of goats up to 6 months. *European Society for Biomaterials.* London, Uk, 2001:T121.

67. Yuan H, de Bruijn JD, van Blitterswijk CA, Zhang X, de Groot K. Osteoinduction by a porous alumina ceramic. *European Society for Biomaterials.* London, UK, 2001:T209.

68. Lie SA, Havelin LI, Furnes ON, Engesaeter LB, Vollset SE. Failure rates for 4762 revision total hip arthroplasties in the Norwegian Arthroplasty Register. *Journal of Bone and Joint Surgery 2004;86-B-4:504-9.*

69. Semlitsch M. CoCrMoC metal/metal articulation as a solution to the problem of wear of hip joint replacements. *SERC/IMechE Annual Expert Meeting on Failure of Joint Prostheses.* 1993:40-5.

70. Scholes SC, Green SM, Unsworth A. The wear of metal-on-metal total hip prostheses measured in a hip simulator. *Proceedings of the Institution of Mechanical Engineers Part H- Journal of Engineering in Medicine 2001;215-H6:523-30.*

71. Clarke IC, Good VD, Williams P, Schroeder D, Anissian L, Stark C, Oonishi H, Schuldies J, Gustafson G. Ultra-low wear rates for rigid on rigid bearings in total

hip replacements. *Proceedings of the Institution of Mechanical Engineers Part H-Journal of Engineering in Medicine 2000;214-H4:331-47.*

72. Chan FW, Bobym JD, Medley JB, Krygier JJ, Yue S, Tanzer M. Engineering issues and wear performance of metal on metal hip implants. *Clinical Orthopaedics and Related Research 1996;333:96-107.*

73. Boehler M, Knahr K, Plenk H, Walter A, Salzer M, Schreiber V. Long-term results of uncemented alumina acetabular implants. *Journal of Bone and Joint Surgery 1994;76-B-1:53-9.*

74. Sedel L, Nizard RS, Kerboull L, Witvoet J. Alumina-Alumina Hip Replacement in Patients Younger Than 50 Years Old. *Clinical Orthopaedics and Related Research 1994;298:175-83.*

75. Boutin P. Arthroplastie totale de la hanche par prothèse en alumine frittée etude experiméntale et premières applications cliniques. *1972;58:229-46.*

76. Sedel L, Hamadouche M, Bizot P, Nizard RS. Long term datas concerning the use of alumina on alumina bearings in total hip replacements. *Engineers and Surgeons - joined at the hip.* London, 2002.

77. Bizot P, Hannouche D, Nizard RS, Witvoet J, Sedel L. Hybrid alumina total hip arthroplasty using press-fit metal-backed socket in patients younger than 55 years - a six- to 11- year evaluation. *Journal of Bone and Joint Surgery 2004;86B-2:190-4.*

78. Hamadouche M, Boutin P, Daussange J, Bolander ME, Sedel L. Alumina on Alumina Total Hip Arthroplasty. *Journal of Bone and Joint Surgery 2002;84-A-1:69-77.*

79. Mahoney OM, Dimon JH. Unsatisfactory Results with a Ceramic Total Hip Prosthesis. *Journal of Bone and Joint Surgery 1990;72-A-5:663-71.*

80. Sedel L, Kerboull L, Christel P, Meunier A, Witvoet J. Alumina-on-alumina hip replacement: results and survivorship in young patients. *Journal of Bone and Joint Surgery 1990;72-B-4:658-63.*

81. Howie DW, Campbell D, McGee M, Cornish BL. Wagner resurfacing hip arthroplasty - the results of one hundred consecutive arthroplasties after eight to ten years. *Journal of Bone and Joint Surgery 1990;72-A-5:708-14.*

82. Treacy RBC, McBryde CW, Pynsent PB. Birmingham hip resurfacing arthroplasty: a minimum follow-up of five years. *Journal of Bone and Joint Surgery 2005;87-B-2:167-70.*

83. Amstutz HC, Beaule PE, Dorey FJ, Le Duff MJ, Campbell PA, Gruen TA. Metal-on-metal hybrid surface arthroplasty: two to six-year follow-up study. *Journal of Bone and Joint Surgery 2004;86-A-1:28-39.*

84. Lerouge S, Huk O, Yahia LH, Witvoet J, Sedel L. Ceramic-ceramic and metal-polyethylene total hip replacements. *Journal of Bone and Joint Surgery 1997;79-B-1:135-9.*

85. Yoo JJ, Kim HJ, Kim Y-M. Damage of an alumina-on-alumina bearing surface from a difficult reduction of a total hip arthroplasty - a report of three cases. *Journal of Bone and Joint Surgery 2004;86-A-2:376-8.*

86. Scholes SC, Green SM, Unsworth A. Nanotribological characterisation of alumina femoral heads using an atomic force microscope. *Key Engineering Materials 2002;218-220:543-8.*

87. Saikko V, Pfaff H-G. Low wear and friction in alumina/alumina total hip joints. *Acta Orthopaedica Scandinavica 1998;69-5:443-8.*

88. Brown SS, Kawanabe K, Manaka M, Williams P, Good VD, Clarke IC. Eliminating the confounding effect of metal transfer in gravimetrical wear assessment of alumina heads. *50th Annual Meeting of the Orthopaedic Research Society.* San Fransisco, California, USA, 2004:Poster No. 1457.

89. Nevelos JE, Ingham E, Doyle C, Streicher R, Nevelos AB, Walter W, Fisher J. microseparation of the centres of alumina-alumina artificial hip joints during simulator testing produces clinically relevant wear rates and patterns. *Journal of Arthroplasty 2000;15-6:793-5.*

90. Stewart T, Tipper JL, Insley G, Streicher RM, Ingham E, Fisher J. The performance of new ceramic articulations in hip sumulator studies with microseparation. *Engineers and Surgeons - joined at the hip.* London, 2002.

91. Dorlot JM, Christel P, Meunier A. Wear analysis of retrieved alumina heads and sockets of hip prosthese. *Journal of Biomedical Materials Research 1989;23-A3 SUPP:299-310.*

92. Nevelos JE, Prudhommeaux F, Hamadouche M, Doyle C, Ingham E, Meunier A, Nevelos AB, Sedel L, Fisher J. Comparative analysis of two different types of alumina-alumina hip prosthesis retrieved for aseptic loosening. *Journal of Bone and Joint Surgery 2001;83-B-4:598-603.*

93. Nevelos JE, Ingham E, Doyle C, Fisher J, Nevelos AB. Analysis of retrieved alumina ceramic components from Mittelmeier total hip prostheses. *Biomaterials 1999;20-19:1833-40.*

94. Eickmann T, Manaka M, Clarke IC, Gustafson A. Squeaking and neck-socket impingement in a ceramic total hip arthroplasty. In: Ben-Nissan B, Sher D, Walsh W, eds. *Bioceramics-15.* Vol. 240-242. Sydney, Australia: Trans Tech Publications Ltd, 2003:849-52.

95. Dorlot JM, Christel P, Meunier A. Analysis of wear on retrieved alumina heads and sockets of hip prostheses. *Symposium on retrieval & analysis of surgical implants & Biomaterials.* Snowbird, Utah, USA, 1988:67.

96. Manaka M, Clarke IC, Gustafson A, Imakiire A. Impingement in ceramic hip patient - a retrieval and wear-scar analysis of femoral head. In: Ben-Nissan B, Sher D, Walsh W, eds. *Bioceramics-15.* Vol. 240-242. Sydney, Australia: Trans Tech Publications Ltd, 2003:847-8.

97. Dennis GA, Komistek RD, Northcut EJ, Ochoa JA, Ritchie A. "In vivo" determination of hip joint separation and the forces denerated due to impact loading conditions. *Journal of Biomechanics 2001;34:623-9.*

98. Amstutz HC, Grigoris P. Metal on metal bearings in hip arthropasty. *Clinical Orthopaedics and Related Research 1996;329S:S11-S34.*

99. Schmalzried TP, Peters PC, Maurer BT, Bragdon CR, Harris WH. Long-duration metal-on-metal total hip arthroplasties with low wear of the articulating surfaces. *Journal of Arthroplasty 1996;11-3:322-31.*

100. Schmalzried TP, Szuszczewicz ES, Akizuki KH, Peterson TD, Amstutz HC. Factors correlating with long term survival of McKee-Farrar total hip prostheses. *Clinical Orthopaedics and Related Research 1996;329S:S48-S59.*

101. Jacobsson S-A, Djerf K, Wahlstrom O. 20-year results of McKee-Farrar versus Charnley prostheses. *Clinical Orthopaedics and Related Research 1996;329S:S60-S8.*

102. De Smet KA, Pattyn C, Verdonk R. Early results of primary Birmingham hip resurfacing using a hybrid metal-on-metal couple. *Hip International 2002;12-2:158-62.*

103. Unsworth A, Vassiliou K, Elfick APD, Scholes SC, McMinn D, Band T. Changes in friction and lubrication during a 3 million-cycle wear test on Birmingham Hip Resurfacing (Metal on metal) device. *World Congress on Medical Physics and Biomedical Engineering.* Vol. 209. Sydney, Australia, 2003:15.06B.

104. van Kampen M, Scholes SC, Unsworth A. The lubrication regime in a metal-on-metal total hip replacement. *Engineers and Surgeons - joined at the hip.* London, 2002:C601/035/2002.

105. Wimmer MA, Sprecher C, Hauert R, Tager G, Fischer A. Tribochemical reaction on metal-on-metal hip joint bearings: a comparison between in-vitro and in-vivo results. *Wear 2003;255-7-12.*

106. McKellop HA, Park S-H, Chisea R, Lu B, Normand P, Doorn P, Amstutz HC. Twenty -year analysis of retrieved metal-metal hip prostheses. *Fifth World Biomaterials Congress.* Toronto, Canada, 1996:854.

107. Naudie D, Roeder CP, Parvizi J, Berry DJ, Eggli S, Busato A. Metal-on-metal versus metal-on-polyetheylene bearings in total hip arthroplasty - a matched case-control study. *Journal of Arthroplasty 2004;19-7 Suppl. 2:35-41.*

108. Thomas P, Barnstorf S, Summer B, Willmann G, Przybilla B. Immuno-allergological properties of aluminium oxide (Al2O3) ceramics and nickel sulfate in humans. *Biomaterials 2003;24-6:959-66.*

109. Catelas I, Petit A, Marchand R, Zukor DJ, Yahia LH, Huk O. Cytotoxicity and macrophage cytokine release induced by ceramic and polyethylene particles in vitro. *Journal of Bone and Joint Surgery 1999;81-B:516-21.*

110. Schmidt MB, Weber H, Schon R. Cobalt chromium molybdenum metal combination for modular hip prostheses. *Clinical Orthopaedics and Related Research 1996;329S:S35-S47.*

111. Clarke IC. Wear of artificial joint materials I - friction and wear studies: validity of wear-screening protocols. *Engineering in Medicine 1981;10-3:115-22.*

112. Rieker C, Konrad R, Schon R. In-vitro comparison of the two hard-hard articulations for total hip replacements. *Proceedings of the Institution of Mechanical Engineers Part H- Journal of Engineering in Medicine 2001;215-H2:153-60.*

113. Smith SL, Unsworth A. An in vitro study of alumina-alumina total hip prostheses. *Proceedings of the Institution of Mechanical Engineers Part H- Journal of Engineering in Medicine 2001;215-H5:443-6.*

114. Clarke IC. Clinical and tribological perspectives of wear in alumina-alumina THR. In: Ben-Nissan B, Sher D, Walsh W, eds. *Bioceramics-15.* Vol. 240-242. Sydney, Australia: Trans Tech Publications Ltd, 2003:755-64.

115. Scholes SC, Green SM, Unsworth A. Nanoscale wear degradation of alumina femoral head bearing surfaces assessed using an atomic force microscope. *Engineers and surgeons - joined at the hip.* London, 2002:C601/036/2002.

116. Scholes SC, Unsworth A. Comparison of friction and lubrication of different hip prostheses. *Proceedings of the Institution of Mechanical Engineers Part H- Journal of Engineering in Medicine 2000;214-H1:49-57.*

117. Barbour PSM, Barton DC, Fisher J. The Influence of Contact Stress on the Wear of Uhmwpe for Total Replacement Hip Prostheses. *Wear 1995;181:250-7.*

118. Rose RM, Goldfarb HV, Ellis E, Crugnola AM. On the pressure dependence of the wear of ultrahigh molecular weight polyethylene. *Wear 1983;92:99-111.*

119. Sathasivam S, Walker PS, Campbell P, Rayner K. The Effect of Contact Area on Wear in Relation to Fixed Bearing and Mobile Bearing Knee Replacements. *Journal of Biomedical Materials Research - Applied Biomaterials 2001;58-3:282-90.*

120. Sathasivam S, Walker PS, Campbell P. Will mobile bearing knees reduce polyethylene wear compared to fixed bearing designs. *International Conference on Knee Replacement 1974-2024.* IMechE Headquarters, 1999.

121. Wang A, Essner A, Klein R. Effect of contact stress on friction and wear of ultra-high molecular weight polyethylene in total hip replacement. *Proceedings of the Institution of Mechanical Engineers Part H- Journal of Engineering in Medicine 2001;215-H2:133-40.*

122. Landry ME, Blanchard CR, Mabrey JD, Wang X, Agrawali CM. Morphology of In Vitro Generated Ultrahigh Molecular Weight Polyethylene Wear Particles as a Function of Contact Conditions and Material Parameters. *Journal of Biomedical Materials Research - Applied Biomaterials 1999;48-1:61-9.*

123. Mazzucco D, Spector M. Effect of contact area on the wear of ultrahigh molecular weight polyethylene in bidirectional pin-on-flat articulation. *49th Annual Meeting of the Orthopaedic Research Society.* Los Angeles, 2003:#0001.

124. Schmidt MB, Farrar R. Effect of diameter on the wear of metal-on-metal hips. Amsterdam, 1996:35.

125. Medley JB, Krygier JJ, Bobym JD, Chan FW, Tanzer M. Metal-metal bearing surfaces in the hip: investigation of factors influencing wear. *41st Annual meeting of the Orthopaedic Research Society.* Orlando, FLorida, USA, 1995:765.

126. Scott RA, Schroeder DW. The effect of radial mismatch on the wear of metal on metal hip prostheses: a hip simulator study. *43rd Annual meeting of the Orthopaedic Research Society.* San Fransisco, California, USA, 1997:764.

127. Smith SL, Dowson D, Goldsmith AAJ. The effect of diametral clearance, motion and loading cycles upon lubrication of metal-on-metal total hip replacements. *Proceedings of the Institution of Mechanical Engineers Part C 2001;215-1:1-5.*

128. Scholes SC, Green SM, Unsworth A. The friction and lubrication of alumina-on-alumina total hip prostheses - the effect of radial clearance and wear testing. *Key Engineering Materials 2002;218-220:535-40.*

129. Scholes SC, Green SM, Unsworth A. The influence of radial clearance and wear testing on the tribology of alumina-on-aumina total hip prostheses. *Engineers and surgeons - joined at the hip.* London, 2002:C601/037/2002.

130. Saikko V, Calonius O, Keranen J. Effect of counterface roughness on the wear of conventional and crosslinked ultrahigh molecular weight polyethylene studied with a multi-directional motion pin-on-disk device. *Journal of Biomedical Materials Research 2001;57-4:506-12.*

131. Smith SL, Elfick APD, Unsworth A. An evaluation of the tribological performance of zirconia and CoCrMo femoral heads. *Journal of Materials Science 1999;34-21:5159-62.*

132. Smith SL, Unsworth A. A five-station hip joint simulator. *Proceedings of the Institution of Mechanical Engineers Part H- Journal of Engineering in Medicine 2001;215-H1:61-4.*

133. Smith SL, Unsworth A. Simplified motion and loading compared to physiological motion and loading in a hip joint simulator. *Proceedings of the Institution of*

Mechanical Engineers Part H- Journal of Engineering in Medicine 2000;214-H3:233-8.

134. Smith SL, Burgess IC, Unsworth A. Evaluation of a hip joint simulator. *Proceedings of the Institution of Mechanical Engineers Part H- Journal of Engineering in Medicine 1999;213:469-73.*

135. Smith SL, Unsworth A. A comparison between gravimetric and volumetric techniques of wear measurement of UHMWPE acetabular cups against zirconia and cobalt-chromium-molybdenum femoral heads in a hip simulator. *Proceedings of the Institution of Mechanical Engineers Part H- Journal of Engineering in Medicine 1999;213:475-83.*

136. Topometrix Corporation. *Topometrix Technical Brief - Contact Mode Data Acquisution - Accurex/Explorer.* Topometrix Corporation, 1996.

137. American Society for Testing and Materials. F 732-00 Standard Test Method for Wear Testing of Polymeric Materials Used in Total Joint Prostheses. In: *Annual book of ASTM Standards*, 2000.

138. Scholes SC. The Tribology of Hard Bearing Surfaces for use in Hip Prostheses. *Centre for Biomedical Engineering.* Durham: University of Durham, 1999.

139. Lloyd A. The Influence of Stress and Load on the Wear of UHMWPE Pins on Stainless Steel Plates. *School of Engineering.* Durham: University of Durham, 2000.

140. Dowson D, Wallbridge NC. Laboratory wear tests and clinical observations of the penetration of femoral heads into acetabular cups in total replacement hip joints I: Charnley prostheses with polytetrafluoroethylene acetabular cups. *Wear 1985;104:203-15.*

141. Hall RM, Siney P, Unsworth A, Wroblewski BM. The association between rates of wear in retrieved acetabular components and the radius of the femoral head. *Proceedings of the Institution of Mechanical Engineers Part H- Journal of Engineering in Medicine 1998;212-H5:321-6.*

142. Saikko V, Ahlroos T. Wear simulation of UHMWPE for total hip replacement with a multidirectional motion pin-on-disk device: Effects of counterface material, contact area, and lubricant. *Journal of Biomedical Materials Research 2000;49-2:147-54.*

143. Charnley J. The wear of plastic materials in the hip joint. *Plastics and Rubber 1976;1:59-63.*

144. Scholes SC, Unsworth A, Goldsmith AAJ. A frictional study of total hip joint replacements. *Physics in Medicine and Biology 2000;45-12:3721-35.*

145. Green RJ, Davies MC, Roberts CJ, Tendler SJB. Surface plasmon resonance for real time in situ analysis of protein adsorption to polymer surfaces. *Biomaterials 1997;18:405-13.*

146. Wang A, Polineni VK, Stark C, Dumbleton JH. Effect of femoral head surface roughness on the wear of ultrahigh molecular weight polyethylene acetabular cups. *Journal of Arthroplasty 1998;13-6:615-20.*

147. Cooper JR, Dowson D, Fisher J. Macroscopic and microscopic wear mechanisms in ultra-high molecular weight polyethylene. *Wear 1993;162-164:378-84.*

148. Daniel J, Pynsent PB, McMinn DJW. Metal-on-metal resurfacing of the hip in patients under the age of 55 years with osteoarthritis. *Journal of Bone and Joint Surgery 2004;86B-2:177-84.*

149. Farrar R, Schmidt MB. The effect of diametral clearance on wear between head and cup for metal-on-metal articulations. *43rd Annual meeting of the Orthopaedic Research Society.* San Fransisco, California, 1997:71-12.

150. Chan FW, Medley JB, Bobym JD, Krygier JJ, Podgorsak GF, Tanzer M. Investigation of parameters controlling wear of metal-metal bearings in total hip arthroplasty. *43rd Annual meeting of the Orthopaedic Research Society.* San Fransisco, California, 1997:763.

151. Barbour PSM, Stone MH, Fisher J. A hip joint simulator study using simplified loading and motions cycles generating physiological wear paths and rates. *Proceedings of the Institution of Mechanical Engineers Part H- Journal of Engineering in Medicine 1999;213-H6:455-67.*

152. McKellop HA, Parl SH, Chiesa R, Doorn P, Lu B, Normand P, Grigoris P, Amstutz HC. In vivo wear of 3 types of metal-on-metal hip prostheses during 2 decades of use. *Clinical Orthopaedics and Related Research 1996;329S:128-40.*

153. Kothari M, Bartel DL, Booker JF. Surface geometry of retrieved McKee-Farrar total hip replacements. *Clinical Orthopaedics and Related Research 1996;329S:141-7.*

154. Bowsher JG, Hussain A, Nevelos JE, Shelton JC. The importance of head diameter of minimising metal-on-metal hip wear. *50th Meeting of the Orthopaedic Research Society.* Vol. 29. San Francisco, California, 2004, 2004:Poster: 1453.

Appendix A – Balance Check

The mass of a small metallic object was measured using both the Mettler Toledo AT20 and the Mettler AE200. The temperature and humidity in the laboratory were also recorded using a digital monitor. The results are shown graphically in Figure 83 and Figure 84 below.

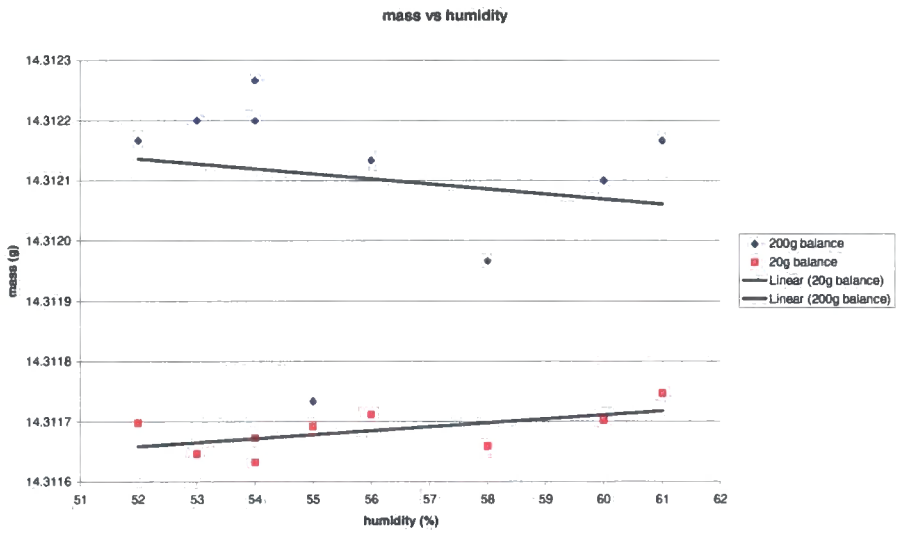

Figure 83. The variation in mass measured by the two balances, depending on the humidity in the laboratory.

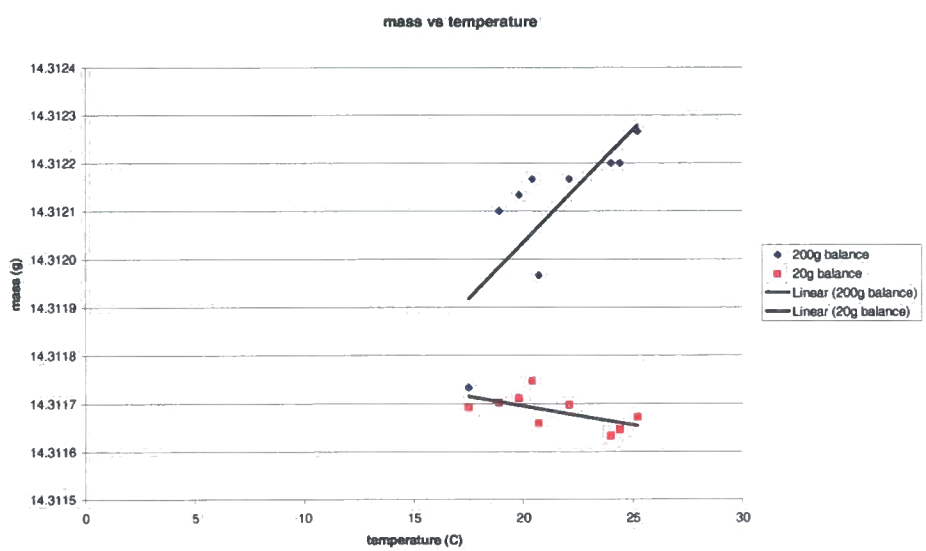

Figure 84. The variation in the mass measured by the two balances depending on the temperature on the laboratory

Appendix B – Actual average sliding distance

Due to the rotational element of the pin's path, the average sliding distance covered is larger than the reciprocation distance. This increase is calculated below.

B.1. Calculation

A computer program written in C[138] was modified in order to calculate the additional sliding distance seen by the wear interface due to the rotational element of the pin's motion. The code is included here. The program was modified, compiled and run in QuickC.

```
#include <stdio.h>
#include <math.h>

struct PT {
     float x,y;
     } ;


struct   PT   pos(float   a,float   r,float   theta,float
theta0,float ratio)
{
struct PT t;

theta0 *= 3.14159 / 180.0 ;
theta  *= 3.14159 / 180.0 ;

t.x = a*sin(theta) + r*cos(theta*ratio+theta0);
t.y =       0      + r*sin(theta*ratio+theta0);

return t ;
}

void draw( struct PT pt ,float a ,float r , int mode )
```

```
{
int x,y;

x = 320 + pt.x*310/(a+r) ;
y = 175 - pt.y*165/(r) ;

}

FILE *fp ;

main()
{
char filename[50];
float a = 0.0125 ;
float r ;
float rmin = 0;
float rmax = 0.002501;
float r0 = 0.0025 ;
float theta,theta0 ;
float sumdistance, average ;
struct PT pt,ptold ;
int i, k;
int color ;
float distance,dx,dy;
float perc;
float ratio = 1.0 ;

printf("Enter file name : ");
scanf("%s",filename);
fp = fopen(filename,"w");
if( fp == NULL )
     {
     printf("Unable to open : %s\n",filename);
```

```
        exit(1);
        }
printf("the value of rmin is: %f\n", rmin);
printf("the value of rmax is: %f\n", rmax);


sumdistance = 0;
k=0;

fprintf(fp,"radii: min, max : %f %f\n", rmin, rmax);
fprintf(fp,"radius theta0 distance\n");
for(theta0 = 0 ; theta0 < 360 ; theta0 += 1)
for( r = rmin ; r <= rmax ; r += 0.00005 )
        {
        ptold = pos( a , r , 0 , theta0 , ratio ) ;

        draw( ptold , a ,r0 , 0 ) ;

        distance = 0 ;
        for( theta = 1 ; theta <= 360 ; theta++ )
                {
                pt = pos( a , r , theta , theta0 , ratio ) ;
                draw( pt , a , r0 , 1 ) ;
                dx = pt.x - ptold.x ;
                dy = pt.y - ptold.y ;
                distance += sqrt( dx*dx + dy*dy) ;
                ptold = pt ;
                }

        fprintf(fp,"%7.5f %4.0f %f\n",r, theta0, distance) ;
        sumdistance=sumdistance+distance;
        k = k+1;
        color++ ;
```

```
        if( color > 7 ) color = 1;
        }
        average = sumdistance /k;
        perc = (average - 0.050)/0.050*100;

fprintf(fp,"average %f\n", average);
printf ("average: %f\n", average);
fprintf(fp,"perc increase: %f\n", perc);
printf("percentage increase: %f\n", perc);
scanf("%d", &i);
}
```

B.2. Results

The percentage additional sliding distance was calculated using the code given above. The results are shown in Table 27, and all results quoted throughout the document are adjusted to account for the additional sliding distance due to the rotational element of the pin motion.

	Inner radius (mm)	Outer radius (mm)	Percentage increase in sliding distance due to rotation.
Leeds tapered	0.0	1.5	0.67
Durham	0.0	2.5	1.69
ASTM	0.0	4.5	4.82
Leeds flat	0.0	4.75	5.30
Pin 1	0.0	2.95	2.27
Pin 2	1.5	3.3	4.51
Pin 3	3.0	4.2	9.04
Pin 4	4.0	4.95	13.22

Table 27. The percentage increase in sliding distance due to the rotational element of the pin motion for all diameters of pin used.

Appendix C - Cleaning Protocols

C.1. Stainless Steel Plates

The plates are cleaned using the following protocol:

- Rinse with tap water to remove bulk contaminants.
- Immerse in a solution of 1% Neutracon and place in an ultrasonic bath for 10 minutes at 37°C.
- Rinse in distilled water.
- Dry with a lint free wipe.
- Wipe with acetone and a lint free wipe.

C.2. UHMWPE Pins

The pins were cleaned according to the following protocol, closely following the ASTM recommendation (ASTM F732-00, part A6).

- Rinse with tap water to remove bulk contaminants.
- Immerse in a 1% solution of Neutracon and place in an ultrasonic bath for 15 minutes at 37°C
- Rinse in a stream of distilled water.
- Immerse in distilled water and place in an ultrasonic bath for 5 minutes at 37°C.
- Dry with a lint free tissue.
- Immerse in Acetone for 3 minutes
- Dry with a lint free tissue.
- Allow to dry in a biological flow cabinet at room temperature for 30 minutes before weighing.

C.3. Ceramic Hip Components

- Rinse components in tap water to remove bulk contaminants.
- Rinse in distilled water
- Clean with acetone and a lint free wipe to remove (most) proteins

- Immerse in 1% Neutracon solution and place in an ultrasonic bath for 30 minutes at 40° C
- Rinse in distilled water
- Immerse in distilled water and place in an ultrasonic bath for 10 minutes at 40° C
- Dry with a lint free wipe
- Wipe with acetone and lint free wipe
- For the ceramic heads, spray the inside of the taper with compressed air.
- Dry for 30 mins in atmosphere with bearing surface exposed
- Sspray the inside of the taper on the ceramic heads with compressed air again before weighing.

C.4. Metal-on-metal resurfacing study

- Rinse in tap water then distilled water
- Wipe with lint free wipe (all surfaces)
- Place in Ultrasonic bath in distilled water for 10 minutes
- Rinse in distilled
- Place in ultrasonic bath in weak neutracon solution for 10 minutes
- Rinse in distilled water
- Place in ultrasonic bath in distilled water for 10 minutes
- Rinse in distilled water
- Place in ultrasonic bath in distilled water for 3 minutes
- Rinse in distilled water
- Rinse in isopropanol and wipe with a lint free wipe (all surfaces)
- Dry with a jet of filtered inert gas
- Place in the vacuum oven at room temperature for 30 minutes to dry
- Weigh to achieve 3 consecutive readings which agree to within 0.1mg.

Appendix D – Ceramic Data

D.1. Ceramic clearance study

Component	cycles:	0	466350	1022535	1640305	2341813
	Cycles					
	(Joint 4)	-	0	556184	1173954	1875462
Head 14	Average	53.39394	53.39404	53.39413	53.39061	53.39047
	Standard Deviation	4.73E-05	4.62E-05	2.40E-04	4.58E-05	4.51E-05
Head 12	Average	53.39171	53.39181	53.39161	53.38838	53.38818
	Standard Deviation	8.02E-05	1.02E-04	1.53E-05	3.61E-05	3.06E-05
Head 3	Average	56.90551	56.90571	56.90557	56.90209	56.90198
	Standard Deviation	5.03E-05	5.77E-06	4.51E-05	4.73E-05	1.73E-05
Head 15	Average		53.35062	53.34969	53.34627	53.34614
	Standard Deviation		1.07E-04	8.14E-05	1.73E-05	1.53E-05
Head 17	Average	53.27816	53.27815	53.27813	53.27483	53.27467
	Standard Deviation	5.13E-05	4.00E-05	1.15E-05	4.04E-05	2.31E-05
Head 20	Average	52.98766	52.98774	52.98765	52.98439	52.98450
	Standard Deviation	3.51E-05	5.86E-05	5.77E-06	2.08E-05	4.73E-05
Cup 21	Average	58.34102	58.34062	58.34095	58.33720	58.33636
	Standard Deviation	6.66E-05	3.06E-05	2.23E-04	9.45E-05	1.40E-04
Cup 18	Average	101.89687	101.89734	101.89705	101.89061	101.88992
	Standard Deviation	5.29E-05	7.02E-05	1.40E-04	3.61E-05	1.87E-04
Cup 15	Average	59.62626	59.62623	59.62626	59.62256	59.62205
	Standard Deviation	6.66E-05	8.19E-05	4.04E-05	2.31E-05	1.01E-04
Cup 11	Average		59.60823	59.60844	59.60444	59.60396
	Standard Deviation		3.06E-05	3.51E-05	4.04E-05	1.25E-04
Cup 3	Average	59.23341	59.23345	59.23368	59.22962	59.22912
	Standard Deviation	4.00E-05	7.23E-05	3.46E-05	4.93E-05	9.85E-05
Cup 8	Average	59.35278	59.35272	59.35261	59.34886	59.34862
	Standard Deviation	3.61E-05	3.00E-05	1.53E-05	1.00E-05	7.55E-05

Component	Cycles:	2984050	3575465	4168925	4716277	5200000
	Cycles (Joint 4)	2517699	3109114	3702575	4249927	4700000
Head 14	Average	53.39073	53.39075	53.39069	53.39057	53.39129
	Standard Deviation	4.04E-05	4.93E-05	4.73E-05	7.00E-05	4.73E-10
Head 12	Average	53.38824	53.38835	53.38831	53.38827	53.38888
	Standard Deviation	6.81E-05	5.77E-06	1.73E-05	8.14E-05	1.73E-10
Head 3	Average	56.90212	56.90197	56.90186	56.90202	56.90254
	Standard Deviation	5.00E-05	1.53E-05	3.79E-05	7.37E-05	3.79E-10
Head 15	Average	53.34622	53.34615	53.34601	53.34602	53.34669
	Standard Deviation	3.21E-05	1.53E-05	5.57E-05	5.20E-05	5.57E-10
Head 17	Average	53.27520	53.27465	53.27463	53.27461	53.27518
	Standard Deviation	6.00E-05	3.61E-05	3.79E-05	6.43E-05	3.79E-10
Head 20	Average	52.98442	52.98467	52.98420	52.98426	52.98520
	Standard Deviation	8.08E-05	1.87E-04	2.08E-05	2.08E-05	2.08E-10
Cup 21	Average	58.33723	58.33672	58.33678	58.33662	58.33730
	Standard Deviation	8.62E-05	1.00E-05	3.79E-05	2.08E-05	3.79E-10
Cup 18	Average	101.89050	101.88935	101.88992	101.88990	101.89037
	Standard Deviation	1.75E-04	5.77E-06	4.04E-05	2.65E-05	4.04E-10
Cup 15	Average	59.62271	59.62264	59.62238	59.62240	59.62323
	Standard Deviation	3.46E-05	6.66E-05	4.58E-05	4.16E-05	4.58E-10
Cup 11	Average	59.60476	59.60445	59.60420	59.60414	59.60505
	Standard Deviation	4.04E-05	6.11E-05	2.65E-05	4.58E-05	2.65E-10
Cup 3	Average	59.22971	59.22935	59.22934	59.22920	59.22994
	Standard Deviation	6.08E-05	3.00E-05	4.04E-05	1.53E-05	4.04E-10
Cup 8	Average	59.34907	59.34778	59.34768	59.34764	59.34838
	Standard Deviation	3.79E-05	2.08E-05	3.06E-05	1.53E-05	3.06E-10

Table 28. Average mass and standard deviation for each component throughout ceramic clearance wear test (all masses in g).

D.2. Ceramic roughness study

Component	Cycles:	0	547394	1076078	1708869	2242938
Head 1	Average	31.72758	31.72731	31.72737	31.72723	31.72718
	Standard deviation	5E-05	3.79E-05	2.65E-05	1E-05	1.15E-05
Head 2	Average	31.76846	31.76823	31.76839	31.76841	31.76837
	Standard deviation	3.79E-05	2.52E-05	3.61E-05	4.36E-05	1.73E-05
Head 3	Average	31.81332	31.81315	31.81325	31.8133	31.81332
	Standard deviation	2.65E-05	3.06E-05	5.77E-06	3.21E-05	4.58E-05
Head 4	Average	31.81521	31.81504	31.81509	31.81511	31.81518
	Standard deviation	2.65E-05	3.06E-05	2.89E-05	4.51E-05	2.65E-05
Head 5	Average	31.82223	31.82206	31.82218	31.8222	31.82223
	Standard deviation	1.53E-05	4.35E-15	7E-05	4.73E-05	3.21E-05
Cup 1	Average	43.02508	43.02479	43.02496	43.02509	43.02496
	Standard deviation	3E-05	4.58E-05	2.08E-05	4.51E-05	3.61E-05
Cup 2	Average	42.70754	42.70725	42.70762	42.70754	42.70731
	Standard deviation	3.06E-05	3.61E-05	3.61E-05	3.61E-05	4.04E-05
Cup 3	Average	42.80885	42.80851	42.80868	42.80874	42.80879
	Standard deviation	4.58E-05	1E-05	2.08E-05	4.16E-05	1.73E-05
Cup 4	Average	43.40726	43.40688	43.40722	43.40723	43.4072
	Standard deviation	2.65E-05	3.46E-05	4.36E-05	4.58E-05	3.51E-05
Cup 5	Average	43.00367	43.00335	43.00355	43.00362	43.00351
	Standard deviation	4.04E-05	3.61E-05	3.61E-05	3E-05	1.15E-05

Table 29. Average mass and standard deviation for all components throughout ceramic roughness wear test (all masses in g)

Appendix E - Publications List

E.1. Conferences and meetings

Boampong D, Scholes SC, Elfick APD, Vassiliou K. Metrology and measurement of artificial joints. *Metrology for Implants.* University of Huddersfield, UK, 2002.

Unsworth A, Vassiliou K, Elfick APD, Scholes SC, McMinn D, Band T. Changes in friction and lubrication during a 3 million-cycle wear test on Birmingham Hip Resurfacing (Metal-on-metal) device. *World Congress on Medical Physics and Biomedical Engineering.* Vol. 209. Sydney, Australia, 2003:15.06B.

Unsworth A, Vassiliou K, Elfick APD, Scholes SC, McMinn D, Band TJ. Fluid film lubrication of metal-on-metal hip joints - Fact or Fiction. *ISTA.* San Fransisco, 2003.

Vassiliou K, Scholes SC, Unsworth A. The effect of TiNbON coating on the wear of Kinemax plus knee arthroplasty and on the presence of metal ions in the lubricant. *Knee arthroplasty: engineering functionality.* London, UK, 2005: 224-226.

Vassiliou K, Elfick APD, Scholes SC, Unsworth A. The effect of "running in" on the tribology of metal-on-metal hip resurfacing device. *Society for Biomaterials.* Memphis, Tennessee, USA, 2005:83.

E.2. Journal Papers

Vassiliou K, Unsworth A. Is the wear factor in total joint replacements dependent on the nominal contact stress in ultra-high molecular weight polyethylene contacts? *Proceedings of the Institution of Mechanical Engineers Part H- Journal of Engineering in Medicine 2004;218-H2:101-8.*

Vassiliou K, Elfick APD, Scholes SC, Unsworth A. The effect of "running-in" on the tribology and surface morphology of metal-on-metal hip resurfacing device (BHR) in simulator studies. *Proceedings of the Institution of Mechanical Engineers Part H-Journal of Engineering in Medicine.* Submitted May 2005.

METROLOGY AND MEASUREMENT OF ARTIFICIAL JOINTS

D. Boampong, S C Scholes, A. Elfick, K. Vassiliou
Centre for Biomedical Engineering, School of Engineering, University of Durham,
South Road, Durham, DH1 3LE
s.c.scholes@durham.ac.uk

The University of Durham has been at the forefront of mechanical testing of artificial implants for nearly thirty years. Our testing equipment includes two friction simulators (for both hips and knees), four hip wear simulators (totalling 20 testing stations), a knee wear simulator (6 station), seven single station finger simulators and several pin-on-plate machines.

An integral part of the analysis of all the different types of implant that are tested is the measurement of the surfaces on a micron and sub-micron level. This is done using a Zygo NewView 100 non-contacting 3D profilometer, an atomic force microscope (TopoMetrix Explorer SPM) and a scanning electron microscope as well as optical microscopes, form talysurf and a coordinate measuring machine. The surfaces of the test components are often measured before and after friction and wear tests. This is usually to get an idea of the general surface topography and therefore an indication of the wear mechanisms acting within the joints. However, sometimes, when the gravimetric method of wear measurement is unsuitable (i.e. for low wearing alumina-on-alumina joints or for polyurethane joints that absorb a lot of water) the surface topography analysis can be used in an attempt to get more quantitative results.

Changes in Friction and Lubrication during a 3 Million-Cycle Wear Test on a Birmingham Hip Resurfacing (metal-on-metal) Device.

A Unsworth[1], K Vassiliou[1], APD Elfick[1], SC Scholes[1], D McMinn[2] and T Band[3]

[1]Centre for Biomedical Engineering, University of Durham, England. [2] Birmingham Nuffield Hospital,[3]UK, Midland Medical Technologies Ltd, UK

Introduction

A long-term wear test was carried out on a 50mm diameter Birmingham Hip Resurfacing device made from as cast, high carbon CoCrMo alloy. The wear test was conducted in a Durham MK1 hip wear simulator with a Paul loading cycle (min load 100N max 2975N) and a realistic motion cycle.

Friction of the joint was measured on the Durham hip friction simulator, care being taken to measure this over the wear area. Measurements of friction were made at 0, 0.5, 1, 2 and 3 million cycles of wear testing using 25% bovine serum as lubricant. The tests were conducted at 5 different viscosities of lubricant covering the range from normal to arthritic fluid.

Results

The results were plotted as a 'Stribeck' curve and from this (figure 1), inferences could be made about the lubrication modes. Prior to any wear testing the friction factor was 0.08 and fairly constant for all viscosities of lubricant. This suggests that little or no fluid film lubrication was being generated and the metal-on-metal surfaces were largely sliding directly on each other. By 1 million cycles a classical mixed lubrication stribeck curve had emerged with friction factors falling from 0.08 at low viscosities to 0.025 at high viscosities. At two million cycles this curve had developed further showing fluid film lubrication at higher viscosities and a minimum friction factor of 0.015. This was maintained at 3 million cycles.

Discussion

As the joint was wearing, although the roughness did not change a great deal, the nature of the roughness did. The starting surface roughness showed positive skewness indicating greater peaks than valleys, which is typical of the block carbides inherent in

the as cast microstructure. With wear, the peaks were lowered and the resulting surfaces exhibited negative skewness indicating a predominance of valleys. This type of surface is easier to lubricate using fluid film techniques.

Conclusion

For the particular combination of materials, design and manufacture of the Birmingham Hip Resurfacing device, friction and lubrication have been shown to improve as the surfaces wear-in during the first 3 million cycles in a hip simulator.

Figure 1 – Stribeck Curve

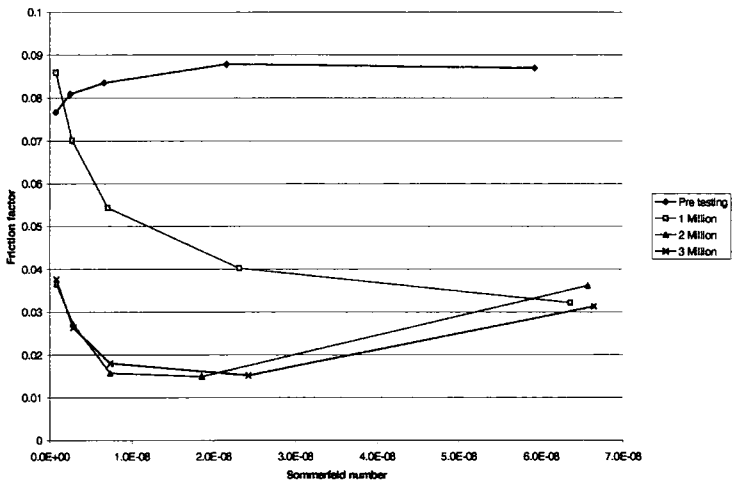

Fluid film lubrication of metal-on-metal hip joints – Fact or Fiction

A Unsworth[1], K Vassiliou[1], APD Elfick[1], SC Scholes[1], D McMinn[2] and T Band[3]
[1]Centre for Biomedical Engineering, University of Durham, England. [2]Birmingham Nuffield Hospital UK. [3]Midland Medical Technologies Ltd, UK.

Introduction

Frictional studies carried out on low carbon, 28mm diameter metal-on-metal hip joint replacements gave friction factors of 0.15 when lubricated with a lubricant containing proteins and 0.3 when no proteins were present. The "Stribeck" curves indicated that the lubrication mode was largely boundary or possibly mixed at high viscosities and entraining velocities [1].

MMT Hip Resurfacing

During a 3 million cycle wear test, a single MMT hip resurfacing device of 50mm diameter, made from high carbon CoCrMo alloy was friction tested at zero, 0.5, 1, 2 and 3 million cycles. The lubricant was 25% bovine serum in aqueous solutions of carboxymethyl cellulose to give a range of viscosities. Figure 1 shows the Stribeck curves at different steps through the wear cycle. Prior to wear testing the friction factor was 0.08 and constant for all viscosities of lubricant. This is consistent with boundary lubrication. By 1 million cycles, a classical mixed lubrication Stribeck curve emerged and by 2 million cycles the curve looked like fluid film lubrication and the friction factor was about 0.015 a value similar to ceramic-on-ceramic when lubricated with a similar lubricant.

Discussion

The roughness of the Hip Resurfacing device as it wore, didn't change much, but the 'skewness' of the asperity distribution moved from positive at the start to negative after 3 million cycles. This indicates that the peaks had been smoothed and the valleys deepened. This surface topography is easier to lubricate than the starting surface.

Conclusion

Unlike earlier, reported tests on metal-on-metal hip joint replacements [1], the Birmingham hip resurfacing device appeared to be subjected to fluid film lubrication as the surface topography modified with wear.

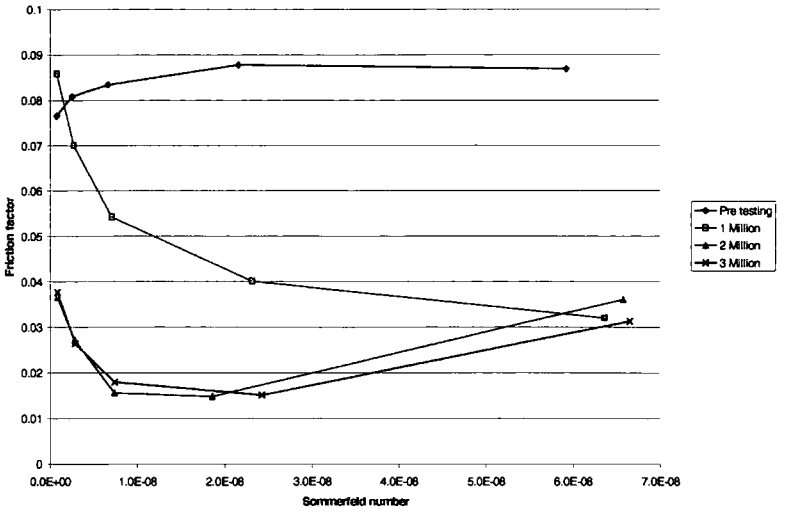

Figure 1 – Stribeck Curve

[1] Scholes SC and Unsworth A (2000). Proc.Inst.Mech.Engrs, 214, 49-58.

The Effect of "Running-in" on the Tribology of Metal-on-Metal Hip Resurfacing Device

Introduction

Metal-on-metal bearings have gained favor in recent years due to concerns over polyethylene debris in conventional joints. Resurfacing prostheses have the added advantage of conserving bone stock, which makes them particularly suitable for younger patients who may need revision arthroplasty during their lifetime.

Friction and wear tests were carried out on the Birmingham Hip Resurfacing (BHR) device and surface roughness data were collected at various intervals.

Frictional studies give an insight into the lubrication mode operating within the device and as such, the effect of "running-in" on the friction, lubrication and surface condition could be studied.

Materials and Methods

Five 50mm diameter BHR devices made from as-cast CoCrMo alloy were tested in a hip wear simulator[1] with a Paul loading cycle (min load 100N max 2975N) and a realistic motion cycle. One joint was friction tested in a friction simulator[2, 3] before the wear test and at 1 million cycle intervals during testing. All joints were friction tested at the end of the wear test. This ensured that the act of friction testing the joints did not alter the wear results in any way.

Joints were worn in the presence of 25% newborn calf serum (protein concentration 18.6mg/ml) with 0.2% sodium azide and 20mM EDTA added to resist bacterial degradation and calcium deposition respectively. Wear was measured gravimetrically at approximately 0.5 million cycle intervals at which point the lubricant was refreshed.

The lubricant for friction testing was prepared identically to that for wear testing. Sodium carboxymethyl cellulose salt was added to 4 batches of this in various concentrations as a viscosity enhancer[4], resulting in 5 different viscosities of lubricant (0.0012, 0.0042, 0.011, 0.036, 0.098 Pa s). This was used to vary the Sommerfeld parameter for 'Stribeck plot' analysis.

Roughness data were collected approximately every 0.5 million cycles using a Zygo NewView100 non-contacting optical interference profilometer and statistical significance was determined by t-test.

Results and Discussion

Friction results are shown in Figure 1. Initially the joint operated in boundary lubrication, but progressed to fluid film lubrication at higher viscosities as the test progressed. This is consistent with the change in skewness of the surface roughness. The surfaces became significantly ($p<0.02$ in all cases) more negatively skewed (move valleys than peaks) during the wear test, which is more favorable for lubrication.

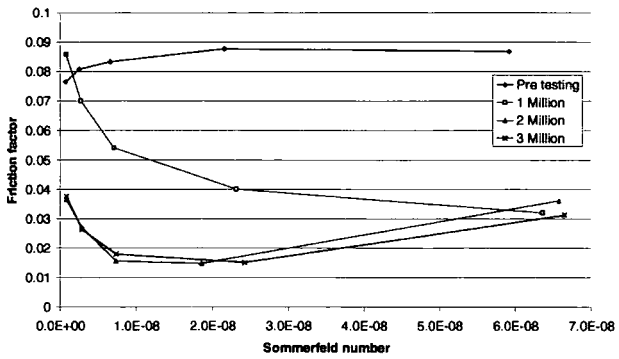

Figure 1. Stribeck curves throughout wear test

Table 1 shows the wear rates calculated by regression analysis. There is a clear reduction in wear rate after wearing in. One joint showed much higher wear throughout than the others. These results are consistent with other findings for this material [5-8] both pertaining to the wear factors and the spread in the results.

mm^3/million cycles	**0 – 1.5 million cycles**	**1.5 - 3 million cycles**
Joint 1	1.79	0.90
Joint 2	6.69	4.81
Joint 3	0.53	0.39
Joint 4	3.21	0.27
Joint 5	0.77	0.25

Table 1. Wear results for each joint.

Conclusions

BHR shows an improvement in tribological characteristics after running-in: the friction factor and wear rate are reduced, and lubrication is closer to fluid film.

References

(1) Smith, S. L., *et al.* **1999**, *213*, 469-473. (2) Unsworth, A., *et al. Engng Medicine* **1988**, *17*, 101-104. (3) Hall, R. M., *et al. Wear* **1994**, *175*, 159-166. (4) Cooke, A. F., *et al. Engng Medicine* **1978**, *7*, 66-72. (5) Kothari, M., *et al. Clin Orthop Rel Res* **1996**, *329S*, 141-147. (6) Farrar, R.; Schmidt, M. B., *43rd Annual meeting of the Orthopaedic Research Society*, San Fransisco, California 1997; 71-12. (7) McKellop, H. A., *et al. Clin Orthop Rel Res* **1996**, *329S*, 128-140. (8) Scholes, S. C., *et al. Proc Inst Mech Engrs Part H: J Engineering in Medicine* **2001**, *215*, 523-530.

Acknowledgements

This research was funded by Midland Medical Technologies, now part of Smith and Nephew.

The effect of TiNbON coating on the wear of Kinemax plus knee arthroplasty and on the presence of metal ions in the lubricant

K Vassiliou, SC Scholes, A Unsworth
Centre for Biomedical Engineering, University of Durham.

Introduction

Six Kinemax knee prostheses were tested in the Durham Knee Wear Simulator to investigate the effect of coating the femoral component on the performance of the joint. ICP-MS was used to determine the concentration of metal ions present in the lubricant and the effect of the presence of bone cement particles on the wear rate of UHMWPE was also investigated.

Materials and Methods

Six Kinemax plus knee joints were tested against UHMWPE in which 4 of the femoral components had a TiNbON coating. After 0.5 million cycles, bone cement particles were added to the lubricant of one coated and one uncoated joint at a concentration of 3 mg/ml. The lubricant was new born calf serum (Harlan-sera lab, batch: 8030901) diluted to 30% with distilled water with 0.2% sodium azide. Every 0.5 million cycles the ion levels of Ti, Co, Cr and Mo in the lubricant were measured using ICP-MS, and the values were normalised per 100,000 cycles.

The joints were tested in the Durham six-station knee wear simulator (1). The simulator is hydraulically driven, and combines a dynamic axial load (maximum 3 kN) with active flexion/extension (65°-0), anterior/posterior translation (±2.5 mm), internal/external rotation (±5°) and passive abduction/adduction. The simulator ran at a frequency of 1Hz.

Results

Figure 1 shows the gravimetric wear results for all the tibial components. The two which show high wear are PE1 which was uncoated, and PE6(3) which was coated neither of which were worn in the presence of cement particles.

ICP-MS showed the presence of Co, Cr, and Mo in much higher concentrations in the lubricant from uncoated joints than from the coated ones. Concentrations of Ti were

higher from coated components than uncoated, and a very high concentration was seen on the coated component worn in the presence of cement particles.

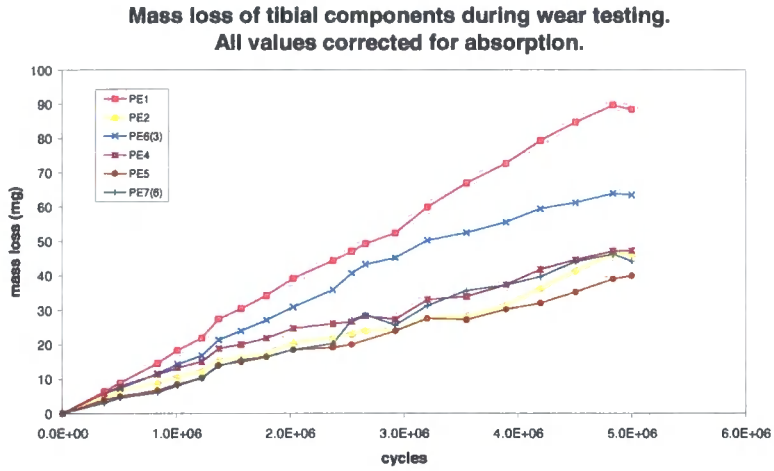

Figure 1. Gravimetric wear results for polyethylene components. PE1 & PE2 Uncoated. PE2 & PE4 bone cement.

Discussion and Conclusions

There is no discernible pattern in the gravimetric wear results based on coated or uncoated femoral component, or even on the inclusion of bone cement particles. More surface damage was noted on the components worn in the presence of particles, however. Inclusions seen on the polyethylene components may have been embedded bone cement particles which would have skewed the gravimetric data to produce a seemingly more favourable wear factor.

The ICP-MS analysis showed that the metal ions present on the surface of the femoral component are detected in the lubricant post wear. The concentration of Ti ions in the lubricant is much higher when bone cement particles are present than when they are not, suggestive of higher wear on that femoral component than on the other coated components.

Acknowledgements

The authors would like to thank Chris Ottley for performing the ICP-MS tests on the batches of serum lubricant and Arthur Newman for his technical assistance.

References

1 H.E.Ash et al *Proc I MechE Part H-J of Engineering in Medicine* **214**, 437 (2000)

Is the wear factor in total joint replacements dependent on the nominal contact stress in ultra-high molecular weight polyethylene contacts?

K Vassiliou* and **A Unsworth**
Centre for Biomedical Engineering, University of Durham, UK

Abstract: The exact dependence of wear factor on contact stress, load and apparent contact area is much disputed in the literature. This study attempts to solve this dispute. Pin-on-plate studies of ultra high molecular weight polyethylene against stainless steel were conducted under different combinations of load (33–250 N), nominal stress (0.56–12.73 MPa) and face diameter, as well as two tests where both stress and load were kept constant, while the diameter was changed. For these tests the centre of the pin face was bored out to create four different average pin diameters with similar face areas. Diameter and load were found to have no significant effect on the wear factor, while the wear factor decreased with increasing contact stress according to the relation $K = 2 \times 10^{-6}\sigma^{-0.84}$.

Keywords: ultra high molecular weight polyethylene wear, contact stress, load, pin-on-plate set-up

NOTATION

K	wear factor ($mm^3/N\,m$)
L	load (N)
R_a	surface roughness parameter (μm)
UHMWPE	ultra high molecular weight polyethylene
V	wear volume (mm^3)
x	sliding distance (m)

1 INTRODUCTION

1.1 Wear

The simple model of wear, according to the Lancaster equation [1] states that $V = KLx$, where V is the wear volume (mm^3), L is the load (N), x is the sliding distance (m) and K is the wear factor ($mm^3/N\,m$). This indicates that the wear volume is dependent on the load and the sliding distance for any given configuration. The nominal contact stress across the interface does not appear. This is because the real contact area increases with increasing load, while the apparent contact area remains constant [2]. The Lancaster equation is a simplified form of the Archard wear equation [3], which included a term for the hardness. In this case, the hardness term has been incorporated into the wear factor. Archard assumed Hertzian contact theory for a flat non-deformable surface in contact with a nominally flat deformable surface with spherical asperities evenly distributed in depth.

1.2 Effect of stress and load on wear factor

Although the Lancaster equation suggests that the wear volume is dependent only on the particular combination of materials, the load and the distance slid, the situation may not be quite so simple. The literature is divided as to the exact effect of load and stress on the wear rate of ultra high molecular weight polyethylene (UHMWPE). This is made more difficult by the different operating conditions in each study, including differences in apparatus and lubricants.

Barbour *et al.* [4], using pin-on-plate apparatus, indicated that the wear factor decreases with increasing nominal contact stress. Wang *et al.* [5] showed the effect of maximum contact stress on the wear of UHMWPE using artificial hips, by altering the radial clearance. These findings agreed with the Barbour *et al* study but contradicted previous work [6, 7].

Rose *et al.* [6] and Rostoker and Galante [7] both found an exponential increase in wear with increasing load and increasing contact stress respectively. The results in these studies were presented as mass loss per unit sliding distance, and penetration depth per unit sliding distance respectively rather than wear factor.

The MS was received on 7 November 2003 and was accepted after revision for publication on 8 December 2003.
* *Corresponding author: Centre for Biomedical Engineering, University of Durham Science Laboratories, South Road, Durham DH1 3LE, UK.*

When the results were converted to a wear factor, this relationship was found to be no longer the case. Rose *et al.* showed very little variation in the wear factor except for a large increase at the very highest stress, while Rostoker and Galante showed lower wear factors for stresses around 10 MPa, but higher wear factors both above and below this.

Sathasivam *et al.* [8] found that the average mass loss on the pins at first increased and then decreased with decreasing nominal stress. This trend does not change when converted to a wear factor since all pins in the study were subjected to the same loads.

More recently, Mazzucco and Spector [9] concluded that the wear factor for UHMWPE pins against CoCrMo plates was not dependent on the load nor on the contact stress. Instead they found it to be dependent on the apparent contact area. However, their results did show a decrease in wear factor with increasing contact stress.

Archard's work appears to be applicable to all the references cited above, in which UHMWPE is tested against a metal. This paper attempts to solve the dispute within the literature concerning the exact relationship between the magnitude of the wear factor and the load applied to the system.

2 APPARATUS

The four-station pin-on-plate machine had independently generated reciprocating and rotational motion. Figure 1 shows the set-up of the rig. The plates reciprocated at 1 Hz with a stroke length of 25 mm, while the pins rotated at 1 Hz around their central vertical axis. Each of the pins had a separate motor to provide rotation. The addition of rotation to the reciprocation motion has been found to give wear rates more comparable with clinically observed wear rates, and to give worn surfaces with similar wear patterns and defects to those seen in clinically retrieved samples. This has been seen in pin-on-plate [10, 11], pin-on-disc [12] and simulator [13] studies.

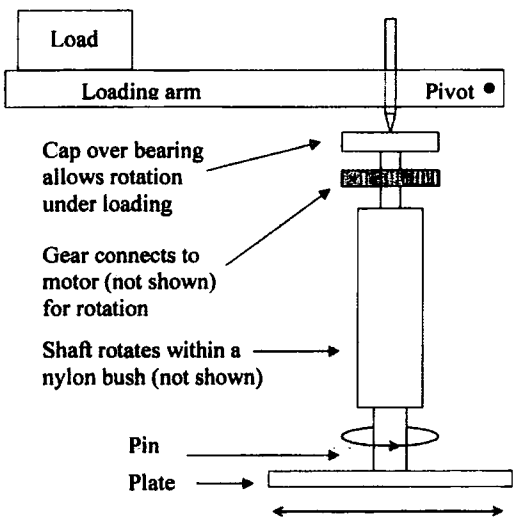

Fig. 1 Schematic diagram of pin-on-plate set-up

The pins were each independently statically loaded by placing masses at various lengths along four loading arms (Fig. 1). Bovine serum diluted to 30 per cent, with 0.2 per cent sodium azide added to retard bacterial degradation, lubricated the pin–plate interface (15.6 g/l protein concentration).

The number of cycles was measured by a non-contacting Hall-effect probe. The temperature was kept at a constant 37 °C. A level sensor was attached to one side of the bath to control the amount of lubricant in the bath. An unloaded control pin was also used to correct for the amount of fluid uptake. This was in the bath to the same depth as the test pins but did not articulate.

3 MATERIALS AND METHODS

3.1 Materials

3.1.1 Stainless steel

Stainless steel plates of dimensions 48 mm × 24 mm × 3 mm were machined from bar stock supplied by RS Components. The stainless steel was 316 highly corrosion resistant material. While the British Standard refers to an initial $R_a < 50$ nm, industry produces joints with surface roughnesses that are much lower than this. The initial R_a values of the plates used were between 5.25 and 13.30 nm, which is comparable with the values produced on artificial joints by manufacturers.

3.1.2 Ultra high molecular weight polyethylene

The pins were machined from a rod of gamma-irradiated UHMWPE (0.254–0.297 MRad). All pins were machined with the same orientation within the bar to prevent any possible directional effects.

All pin designs and test conditions are detailed in Table 1 and had a connector of 5 mm diameter to fit into the pin holder. For tests B and C, the pins were required to have similar face areas, while differing in radius. As such the centres of pins 2 to 4 were machined out to a depth of 2 mm, causing the pin's face to be an annulus for those pins. For test F, a pin of face diameter 5 mm was used. However, owing to the large loads applied during this test, a pin with a larger midsection was manufactured to decrease any buckling or bending of the pin under load.

One pin was tested under each set of conditions, except in the case of tests D and E which were conducted under identical conditions. The results from these two tests agreed well but were presented as individual data points in accordance with the other tests. This gave an overall indication of the trend for each of the factors investigated.

Table 1 Conditions and pin design for each test

Test ID	Test pair	Load (N)	Contact stress (MPa)	Pin type	Pin name
A	1	40	5.66	Tapered; initial face diameter, 3 mm	Leeds tapered
	2	40	2.04	Cylinder; diameter, 5 mm	Durham
	3	40	0.63	Cylinder; diameter, 9 mm	ASTM
	4	40	0.56	Cylinder; diameter, 9.5 mm	Leeds flat
B	1	40	1.46	Cylinder; diameter, 5.9 mm	Pin 1
	2	40	1.47	External diameter, 3 mm; internal diameter, 6.6 mm	Annulus face pin 2
	3	40	1.47	External diameter, 6 mm; internal diameter, 8.4 mm	Annulus face pin 3
	4	40	1.50	External diameter, 8 mm; internal diameter, 9.9 mm	Annulus face pin 4
C	1	70	2.56	Cylinder; diameter, 5.9 mm	Pin 1
	2	70	2.58	External diameter, 3 mm; internal diameter, 6.6 mm	Annulus face pin 2
	3	70	2.58	External diameter, 6 mm; internal diameter, 8.4 mm	Annulus face pin 3
	4	70	2.62	External diameter, 8 mm; internal diameter, 9.9 mm	Annulus face pin 4
D and E	1	33	1.68	Cylinder; diameter, 5 mm	Durham
	2	61	3.11	Cylinder; diameter, 5 mm	Durham
	3	79	4.02	Cylinder; diameter, 5 mm	Durham
	4	49	2.50	Cylinder; diameter, 5 mm	Durham
F	1	180	9.17	Face diameter, 5 mm	Durham larger midsection
	2	250	12.73	Face diameter, 5 mm	Durham larger midsection
	3	90	4.58	Face diameter, 5 mm	Durham larger midsection
	4	120	6.11	Face diameter, 5 mm	Durham larger midsection

3.2 Methods

3.2.1 Cleaning and weighing protocols

The pins and plates were cleaned according to the protocols in the Appendix. Each component was weighed four times and the mean and standard deviation of the readings was found. The pin mass change was adjusted for fluid uptake using the mass of the control pin.

3.2.2 Experimental procedure

After approximately 250 000 cycles the experiment was stopped and the pins and plates removed, cleaned and weighed. The mass loss measured was converted to a volume loss using the density of UHMWPE (953 $\mu g/mm^3$) and the density of stainless steel (7.85 mg/mm^3) for the pins and plates respectively. The wear factors were found by using the Lancaster equation.

The lubricant was discarded and replaced with fresh serum each time that the machine was stopped to enable the pins and plates to be weighed. Each test was stopped after a minimum of 1.5×10^6 cycles of steady state wear, and all wearing-in data were disregarded. The plates were analysed on the Zygo NewView 100 non-contact profilometer approximately each 0.5×10^6 cycles and both pins and plates were analysed post-testing.

3.2.3 Effect of the rotational element of motion on the sliding distance

Because of the rotational motion, paths taken by different points on the pin surface differed according to position [**11**]. Since the rotation and reciprocation frequencies were both 1 Hz, the path lengths of different points on the perimeter also differ. Figure 2 [**11**] shows the paths taken by points which began at different positions on the circumference of the pin. Clearly not all points traversed the same path or have the same path length.

Scholes [**14**] developed a computer program to find the actual sliding distance of pins undergoing the particular motion used in the Durham machines. For the purposes of the present study, Scholes' program was modified to take into account the different pin designs. This is a numerical integration over the surface of the pin for small increments of angles and radii.

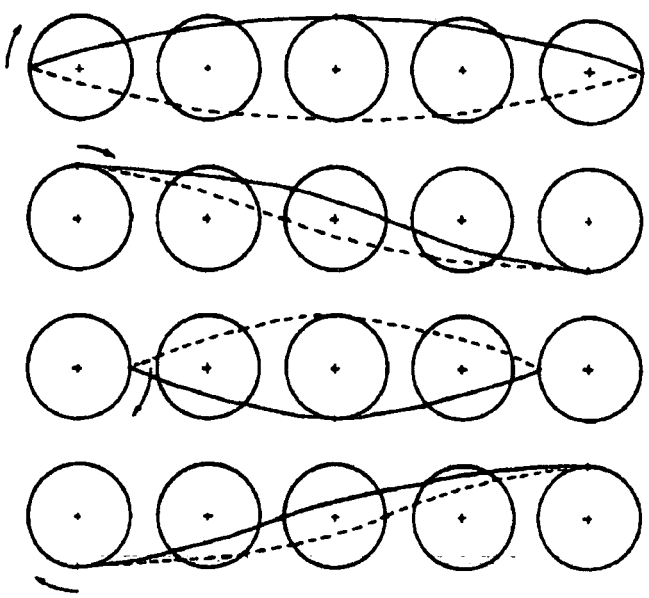

Fig. 2 The paths taken by various points along the circumference of the pin during 1 cycle [**11**]

Table 2 Percentage increase in sliding distance due to rotational element of motion for all pins used in this study

	Increase in sliding distance due to rotation (%)
Leeds tapered	0.67
Durham and test F	1.69
ASTM	4.82
Leeds flat	5.30
Tests B and C: pin 1	2.27
Tests B and C: pin 2	4.51
Tests B and C: pin 3	9.04
Tests B and C: pin 4	13.22

As the number of points taken into account was increased, the output values settled to the values given in Table 2. The percentage increase found for each pin was used to adjust the values of the sliding distance, and it was always these adjusted values that were used for the sliding distance rather than the reciprocation distance.

4 RESULTS

4.1 The effect of pin radius on wear factor

As can be seen in Fig. 3, the wear factor was not affected by the radius of the pin when both the load and the stress remained constant.

Taking into account all the other tests, regardless of experimental conditions, this became more evident. The external radius of each pin was plotted against the wear factor. Figure 4 shows that there was no clear correlation between the pin radius and the wear on the pin. The results for the 2.5 mm radius were particularly indicative since they spanned almost the entire range of the wear factors seen.

4.2 The effect of load on wear factor

As can be seen from Fig. 5, the magnitude of the wear factor is not greatly affected by the applied normal load for a constant nominal contact stress. This is as expected since the load is used in the calculation of the wear factor. This implies that some other factor affects the wear factor more significantly than just the load applied.

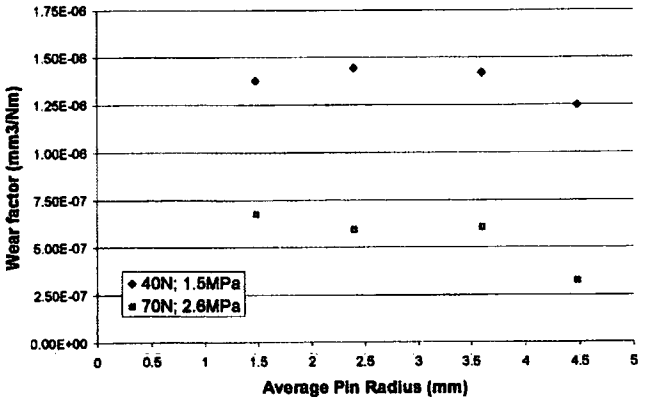

Fig. 3 Dependence of wear factor on average pin radius for two conditions of constant stress: 1.5 and 2.6 MPa

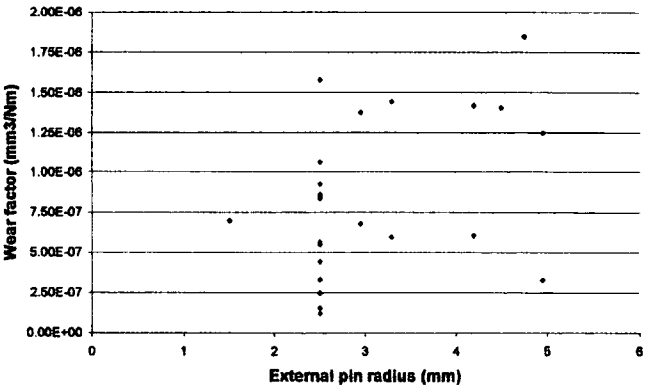

Fig. 4 The effect of external pin radius on wear factor for all test conditions

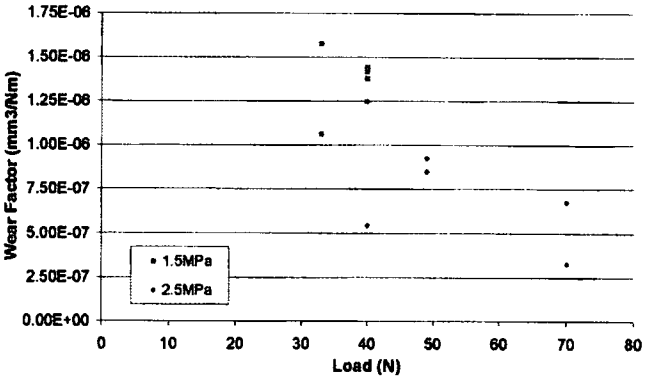

Fig. 5 The effect of normal load on wear factor for two nominal contact stress values: 1.5 and 2.5 MPa

4.3 The effect of nominal contact stress on wear factor

From the results in Fig. 3, we can see that, at higher loads and stresses, lower wear factors are achieved. This difference is found to be statistically significant ($p < 0.05$); a closer analysis including results from all test conditions follows.

Including all data at 40 N the effect of the stress on the pin wear can be seen, and this is shown in Fig. 6. A decrease in wear factor is noted with increasing stress.

Figure 7 shows all data regardless of the experimental conditions. The remaining data were found largely to overlap the 40 N data and are thus considered as one data set. A power-law fit to these data gives the relation $K = 2 \times 10^{-6}\sigma^{-0.84}$. This means that at low stresses the magnitude of the wear factor changes more rapidly as the stress increases than it does at higher stresses.

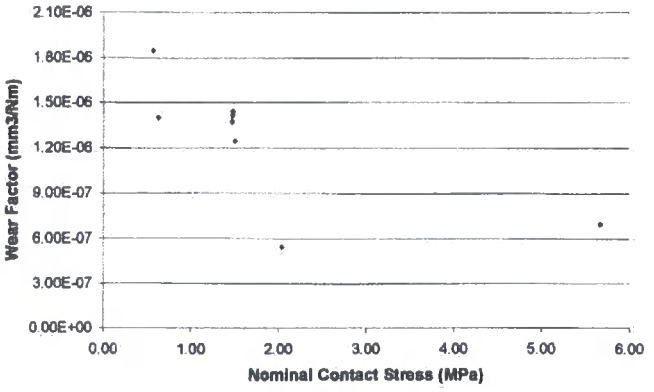

Fig. 6 The dependence of wear factor on nominal contact stress at a constant load of 40 N

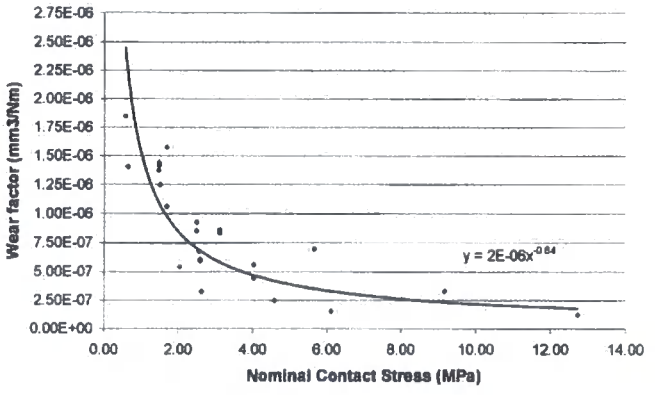

Fig. 7 The dependence of wear factor on nominal contact stress

4.4 Surface study

4.4.1 Plates

All but two plates showed a significant ($p<0.05$) increase in surface roughness between the start and end of the test. Final mean surface roughnesses were in the range 8.81–90.0 nm. Multidirectional scratching was seen on the wear track. No correlation was found between the final roughness for each plate and the conditions of testing ($R^2=0.1$ for both load and contact stress). This indicates that, although the roughness of the plates increased significantly, the increase was not directly related to either the load or the stress under which the test was conducted, nor was the final roughness dependent on the initial roughness. In addition, no correlation was found between the wear factor of the polyethylene and either the initial or the final roughness value of the plate ($R^2=0.2$ and 0.0 respectively).

4.4.2 Pins

During the course of testing, the machining marks visible on the pin faces were removed, leaving a more polished surface. The mean final R_a was in the range 221–803 nm. No correlation was found between the final Ra and either the load or the stress under which the pins were tested ($R^2=0.4$ and 0.2 respectively).

For all solid cross-section pins, a nipple became visible at the centre of the pin (Fig. 8). Some smaller features were seen on the micrographs both at the edges and towards the centre of the pin faces. Multidirectional scratching was noticed in some areas on many pins.

5 DISCUSSION

5.1 General comments

The wear factors found by Barbour *et al.* [4] were lower than those found in this study by a factor of 100 while those found by Rose *et al.* [6] were higher by a similar order of magnitude. The values found in the Durham Laboratories are, however, comparable with those found clinically. From Dowson and Wallbridge [15] the relationship between volume of wear and clinical wear factor is seen to be $k_{\text{clinical}} = \text{volume}/2.376NWr$ (neglecting creep). For a volumetric loss of 50 mm^3/year on a Charnley joint of 22 mm diameter, implanted in a 75 kg (750 N) person, this yields a wear factor of 2.55×10^{-6} $mm^3/N\,m$. This figure was confirmed in a study of over 200 explanted acetabular components [16]. Therefore, while the literature contains a wide range of reported wear factors, those from the current work do have clinical relevance.

5.2 The effect of pin radius on wear factor

The radius of the pin does not affect the wear factor, when all other conditions are kept the same. In these tests the nominal face areas of each pin are very similar, allowing both load and stress to be kept constant. As such, it is expected that the actual contact areas will be very similar for all designs of pin [2], and subsequently there is very little difference in the contact of the surfaces on a microscopic scale. This was expected but Lloyd [17]

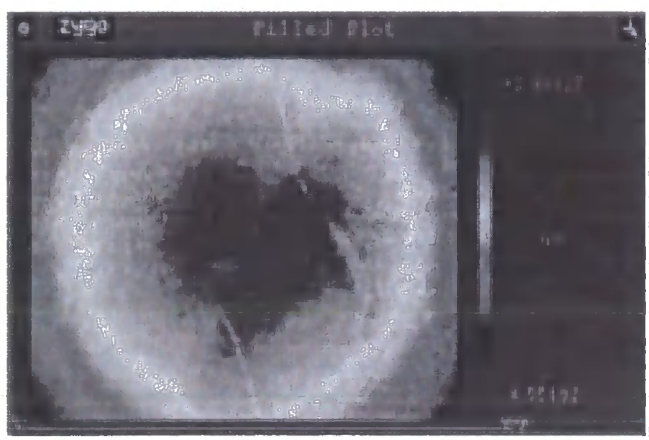

Fig. 8 Central nipple on pin 1 of test B, tested under 40 N load and 1.46 MPa stress

in his thesis suggested that there was a link between the wear factor and the radius.

5.3 The effect of applied normal load on wear factor

The wear factor does not seem to be affected by the normal load. This is in agreement with the Archard equation [3] and the Lancaster equation [1], such that the wear factor is a constant of proportionality between the volume loss and the product of the load and distance slid for a particular material combination. The Lancaster equation is used to calculate the wear factor and, as such, the load is not expected to have an effect on the wear factor.

5.4 The effect of nominal contact stress on wear factor

A decrease in wear factor is seen with increasing nominal contact stress. The relation is found to fit a power law such that $K = 2 \times 10^{-6}\sigma^{-0.84}$. This indicates that the magnitude of the wear factor reduces more as the contact stress increases at low stresses than it does at high stresses. This is consistent with the work of Barbour *et al.* [4], but not with the studies of Rostoker and Galante [7] or of Rose *et al.* [6]. Rostoker and Galante found an exponential increase in penetration depth per unit sliding distance with increasing contact pressure, while Rose *et al.* reported an increasing trend in mass loss with increasing load. This is also contrary to the findings of Mazzucco and Spector [9].

5.5 Surface study

The polymeric components became smoother as the concentric machining marks were removed during the test. At the centre of each of the pins with a circular face geometry, a nipple became visible. This has been noted in the past by other researchers [18, 19]. No correlation was found between the final surface roughness of the pin faces and the conditions of testing (load and stress). Saikko *et al.* [20] found a power-law relation with R_a raised to a power less than one. This would suggest a maximum of a twofold variation in wear factor over the range of roughnesses seen in this study. Even this variation would not obscure the results found herein, where the wear factors vary by an order of magnitude.

6 CONCLUSIONS

The wear factor of UHMWPE when tested against stainless steel increases as the nominal contact stress increases according to a power law $K = 2 \times 10^{-6}\sigma^{-0.84}$. This indicates that there is a high dependence on contact stress for low stresses, but at higher stresses the wear factor is not affected to the same degree. The radius of the pin and the load do not affect the wear factor at all, as expected.

During the testing, the concentric machining marks were removed from the surface of the pins early in the testing, leaving a more polished appearance. A nipple became visible at the centre of the pins. Multidirectional markings were noted on the pin surface.

The plates became significantly rougher during the course of testing, although this increase in roughness was not found to correlate with the testing conditions or the initial roughness of the plate. Neither the initial nor the final roughness value of the plate was found to correlate with the wear factor of the polyethylene component tested against them ($R^2 = 0.2$ and 0.0 respectively).

ACKNOWLEDGEMENTS

The authors would like to thank the School of Engineering Workshop technicians, Mr Kevan Longley and Mr Colin Wintrip, for their help and support on this project. Miss Vassiliou was supported by a School of Engineering Scholarship.

REFERENCES

1 **Lancaster, J. K.** Dry bearings: a survey of materials and factors affecting their performance. *Tribology*, 1973, **6**, 219–251.

2 **Greenwood, J. A.** and **Williamson, J. B. P.** Contact of nominally flat surfaces. *Proc. R. Soc. Lond. A*, 1966, **295**, 300–319.

3 **Archard, J. F.** Contact and rubbing of flat surfaces. *J. Appl. Phys.*, 1953, **24**(8), 981–988.

4 **Barbour, P. S. M., Barton, D. C.** and **Fisher, J.** The influence of contact stress on the wear of UHMWPE for total replacement hip prostheses. *Wear*, 1995, **181**, 250–257.

5 **Wang, A., Essner, A.** and **Klein, R.** Effect of contact stress on friction and wear of ultra-high molecular weight polyethylene in total hip replacement. *Proc. Inst. Mech. Engrs, Part H: J. Engineering in Medicine*, 2001, **215**(H2), 133–140.

6 **Rose, R. M., Goldfarb, H. V., Ellis, E.** and **Crugnola, A. M.** On the pressure dependence of the wear of ultrahigh molecular weight polyethylene. *Wear*, 1983, **92**, 99–111.

7 **Rostoker, W.** and **Galante, J. O.** Contact pressure dependence of wear rates of ultra high molecular weight polyethylene. *J. Biomed. Mater. Res.*, 1979, **13**, 957–964.

8 **Sathasivam, S., Walker, P. S., Campbell, P.** and **Rayner K.** The effect of contact area on wear in relation to fixed bearing and mobile bearing knee replacements. *J. Biomed. Mater. Res., Appl. Biomat.*, 2001, **58**(3), 282–290.

9 **Mazzucco, D.** and **Spector, M.** Effects of contact area and stress on the volumetric wear of ultra-high molecular weight polyethylene. *Wear*, 2003, **254**(5–6), 514–522.

10 **Scholes, S. C.** and **Unsworth, A.** Pin-on-plate studies on the effect of rotation on the wear of metal-on-metal samples. *J. Mater. Sci. Mater. Medicine*. 2001, **12**(4), 299–303.

11 **Joyce, T. J., Monk, D., Scholes, S. C., Unsworth, A.** A

multi-directional wear screening device and preliminary results of UHMWPE articulating against stainless steel. *BioMed. Mater. Engng*, 2000, **10**(3–4), 241–249.

12 **Saikko, V.** A multidirectional motion pin-on-disk wear test method for prosthetic joint materials. *J. Biomed. Mater. Res.*, 1998, **41**(1), 58–64.

13 **Bragdon, C. R., O'Connor, D. O., Lowenstein, J. D.** and **Syniuta, W. D.** The importance of multidirectional motion on the wear of polyethylene. *Proc. Instn Mech. Engrs, Part H: J. Engineering in Medicine*, 1996, **210**, 157–165.

14 **Scholes, S. C.** The tribology of hard bearing surfaces for use in hip prostheses. PhD thesis, University of Durham, Durham, 1999.

15 **Dowson, D.** and **Wallbridge, N. C.** Laboratory wear tests and clinical observations of the penetration of femoral heads into acetabular cups in total replacement hip joints. I: Charnley prostheses with polytetrafluoroethylene acetabular cups. *Wear*, 1985, **104**, 203–215.

16 **Hall, R. M., Siney, P., Unsworth, A.** and **Wroblewski, B. M.** The association between rates of wear in retrieved acetabular components and the radius of the femoral head. *Proc. Instn Mech. Engrs, Part H: J. Engineering in Medicine*, 1998, **212**(H5), 321–326.

17 **Lloyd, A.** The influence of stress and load on the wear of UHMWPE pins on stainless steel plates. MEng thesis, University of Durham, Durham, 2000.

18 **Saikko, V.** and **Ahlroos, T.** Wear simulation of UHMWPE for total hip replacement with a multidirectional motion pin-on-disk device: effects of counterface material, contact area, and lubricant. *J. Biomed. Mater. Res.* 2000, **49**(2), 147–154.

19 **Charnley, J.** The wear of plastic materials in the hip joint. *Plastics Rubber*, 1976, **1**, 59–63.

20 **Saikko, V., Calonius, O.** and **Keranen, J.** Effect of counterface roughness on the wear of conventional and crosslinked ultrahigh molecular weight polyethylene studied with a multi-directional motion pin-on-disk device. *J. Biomed. Mater. Res.*, 2001, **57**(4), 506–512.

APPENDIX

Cleaning protocols

(a) Stainless steel plates

The plates are cleaned using the following protocol:

1. Rinse with tap water to remove bulk contaminants.
2. Immerse in a solution of 1% Neutracon and place in an ultrasonic bath for 10 min at 37 °C.
3. Rinse in distilled water.
4. Dry with a lint-free wipe.
5. Wipe with acetone and a lint-free wipe.

(b) UHMWPE pins

The pins were cleaned according to the following protocol, closely following the ASTM recommendation (ASTM F732-00, part A6):

1. Rinse with tap water to remove bulk contaminants.
2. Immerse in a 1% solution of Neutracon and place in an ultrasonic bath for 15 min at 37 °C.
3. Rinse in a stream of distilled water.
4. Immerse in distilled water and place in an ultrasonic bath for 5 min at 37 °C.
5. Dry with a lint free tissue.
6. Immerse in acetone for 3 min.
7. Dry with a lint-free tissue.
8. Allow to dry in a biological flow cabinet at room temperature for 30 min.